THE STRUCTURAL AND SEDIMENTOLOGICAL EVOLUTION OF THE SOMALI BASIN: PALEOOCEANOGRAPHIC INTERPRETATIONS

By

RICHARD H. BURROUGHS III
AB Princeton University
1969

SUBMITTED IN PARTIAL FULFILLMENT OF THE REQUIREMENTS FOR THE DEGREE OF DOCTOR OF PHILOSOPHY

at the

MASSACHUSETTS INSTITUTE OF TECHNOLOGY

and the

WOODS HOLE OCEANOGRAPHIC INSTITUTION
August 1974

Signature of Author.....

Joint Program in Oceanography, Massachusetts Institute of Technology - Woods Hole Oceanographic Institution, and Department of Earth and Planetary Sciences, and Department of Meteorology, Massachusetts Institute of Technology, August 1974

Certified by.....
Thesis Supervisor

Accepted by.....

Chairman, Joint Oceanography Committee in the Earth Sciences, Massachusetts Institute of Technology-Woods Hole Oceanographic Institution

The Structural and Sedimentological Evolution of the Somali Basin: Paleooceanographic Interpretations

Richard H. Burroughs III

Submitted to the Massachusetts Institute of Technology - Woods Hole Oceanographic Institution Joint Program in Oceanography on August 12, 1974 in partial fulfillment of the requirements for the degree of Doctor of Philosophy

ABSTRACT

The paleooceanographic development of the Somali Basin in the Northwestern Indian Ocean is determined through considering the structural evolution of the area; its influence on Neogene atmospheric and oceanic circulation as indicated in the sediment record; and variation in these circulation systems as seen in late Quaternary sediments. Chain Ridge forms the main structural element of the Somali Basin. Correlation of geophysical measurements along its topographically elevated portion with geophysical transects in the southern Somali Basin indicates that a buried portion of the Chain Ridge sector of Owen Fracture Zone extends at least to 7.5°S. In areas where crustal age may be estimated on both sides of the fracture zone either by elevation or by other methods, the sea floor to the west is at least 30 m.y. older than that to the east and may be considerably older. The trend of the fracture zone and the age of its segments control the time and direction of movement for India relative to Africa and Madagascar. In addition, they limit the number of proposed reconstructions and indicate that the Western Somali Basin is a small remaining part of the original Tethys. These constraints result in a model for the area which considers Gondwanaland dispersal in the Western Indian Ocean.

The final stages of development of the Somali Basin correspond with the destruction of the Tethys with the final marine regression in northern India during Middle Miocene. Neogene

sedimentation rate determinations for the Somali Basin show considerable increases between the Miocene and Recent, in spite of the fact that the basin is becoming larger and deeper. It is proposed that the dessication and subsequent elevation of the area in northern India caused by structural evolution resulted in the development of a land-sea heating contrast which drives the southwest monsoon, and due to increased upwelling and productivity it is recorded by increased sedimentation rates in the Somali Basin.

The late Quaternary sediment record of the area indicates maintenance of these large scale circulations with little change in sea surface temperature as determined from nannofossil assemblage variation, and occurrence of upwelling over a broader area as indicated by the distribution of coarse carbonate. Several significant bottom water incursions into the basin are interpreted from analyzing the total carbonate curves but their effects do not extend to the area of maximum upwelling due to depression of the CCD by high productivity.

Thesis Supervisors: Dr. J. R. Heirtzler (Senior Scientist)
Dr. D. A. Johnson (Assistant Scientist)

TABLE OF CONTENTS

ACKNOWLEDGEMENTS

Instrumental to the completion and success of this project was the help of my advisors J. R. Heirtzler, D. A. Johnson, J. B. Southard, E. T. Bunce, and B. U. Haq. In addition, I would also like to thank my colleagues at Massachusetts Institute of Technology, the Woods Hole Oceanographic Institution and elsewhere who have taken the time to informally discuss the project with me. The officers and crew of the CHAIN, as well as the technical staff of the Geology and Geophysics Department at Woods Hole made the necessary data collection at sea possible.

A Graduate Research Fellowship at the Woods Hole Oceanographic Institution supported my work and in addition provided support for travel, radiocarbon dating, and some of the expenses involved in producing figures for the final manuscript.

Two cruises in the Somali Basin area, CHAIN 99, leg 8, (ONR contracts N00014-66-C-0241;NR083-004; J. R. Heirtzler, Chief Scientist) and CHAIN 100, legs 4 and 5 (NSF Grant 27516; E. T. Bunce, Chief Scientist) formed the data base for the area with additional material from Deep Sea Srilling Project Indian Ocean legs 24 and 25. Scanning electron microscope studies were supported by D. A. Johnson and B. U. Haq, who also aided in

identifications. Some initial typing and drafting expenses were covered by NSF Grant 27516. The final typing of the manuscript was ably done by F. Mellor and D. Allison.

LIST OF FIGURES

Figure

Figure

Figure

LIST OF TABLES

I INTRODUCTION

The sea floor spreading hypotheses (Hess, 1962) and related work on magnetic anomalies (Vine and Matthews, 1963; Heirtzler, et al., 1968) structural features (Wilson, 1965) their global implications (McKenzie and Parker, 1967; Morgan, 1968), and related sea floor elevation (Sclater, et al., 1971) have in little over one decade revolutionized the understanding of the structural evolution of ocean basins.

During the latter part of this decade routine drilling in the deep ocean provided the necessary data to begin to interpret the sediment record in terms of this mobile framework. Using the shorter Pleistocene deep sea sections as a conceptual model, the initial studies examined direct corollaries that grew from knowledge of the structural evolution such as alterations in current paths (Berggren and Hollister, 1974) or calcium carbonate compensation depth (Berger, 1973) and the first paleoceanographic studies that directly investigated past oceanic conditions through analysis of components of deep sea sediments were completed. One of the next steps in utilizing plate tectonics to understand all phases of earth history will be in examining the indirect corollaries to ocean evolution that

are due to changing plate geometries such as long term effects on climatic and meterological variables which in turn are recorded as significantly different ocean conditions.

These problems in paleooceanography which recent technical and intellectual developments have fostered require ability in a variety of fields. The investigator must in general be able to develop the structural evolution of the ocean basin, understand the salient characteristics of the Pleistocene sedimentary record, and through examining the Cenozoic or earlier sediments from the area consider the variety of changes that they may indicate.

This thesis will consider the paleooceanographic record in sediments of the Somali Basin, northwestern Indian Ocean, and its relation to the structural development of the area. Obviously, such a broad scale undertaking, even though limited to a specific geographic area, requires specific investigations with the framework of the overall problem if it is to meet with any success. Accordingly, processes involved in three specific areas of ocean evolution will be examined.

First, as in studies of other oceans the structural framework for the evolution of the area is developed. Second, the initiation of the most prominent oceanographic feature, the monsoon, is investigated by comparing Neogene sedimentation with Recent sedimentation. Third, late Quaternary sedimentation is treated in more detail to determine Recent oceanographic variation.

II. CHAIN RIDGE AND THE STRUCTURAL EVOLUTION OF THE SOMALI BASIN

INTRODUCTION

The complex and relatively recent evolution of the Indian Ocean has attracted work on the structure of the area both to examine its development and to consider the basic mechanisms of plate motion. In the western Indian Ocean these examinations of structural history have, in the past, been confined to those areas where a readily discernible magnetic record of sea floor evolution is available. However, a major portion of the western Indian Ocean, the Somali Basin, has not been incorporated in general evolutionary schemes because initial analyses of available data from the area did not yield readily interpretable structural or magnetic trends. Nonetheless, an understanding of the evolution of this area is crucial to understanding the initial stages of Gondwanaland dispersal as well as the more recent stages of basin evolution.

The objective of this section is to place constraints on plate motions occurring during Gondwanaland dispersal by examining the basic properties of the major fracture zone in the Somali Basin area. In order to do this the southwestern extent of Chain Ridge has been examined; the age of the sea floor on

opposite sides of the ridge has been inferred; and a model for the origin and evolution of the ridge and surrounding basins has been constructed.

Past examination and speculation about the Somali Basin have led to a variety of possible interpretations of its history. Gregory (1920) shows the first indication of a major fault in the northwestern Indian Ocean which he indicates borders the coasts of Africa and Arabia. The John Murray Expedition (Wiseman and Seymour Sewell, 1937) showed the first bathymetric interpretations of the area which enabled Matthews (1963) after the initial International Indian Ocean Expedition investigations to realize that a major fault scarp, called Owen Fracture Zone, displaced the northern end of the Carlsberg Ridge. Wilson (1965) considered this offset a transform fault, and its southwestern extension was mapped tangent to the East African coastline by him. Further work during the International Indian Ocean Expedition (Heezen and Tharp, 1964) resulted in a physiographic diagram of the area which tended to align Owen Fracture Zone with the Amirante Trench and the east coast of Madagascar. Specific investigations of the Chain Ridge portion of Owen Fracture Zone and surrounding Somali Basin were reported by Bunce et al. (1966, 1967) who related a change in the seismically

determined sediment thickness to the location of Chain Ridge. Fisher et al. (1968) on the basis of previous International Indian Ocean Expedition results and their own investigations of the Amirante Trench and surrounding magnetic patterns concluded that a major left lateral shear occurred since mid-Mesozoic along 52° - 54° E and moved Madagascar south with respect to the Seychelles.

A more recent phase of work in the Northwestern Indian Ocean has been the major syntheses which are often based on sea-floor spreading and and plate tectonics (McKenzie and Parker, 1967; Morgan, 1968). Morgan (1968) considered the Arabia-India branch of Owen Fracture Zone as a transcurrent fault. Le Pichon and Heirtzler (1968) examined magnetic anomalies and were able to determine a late Cenozoic pole of opening for the Carlsberg Ridge. Ewing et al. (1969) assembled sediment thicknesses throughout the area, and Laughton, Matthews and Fisher (1970) summarized results from all preceding investigations. McKenzie and Sclater (1971) developed an evolutionary sequence based on observed magnetic anomalies, their synthetic equivalents, and a major change in spreading direction.

The present analysis relies on a combination of geophysical survey results and those from deep ocean drilling. Fisher and

Bunce et al. (1972) and Simpson and Schlich et al. (1972), in preliminary reports of Deep Sea Drilling results were able to indicate minimum and in some cases tentative ages for basement in the Somali Basin area. Burroughs and Bunce (1973) mapped part of the buried extension of Chain Ridge and established that the feature forms a major age discontinuity in the Somali Basin.

The general principles of sea-floor spreading and plate tectonics (Hess, 1962; Vine and Matthews, 1963; McKenzie and Parker, 1967; and Morgan, 1968) allow a variety of methods for determining past plate motions. Crustal age and relative spreading rates may be determined by sea floor magnetic anomalies or the thermal and hence elevation history of the plate. Motion of an individual continent or groups of continents with respect to the earth's dipole may be determined by paleomagnetism and polar wandering paths (McElhinny, 1973). As earthquakes often define present plate boundaries their focal plane solutions may be used to determine relative motion directions between plates which may also be determined by the strike of transform faults. If continents were at one time together, matching of continental edges may also prove useful.

Of the above, three approaches are most useful considering the limitations of the available data in the Somali Basin. First,

the trend of the fracture zone if adequately mapped and understood will provide information on the relative direction of plate motion. Second, sea floor age determinations on each side of the fracture zone place constraints on the chronology of the plate motions. Third, the fit of continents that were at one time contiguous provides additional constraints.

GENERAL CHARACTERISTICS OF FRACTURE ZONES AND RIDGES

Partially or completely buried ridges similar to Chain Ridge occur in many areas of the oceans and are often due to shearing along faults. A brief analysis of their morphologic and geometric variability forms a basis for investigating Chain Ridge. Although all gradations occur, most of these lineaments lie either roughly parallel or roughly perpendicular to the spreading direction.

Explanations for ridges parallel to the spreading direction have grown out of analyses of the properties of a transform fault (Wilson, 1965) extended to a sphere (McKenzie and Parker, 1967; Morgan, 1968). Structural trends extending from the offsets of the spreading axis became known as fracture zones. Menard and Chase (1970) have summarized an earlier definition of fracture zones as long and narrow bands of irregular topography characterized by volcanoes, ridges, and scarps and often separating different regional depths. While the morphology of the associated ridges or scarps may vary, the trend of the fracture zone is presumed to lie parallel to the spreading direction at the time of its creation along the transform fault (Menard and Atwater, 1968).

Other ridges occur perpendicular to the spreading direction as a part of the continental margin or nearby deep sea. Early work by Drake, Ewing, and Sutton (1959) delineated a prominent basement ridge at the edge of the shelf along the east coast of the United States. Such features are presumably due to the initial rifting processes. If the initial rifting occurs along a zone parallel to the spreading direction, the resultant strike-slip motion between two sectors of continental crust may result in a shelf edge basement ridge that runs parallel to the spreading direction. As margins are more commonly of the normal rifting type, this is rare.

In the Equatorial Atlantic the deep sea ridges associated with fracture zones merge in some cases with continental offsets resulting in a series of transitional features (Le Pichon and Hayes, 1971; Hayes and Ewing, 1970). To deal with the variety of ridges found in this setting Le Pichon and Hayes (1971) suggested several definitions: marginal fracture ridge, a high standing ridge from shear between two sections of continental crust or shearing of continental crust against ocean crust; intermediate ridge, a marginal fracture ridge shearing against a marginal fracture ridge; ocean fracture zone, shear between two sections of oceanic crust; transverse ridge, ridge joining

a prolongation of marginal offsets. These general ridge characteristics and their relationship to the spreading process form a background for Chain Ridge studies.

GEOPHYSICAL PROFILES IN THE SOMALI BASIN

Bathymetric, gravity, magnetic and seismic profiling data from recent cruises were examined to investigate the southwestern extension of Chain Ridge and the basins bordering it. The track lines (figure 1) cross the ridge and its buried extension at several locations, and in addition give limited coverage of the basins on either side.

Chain Ridge 8°N Profiles

Seismic profiles in the vicinity of 8°N on Chain Ridge near the junction with the Carlsberg Ridge show a series of four or five acoustic basement ridges (figures 2-5). Here, as elsewhere, acoustic basement is defined as the coherent reflector that forms the main elevated portions of the ridge and where visible below sediments a rough paraboloid surface. When sampled it is basalt (Bunce et al., 1967) and, therefore, corresponds to layer 2 material as defined for other oceans (Ludwig et al., 1970). As the morphology of this surface must reflect some of the processes in fracture zone formation it will be examined in light of the general characteristics of ridges and fracture zones mentioned previously. In all crossings (figures 2-5) a prominent peak to the west is noted. Often

Figure 1.

Location of ship track in vicinity of Chain Ridge (inset) with respect to major northwestern Indian Ocean features. Bathymetry is simplified from Laughton (1966) and Fisher et al. (1968), and magnetic anomalies are from McKenzie and Sclater (1971).

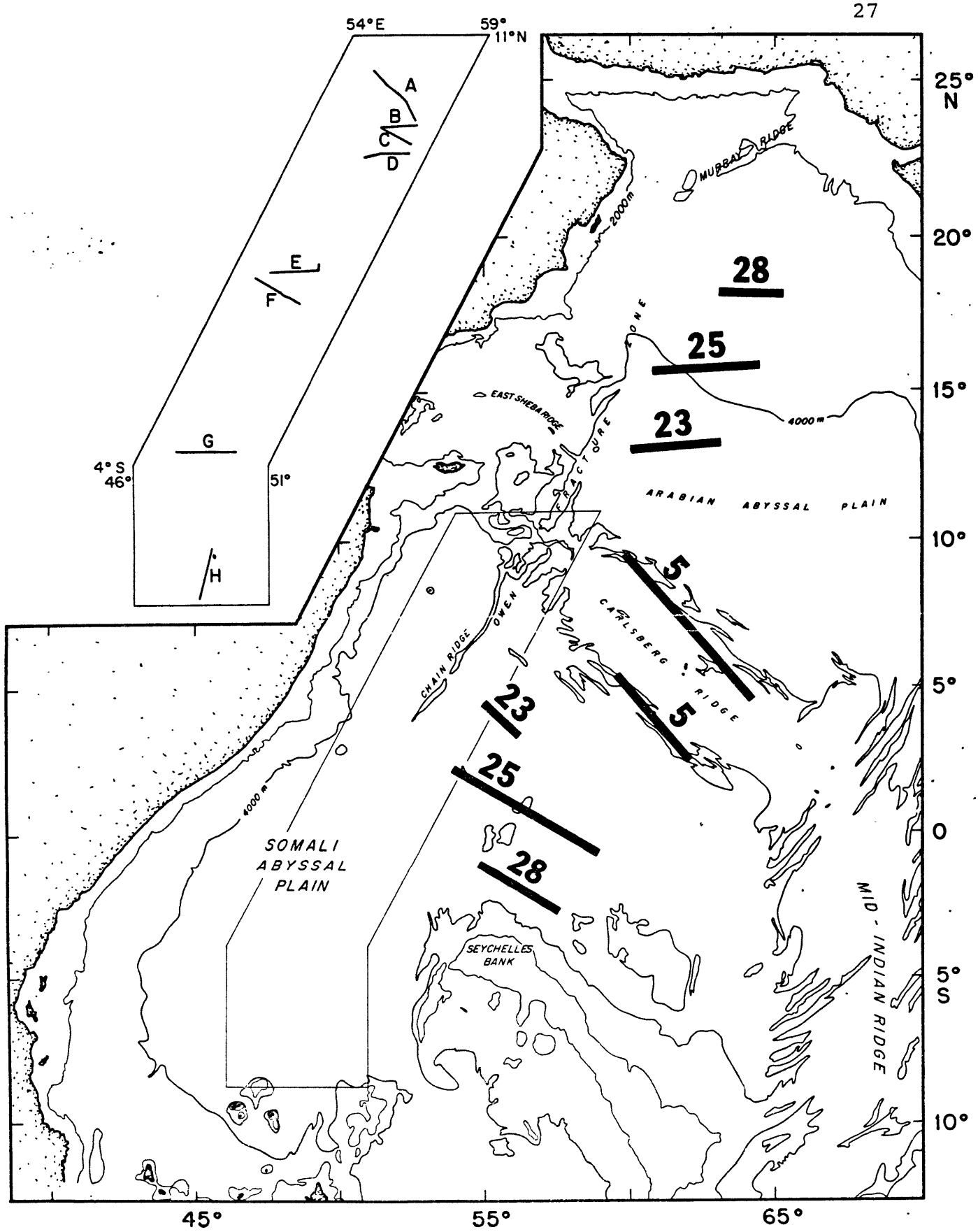
54°E
59°
11°N
A
B
C
D
E
F
G
H
4° S
46°
51°
25°
N
20°
15°
10°
5°
0
5°
S
10°
45°
55°
65°
MURRAY RIDGE
2000m
28
25
23
EAST SHEBA RIDGE
OWEN FRACTURE ZONE
4000m
ARABIAN ABYSSAL PLAIN
5
CARLSBERG RIDGE
5
23
25
28
CHAIN RIDGE
4000 m
SOMALI ABYSSAL PLAIN
SEYCHELLES BANK
MID - INDIAN RIDGE

Figure 2.

Line A. Free-air gravity profile, magnetic profile (with regional field removed) and continuous seismic profiles from west to east in the Somali Basin.

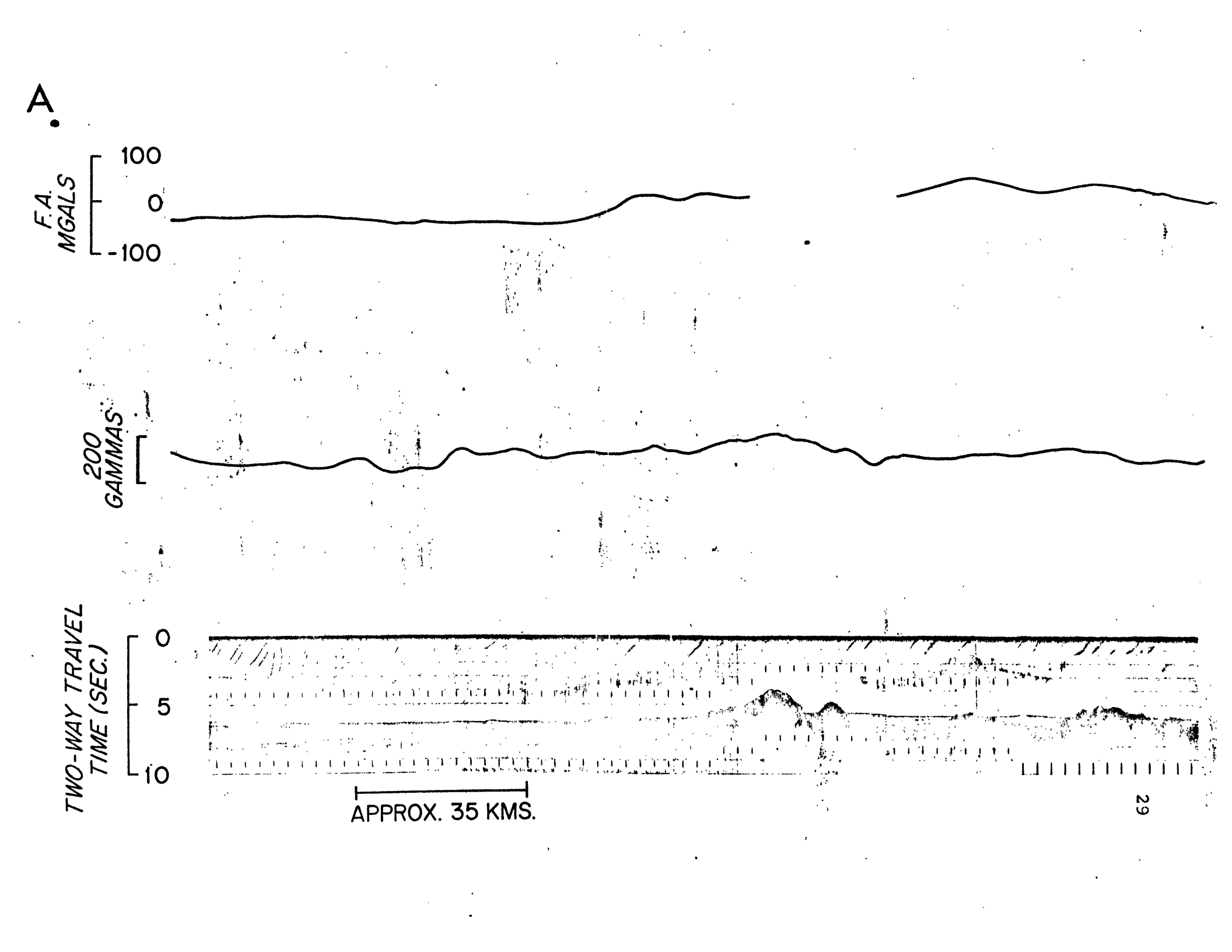
A.
F.A. MGALS
100
0
-100
200 GAMMAS
TWO-WAY TRAVEL TIME (SEC.)
0
5
10
APPROX. 35 KMS.
29

Figure 3.

Line B. Free-air gravity profile, magnetic profile (with regional field removed) and continuous seismic profile from west to east in the Somali Basin.

B

F.A.
MGALS
+100
0
-100
200
GAMMAS
TWO-WAY TRAVEL
TIME (SEC.)
0
5
10
APPROX. 35 KMS

Figure 4.

Line C. Free-air gravity profile, magnetic profile (with regional field removed) and continuous seismic profile from west to east in the Somali Basin.

C

F.A.
MGALS
+100
0
-100
200
GAMMAS
TWO WAY TRAVEL
TIME (SEC.)
0
5
10
APPROX. 35 KMS.

Figure 5.

Line D. Free-air gravity profile, magnetic profile (with regional field removed) and continuous seismic profile from west to east in the Somali Basin.

D

F.A.
MGALS
+100
0
-100
200
GAMMAS
TWO-WAY TRAVEL
TIME (SEC.)
0
5
10
APPROX. 35 KMS.

a similar large peak to the east is present (Lines B, C, D) together with other basement highs. These elevations to the east may form shorter length ridges as suggested by Laughton's (1966) bathymetry and Matthews (1966) discussion although the line to line morphologic similarity of the observed topographic features here is not striking. These basement ridges display true slopes of up to approximately 8° similar to other fracture zones (Menard and Chase, 1970). The free-air gravity is observed to change from slightly negative to slightly positive on every crossing from west to east (figures 2-5). In lines B, C, and D the two major ridges show a slight reduction of associated magnetic signal amplitude while the area in between shows an increase.

The sediment sequence in lines A-D is recorded as a series of closely spaced acoustic reflectors which in some lines (western sectors of A, B, and D) is underlain by a transparent section. The thickness of sediments overlying basement varies from over 2 seconds of two-way travel time to the west to sediment-free elevated portions of the ridge, to 0.5 seconds or less sediment cover in the eastern sectors of lines A and B. Acoustic reflectors are generally assumed to represent variability in sediment properties and the large horizontal

extent of the reflecting surfaces should then indicate a sedimentation process resulting in similar properties is present over an area as extensive as the reflector itself. Almost all the reflectors in lines B, C, and D are flat lying and generally parallel although they are truncated by the ridge. To the west of the main peak in line A some reflectors lie conformably over the basement structure while others are flat lying. Depth to sediment surface is similar throughout lines C and D with the exception of a small elevated pond in line D. However, line A shows 3 areas of sediments to the east of the ridge whose sediment-water surface is nearer sea level to the east than the corresponding surface to the west of the ridge. Similarly line B shows two elevated sediment ponds.

The level of the sediment-water interface together with the morphology of the reflecting surfaces may be used to develop some qualitative arguments concerning the history of the area. With much less detailed seismic profiling coverage of the area Ewing et al. (1969) proposed that since the reflectors in the Somali Basin appeared similar to those in the Indus Cone, they must have been deposited by turbidites. Neither a reasonable source area nor geologic evidence for the proposed turbidites

has been identified to the north or west of Chain Ridge. Examination of lines A-D shows extensive pockets of sediments between Chain Ridge and the Carlsberg Ridge. The sediment-water interface to the east can be closer to sea level than that to the west (lines A,B). In other cases (lines C and D) the sediment-water interface is at the same level on both sides. Line D also shows a prominent elevated sediment pond in the ridge area. Thus, the favored explanation from these observations may be predominantly pelagic sedimentation. However, turbidite movement along strike or from the east and west of the ridge might result in the same pattern. Uplift may be indicated but not required by sediment ponding in the central portion of the ridge (line D).

In addition to analysis of the shape and level of the upper surface of sediment the lower surface is also important. To the west of the major ridge on line A, the strong basement reflector dips under two parallel reflectors in the sediment sequence. The lowermost becomes the deepest observed reflector in the western basin and the absolute depth to basement remains uncertain although it is clearly greater than the deepest observed reflectors. Thus, in the western basin only a minimum depth for basement may be specified.

Chain Ridge 2°N Profiles

Basement morphology in lines E and F (figures 6, 7) shows an area of major basement elevation of about 35 kms in width. In line E two major peaks to the west are bordered by other smaller peaks to the east. To the south in line F the total width of the fracture zone is somewhat less. Total elevation of basement over the surrounding sediment surface in this area is only approximately 300 m whereas in the 9°N sections it was 2000 m. Although the basement structure here is similar to the sections further north the expression of all ridge features is reduced and no associated magnetic variation across the ridge is apparent.

The sedimentary sequence is thicker to the west, in excess of 2 seconds, and thin (0.5 sec) to the east where it displays a more prominent transparent zone (figures 6, 7). The sea floor is at a similar depth on both sides of the ridge. At 2°N the ridge is characterized by subdued, but similar, features to those farther north.

Figure 6.

Line E. Magnetic profile (with regional field removed) and continuous seismic profile from west to east in the Somali Basin.

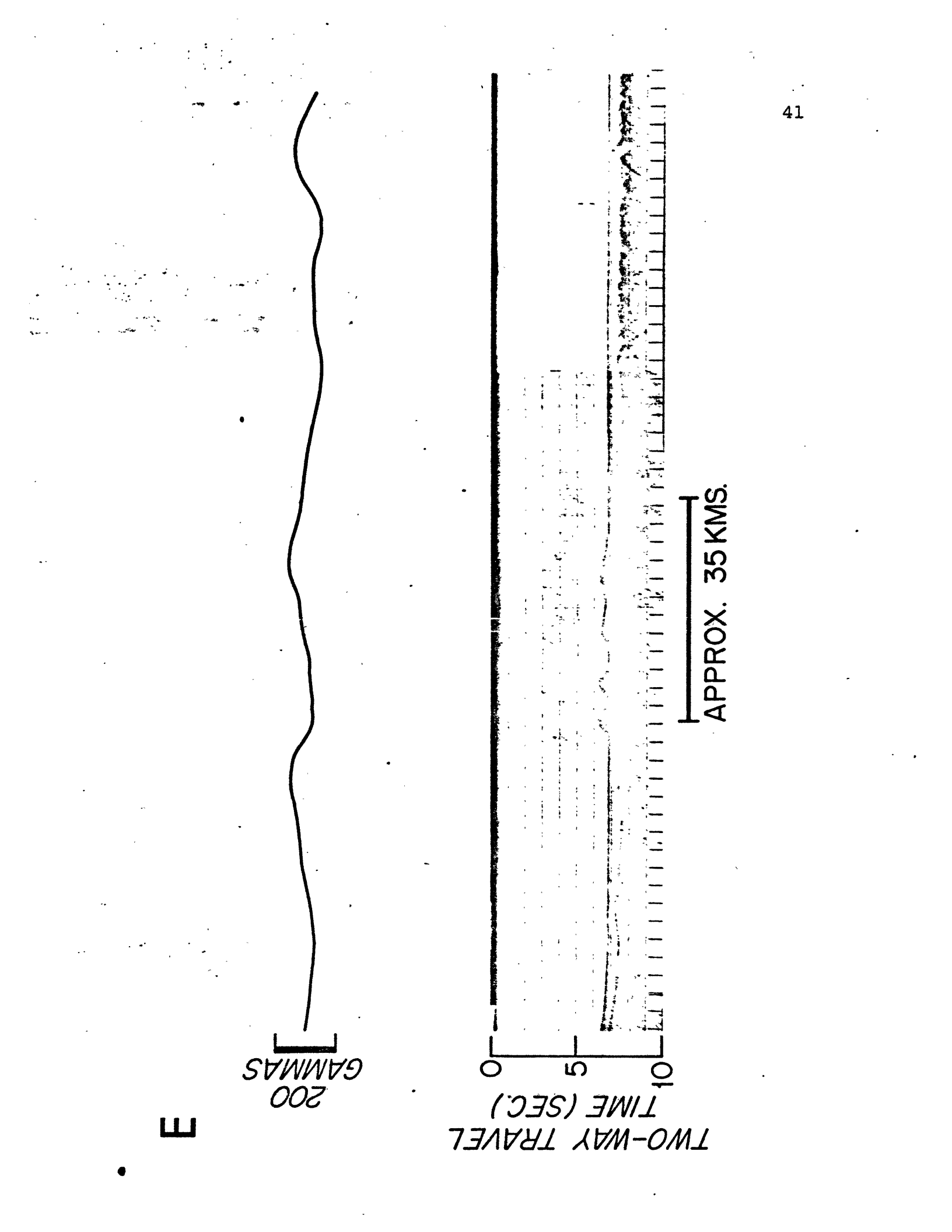
E
200
GAMMAS
TWO-WAY TRAVEL
TIME (SEC.)
0
5
10
APPROX. 35 KMS.

Figure 7.

Line F. Magnetic profile (with regional field removed) and continuous seismic profile from west to east in the Somali Basin.

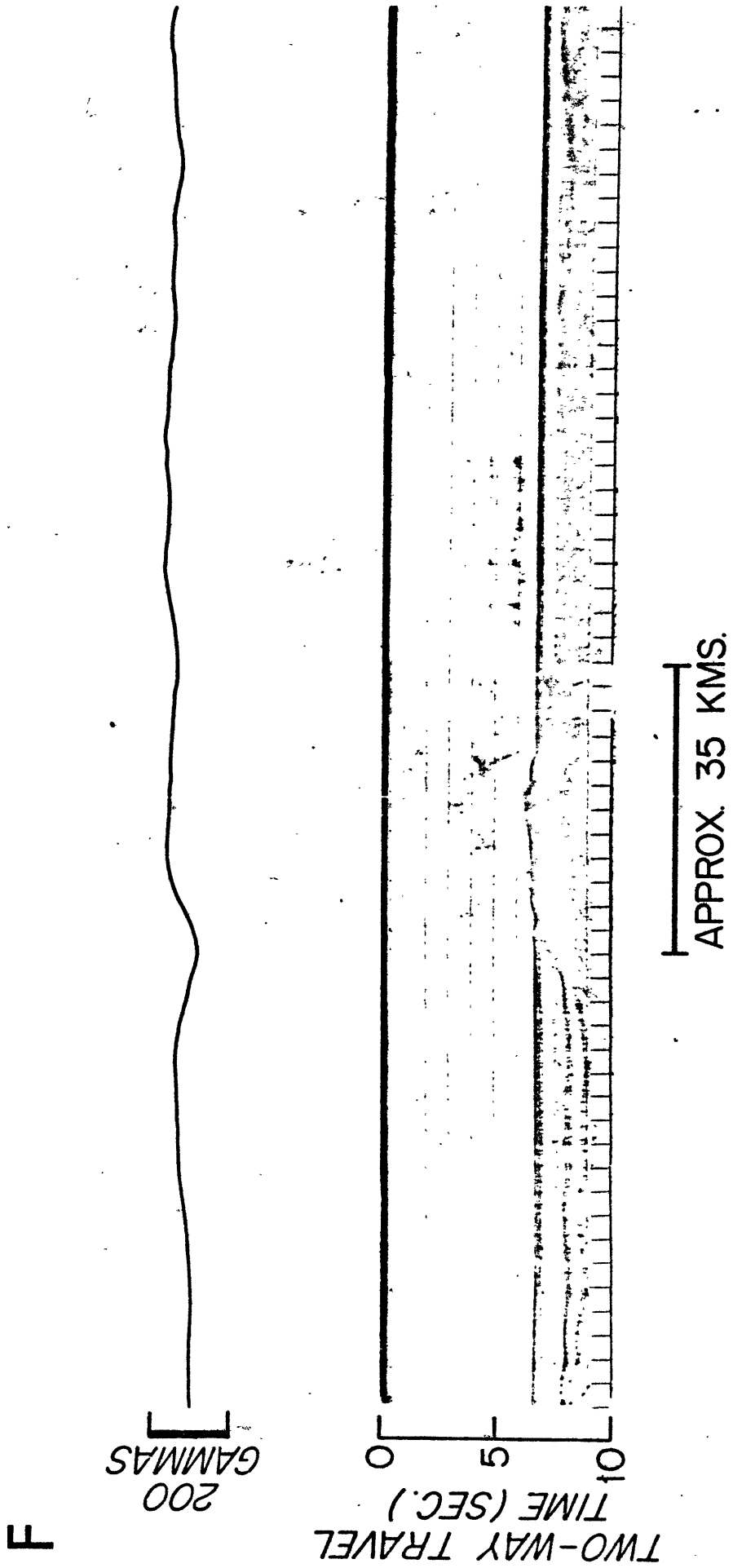

F

Chain Ridge Buried Scarp 3.5°S and 7.5°S

Line G (figure 8) at 3.5°S and line H (figure 9) at 7.5°S in addition to other work in the area (Francis et al., 1966; Schlich et al., 1972) demonstrate a significant change in the depth and in the configuration of basement reflectors in the central Somali Basin. The features are remarkably similar to those described at 2°N and therefore suggest the continuation of the fracture zone southward through this area. A sedimentary sequence with acoustic layering and a gently undulating deepest observed reflector at two seconds or greater (figures 8, 9) terminates at the buried scarp. Beyond the buried scarp, to the east, a sediment sequence of 1 second or less lies above a rough layer 2-type oceanic basement. This change is observed in line G (3.5°S, 48.5°E), in line H (7.5°S, 48.5°E), by Francis et al. (1966) (2.7°S, 47°E; exact location not determined due to station spacing and navigation system), and by Schlich et al. (1972)(3.5°S, 48.5°E) where it is most clearly shown. To the east of the buried scarp the basement reflector outcrops (Schlich et al., 1972, line H) as it does to the north. It must be emphasized that the data presented here indicate that the present fracture zone and therefore past plate boundary is the buried scarp and not the first linear topographic high to the

Figure 8.

Line G. Free-air gravity profile, magnetic profile (with regional field removed) and continuous seismic profile from west to east in the Somali Basin. Arrow to left shows relatively flat lying deepest observed reflector which is presumed to be a sedimentary horizon above basement. Arrow to right (east) shows rough reflector typical of oceanic basement.

G

-20
F.A. MGALS
-40
-60

200 GAMMAS

TWO-WAY TRAVEL TIME (SEC.)
7
8

APPROX. 35 KMS.

45

Figure 9.

Line H. Free-air gravity profile, magnetic profile (with regional field removed) and continuous seismic profile from northeast to southwest in the Somali Basin. Arrow to left of figure indicates deepest observed reflector there which has rough upper surface typical of oceanic basement layer 2. Arrow to right of figure shows relatively flat lying deepest observed reflector which is assumed to be sedimentary indicating far greater depth to basement.

TWO-WAY TRAVEL
TIME (SEC.)
10
5
200
GAMMAS
F.A.
MGALS
-60
0
60

east of it. In line G the free-air gravity anomaly increases to the east of the buried scarp and the magnetic record indicates some possible low amplitude variation in contrast to the smooth zone to the west. However, neither of these clearly demark the structural boundary that is observed by seismic profiling.

CHARACTERISTICS AND EXTENT OF CHAIN RIDGE AND THE BURIED SCARP

The total extent and general characteristics of Chain Ridge may be compiled from data presented here and elsewhere in the literature. The morphology of the oceanic basement that characterizes the fracture zone consists of a distinct change in regional depth to basement across the feature which is obscured by sedimentation throughout its length, and to the north prominent peaks that extend well above the abyssal plains.

The bathymetric expression of the fracture zone is shown in figure 10. In the northern section, lines A-D, often two major peaks,as well as other smaller peaks, rise over 2 kms above the abyssal plain on both sides of the fracture zone. In the more southerly corssings peaks of diminished size rise only a few hundred meters above the surrounding abyssal plain.

The change in depth to regional basement is consistent in seismic profiles across the fracture zone and will be treated in more detail later. This difference exceeds about 2 kms as examination of the seismic profiles shows nearly similar levels for the abyssal plain on either side of the fracture zone but a change in total sediment thickness. In the central Somali Basin near 3.5°S where sediments mask any bathymetric expression of the ridge, the variation in regional depth is most clearly shown by Schlich et al. (1972).

Figure 10.

Bathymetric cross sections of Chain Ridge. In each case the abyssal plain to the west of the ridge is at about 5000 m.

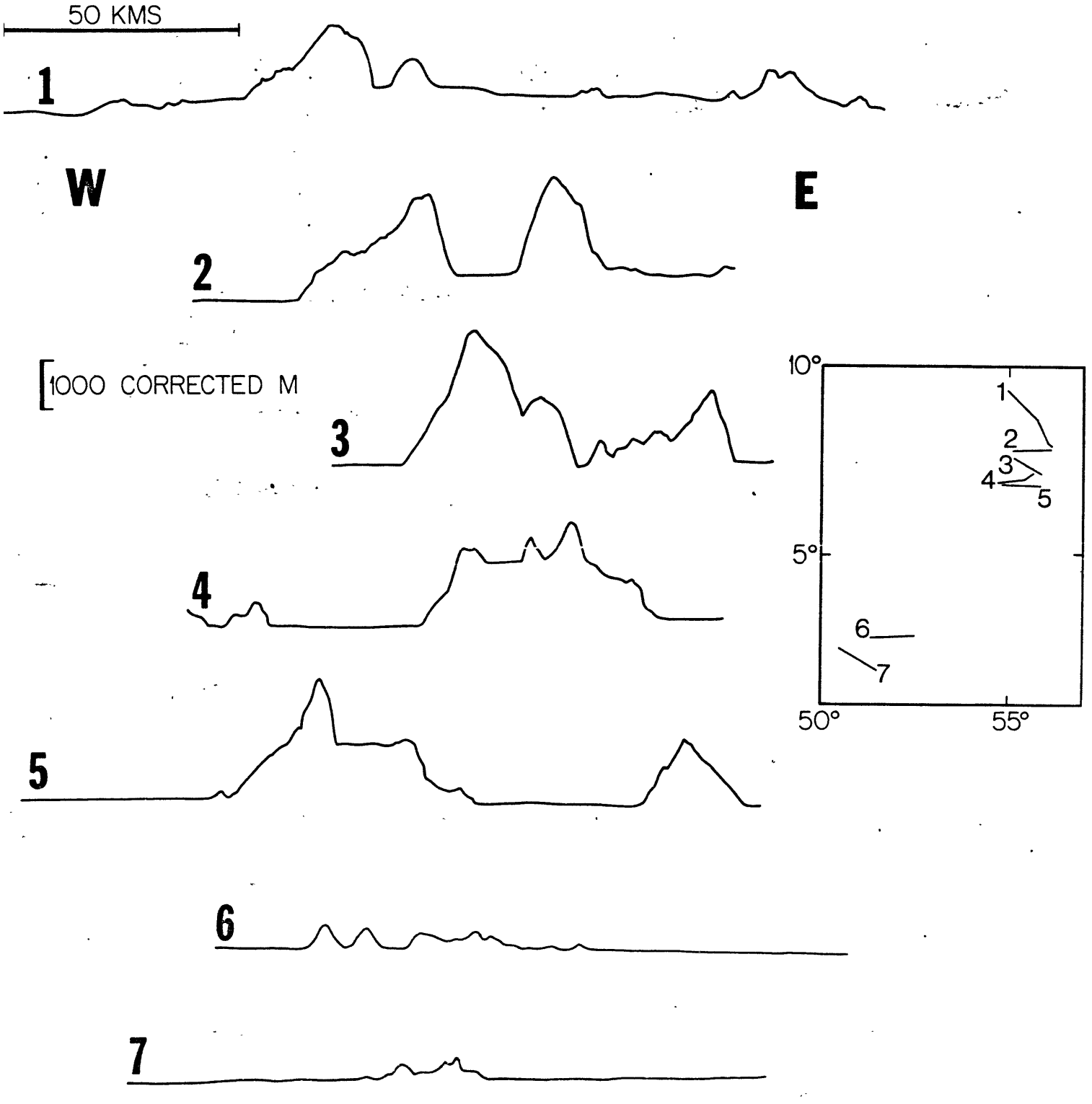
50 KMS
1
W
E
2
1000 CORRECTED M
3
4
5
6
7
10°
5°
50°
55°
1
2
3
4
5
6
7

Analysis of the morphology of Chain Ridge in available bathymetric and seismic data indicates at least two types of deformation may be responsible for the fracture zone. In the northern sections and at its southern topographic extreme the fracture zone often has two major peaks separated by a trough which could be due to shear between two plates. At 5.5°N (Bunce et al., 1967, figure 3, p. 2549) block faulting is indicated. Line D slightly north of there and data from 3.5°S (Schlich et al., 1972, plate 1) indicate block faulting may be important. The multiple ridge morphology is characteristic of other fracture zones (Menard and Chase, 1970) as is the scarp shown by Schlich et al. (1972).

Variation in free-air gravity and in magnetics across the structure is of little help in mapping its extent with the present coverage. Free-air gravity follows topography in the elevated portions of the ridge (lines A-D) but is insensitive to the variation in basement depth across the feature in the southern portions of the basin (line G or Talwani and Kahale, in press). Available magnetic data do not indicate that the fracture follows an identifiable pattern as has been proposed for these features elsewhere (Schouten, 1974).

The extent of the fracture zone may be examined both by its own characteristic features and by those of the sea floor it bounds. The Chain Ridge portion of Owen Fracture Zone extends as a topographic feature from the Carlsberg Ridge to about 2°N in the Somali Basin (figure 11). A buried scarp separates two different sediment thicknesses and types of sea floor south of that point; the scarp continues to 7.5°S. At 3.5°S these data together with some of Schlich et al. (1972) and Francis et al. (1966) demonstrate the same consistent change in sediment thickness. Chain Ridge with its buried scarp trends semi-parallel to the coastline and approximately 380 to 860 kms offshore along the entire mapped length of the ridge (figure 11).

While the extent of the fracture zone may be extrapolated to 7.5°S its relationship with sea floor and continental structures at the northern tip of Madagascar (12°S) cannot be defined on the basis of this data alone. An alignment with one of the roughly north-south trending structures on Madagascar appears likely. The eastern boundary fault of Madagascar (Pepper and Everhart, 1962) trends north-northeast on a line parallel to but east of the fracture zone; this precludes a simple relationship between the two. Fisher et al. (1968) found

Figure 11.

Morphology and extent of fracture zone. The single bold line to the south separates areas of regional basement depth variation only. Triangles indicate bathymetric extent of ridge. Line to north is presumed trend of fracture zone through ridge area.

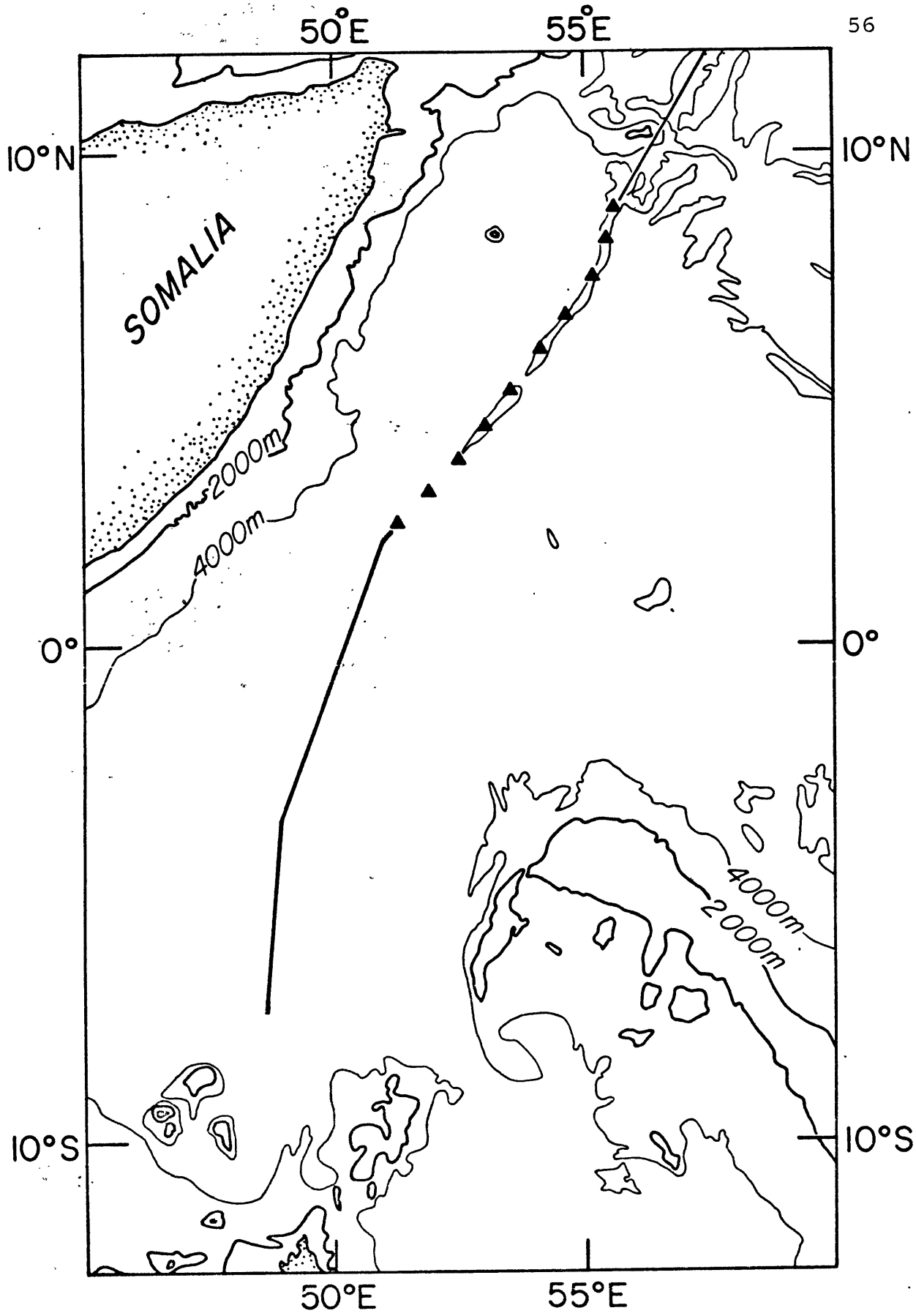
50°E
55°E
10°N
0°
10°S
SOMALIA
2000m
4000m
4000m
2000m
50°E
55°E

this eastern boundary fault coincident with other sea floor structures along its strike to the north. Various western boundary faults on Madagascar have been identified (Gregory, 1920; Pepper and Everhart, 1962) and could also be related to the extension of Chain Ridge. An extension of the short northeastward facing portion of coast at the northern tip of Madagascar if extended would intersect the fracture zone at 7.5°S. Each of these possibilities has significantly different implications for the tectonic features and evolution of the area and will be treated in more detail later.

ELEVATION-AGE DETERMINATIONS FOR BASINS BORDERING CHAIN RIDGE 2°N - 8°N

An indication of age may be derived by considering crustal elevation (Sclater, Anderson, and Bell, 1971). By compiling the seismic profiles already discussed with others from the area (CHAIN 43, VEMA 19, and GLOMAR CHALLENGER, Leg 24) the two-way travel time to oceanic basement may be contoured for an area in the Somali Basin (figure 12). Basement is assumed to be typical oceanic layer 2 material, basalt similar to that dredged from Chain Ridge, and is traced on the profiles from the ridge area outcrop where it was sampled (Bunce et al., 1967) outward into the basins to either side. To the west of the ridge the deepest observed reflector is not continuous with the ridge reflector, and exhibits a smoother character as well; so it is assumed to overlie oceanic basement which in that area remains undefined. A second map of the area (figure 13) shows the two-way travel time from the sediment surface to the deepest observed reflector. From these two sets of information and using assumed compressional wave velocities for water (1.45 km/sec) and unconsolidated sediment (2 km/sec) (Ewing et al., 1969) the distance from sea level to oceanic basement may be computed on both sides of Chain Ridge from visually determined average

Figure 12.

Two-way travel time in seconds to oceanic basement. The basement reflector has been traced from where it outcrops on Chain Ridge into the basins on either side. Where the reflector outcrops on Chain Ridge it has been sampled, identified as basalt, and dated as approximately 90 m.y. (Bunce et al., 1967). To the west of the ridge oceanic basement is greater than 8 seconds but not specifically defined as it is below the deepest observed reflector.

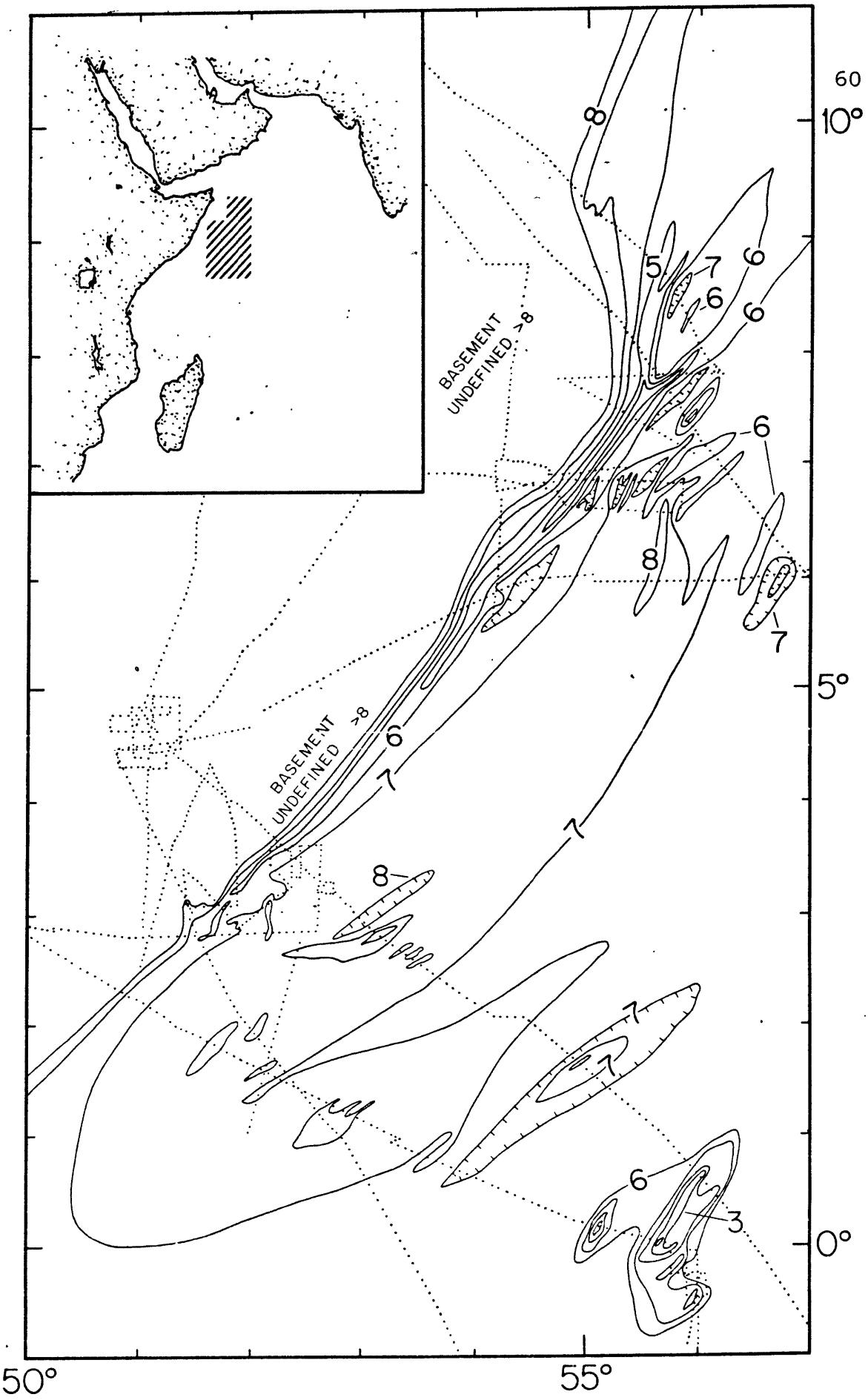
60
10°
5°
0°
50°
55°
BASEMENT UNDEFINED >8
BASEMENT UNDEFINED >8
8
5
7
6
6
6
6
8
7
6
7
7
8
7
7
6
3

Figure 13.

Two-way travel time in seconds from the sediment surface to the deepest observed reflector. In the ridge area and to the east this chart is representative of total sediment thickness. To the west of the ridge it represents sediment thickness above the deepest observed reflector which is assumed to be a sedimentary horizon.

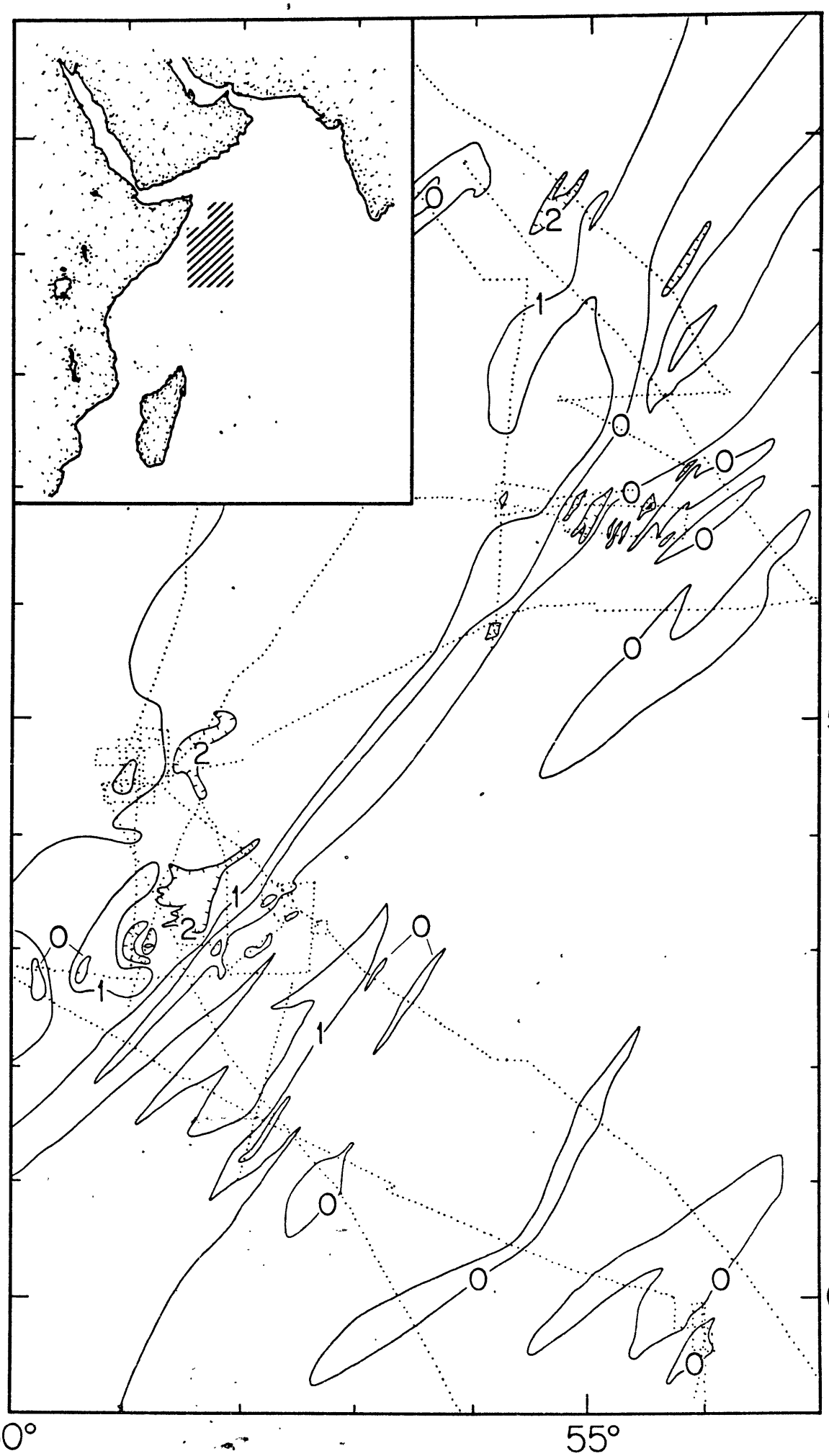
10°
5°
0°
50°
55°
0
1
2

sediment thickness values as follows:

$$\text{East} \quad \frac{6.7 \text{ sec}}{2} \quad 1.45 \text{ km/sec} + \frac{0.3 \text{ sec}}{2} \quad 2 \text{ km/sec} = 5.2 \text{ km}$$

$$\text{West} \quad \frac{7.0 \text{ sec}}{2} \quad 1.45 \text{ km/sec} + \frac{2.0 \text{ sec}}{2} \quad 2 \text{ km/sec} = 7.1 \text{ km}$$

These sea floor elevations may be corrected by considering the effects of sediment loading (Sclater, Anderson and Bell, 1971; Hyndman, 1973). If an isostatic model which assumes a negligible density contrast at the base of the lithosphere is used, the equivalent depth from sediment loading is:

$$d_e = d_w + \frac{\rho_m - \rho_s}{\rho_m - \rho_w} \, d_s$$

where d_e = equivalent depth

d_w = water depth

$\rho_m = 3.3 \text{ gm/cm}^3$

$\rho_s = 2.4 \text{ gm/cm}^3$

$\rho_w = 1.0 \text{ gm/cm}^3$

d_s = sediment thickness

then to the west of the ridge:

$$d_e = 5 \text{ km} + \frac{3.3 \text{ gm/cm}^3 - 2.4 \text{ gm/cm}^3}{3.3 \text{ gm/cm}^3 - 1.0 \text{ gm/cm}^3} 2 \text{ km} = 5.8 \text{ km}$$

whereas to the east:

$$d_e = 4.8 \text{ km} + \frac{3.3 \text{ gm/cm}^3 - 2.4 \text{ gm/cm}^3}{3.3 \text{ gm/cm}^3 - 1.0 \text{ gm/cm}^3} 0.5 \text{ km} = 5.0 \text{ km}$$

To translate these elevations into ages and determine the accuracy of the method several data sets must be compared as in figure 14. The axis of present day spreading forms the reference point for theoretical and observed bathymetric profiles, the elevation determined ages, and the magnetic anomalies which are all plotted in kms from the crest. Comparison of observed bathymetry (thin line) with continuous spreading theoretical bathymetry (bold line) and theoretical bathymetry incorporating a pause in spreading (dashed line) from McKenzie and Sclater (1971) shows that an uncertainty of 5 m.y. on the theoretical bathymetry time scale is not uncommon and that the elevation on this profile is not particularly sensitive to the proposed pause in spreading. The divergence between observed and theoretical bathymetry may be even greater beyond 500 kms due to sedimentation. For these reasons the theoretical curve (bold line) is

Figure 14.

Sea floor age estimate from basement elevation. Theoretical Indian Ocean depth curve (bold line), theoretical curve with pause in spreading (dashed line) and observed bathymetry (thin line located as shown in inset) are plotted versus distance from the spreading axis (Sclater, Anderson and Bell, 1971; McKenzie and Sclater, 1971). For reference age as determined by the theoretical curve and accompanying magnetic anomalies (Heirtzler et al., 1968) are plotted below.

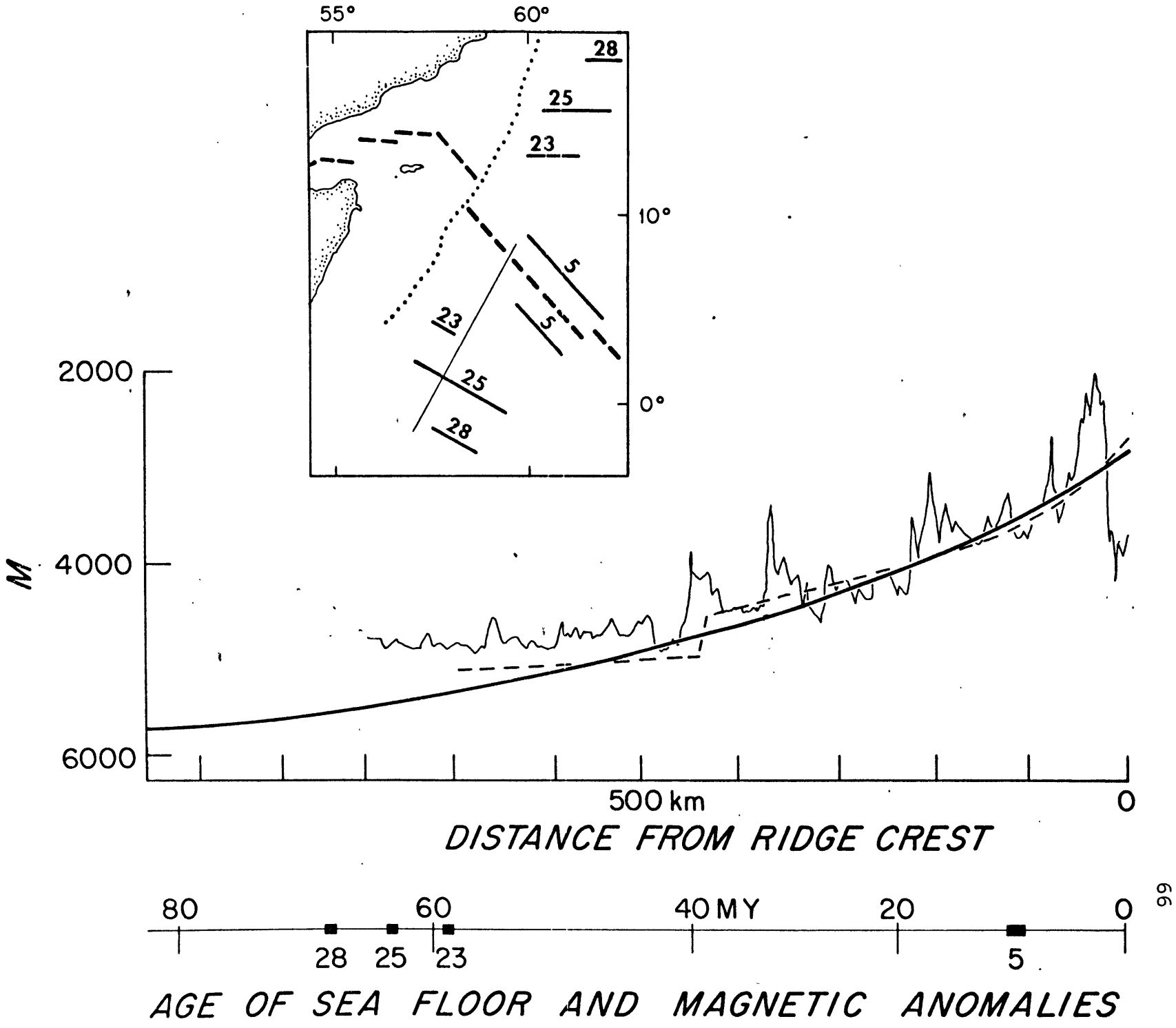
55°
60°
28
25
23
10°
5
5
23
25
28
0°
2000
4000
6000
M
500 km
0
DISTANCE FROM RIDGE CREST
80
60
40 MY
20
0
28
25
23
5
AGE OF SEA FLOOR AND MAGNETIC ANOMALIES

used to estimate the ages of the contrasting sides of the fracture zone assuming the basins on either side are underlain by normal oceanic basement.

The age of the sea floor may then be inferred by plotting the depth to basement from contrasting sides of the fracture zone on the theoretical curve of depth versus age for the Indian Ocean (figure 14) derived by Sclater, Anderson, and Bell (1971). The average corrected oceanic basement depth to the east of Chain Ridge between 2° and 8°N (figure 14) yields an Eocene age (approximately 50 m.y.). To the west of Chain Ridge the average corrected depth of oceanic basement is at least 6 kms, which by this interpretation gives an age in excess of 80 m.y. (upper Cretaceous) if this sector of the basin has been formed by the normal spreading process. The exact age may not be determined by this method in this area, however, because of the bathymetry versus age relation used here is insensitive beyond 80 m.y. Thus, the sea floor could be much older, making the age discontinuity across the ridge even greater.

The age-elevation calculations presented are corrected for the great thickness of sediments to the west of the ridge

and presume that the basin there is underlain by normal oceanic layer 2 basement with a velocity of approximately 5 km/sec as has been observed elsewhere in the oceans (Ludwig et al., 1970). This assumption is supported by the work of Francis et al. (1966) who report such a velocity in some of their western Somali Basin lines.

Menard (1967) in considering basins of abyssal depths but containing extensive thicknesses of sediment established some criteria for their recognition on the basis of refraction data and speculated they could be found in the geologic record. The Gulf of Mexico (Menard, 1967) is considered to be the type example of the advanced stage of development for a small basin surrounded by continent (figure 15). The western Somali Basin may well qualify as having been a small ocean basin underlain by transitional crust as is indicated by a comparison of refraction results there (Francis et al., 1966) with the Gulf of Mexico. In each case 2-6 kms of sediments (velocity 1.8-3.8 km/sec) overlie approximately 3 kms of layer 2 material (velocity around 5 km/sec) with layer 3 and upper mantle below.

Figure 15.

Comparison of crustal sections in the Somali Basin (Francis et al., 1966) 2°55'S, 47°02'E and Gulf of Mexico (Menard, 1967). Other Somali Basin sections nearer Africa show up to 4 kms of sediments (Francis et al., 1966).

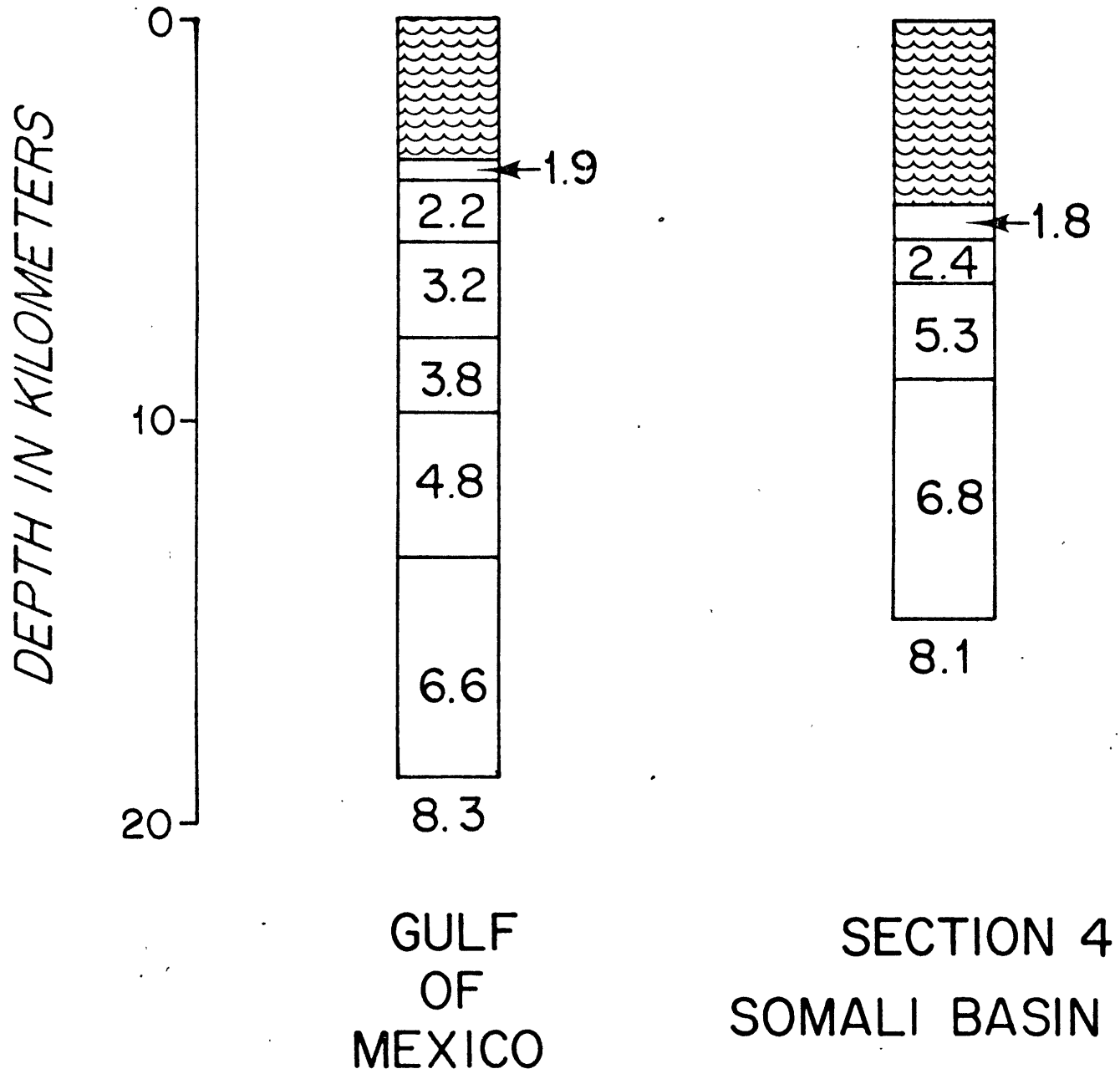
DEPTH IN KILOMETERS
0
10
20
1.9
2.2
3.2
3.8
4.8
6.6
8.3
1.8
2.4
5.3
6.8
8.1
GULF OF MEXICO
SECTION 4
SOMALI BASIN

DISCUSSION

Summary of Somali Basin Sea Floor Ages

The existence of an age difference across Chain Ridge and its southern extension may be examined in several ways (figure 16). The most direct evidence comes from sampling the sediment sequence on either side of the structure. This has been done to the north (Sites 234 and 235) but the results are inconclusive due to the shallowness of the penetration to the west (Fisher and Bunce et al., Site 235, 1972). However, the data presented here indicate the lineation extends into the south central Somali Basin where two additional Deep Sea Drilling Project sites (240, 241) are located (Simpson and Schlich et al., 1972). If the fracture zone bounds sea floor of different origins then this should be evident over its southern section as well as in the north where it is a topographic structure. In this southern section the basal sediments at the eastern site, 240, were early Eocene on top of basalt (Simpson, Schlich et al., 1972). At site 241 on the East African side of the fracture zone the drilling was terminated considerably above basement in middle Eocene to middle Cretaceous lithified brown mudstone shale and chalk (Simpson, Schlich et al., 1972). Thus, site

Figure 16.

Somali Basin seafloor ages. Ages in brackets are determined by elevation (where they border Chain Ridge) and by the magnetic anomaly sequence (McKenzie and Sclater, 1971). Deep Sea Drilling Sites in the area are shown by large solid dots (Fisher and Bunce et al., 1972; Simpson and Schlich et al., 1972). Ages in parentheses indicate a sediment age above basement while other ages are at or very near basement. The small solid dot is the age at the base of a piston core (Pimm et al., 1972). Ages with wavy underline are potassium-argon dates on dredged basalts (Bunce et al., 1967; Fisher et al., 1968). Continental areas are dated by Baker and Miller, 1963; and Pepper and Everhart, 1963. Island dates are by Hajash and Armstrong, 1972.

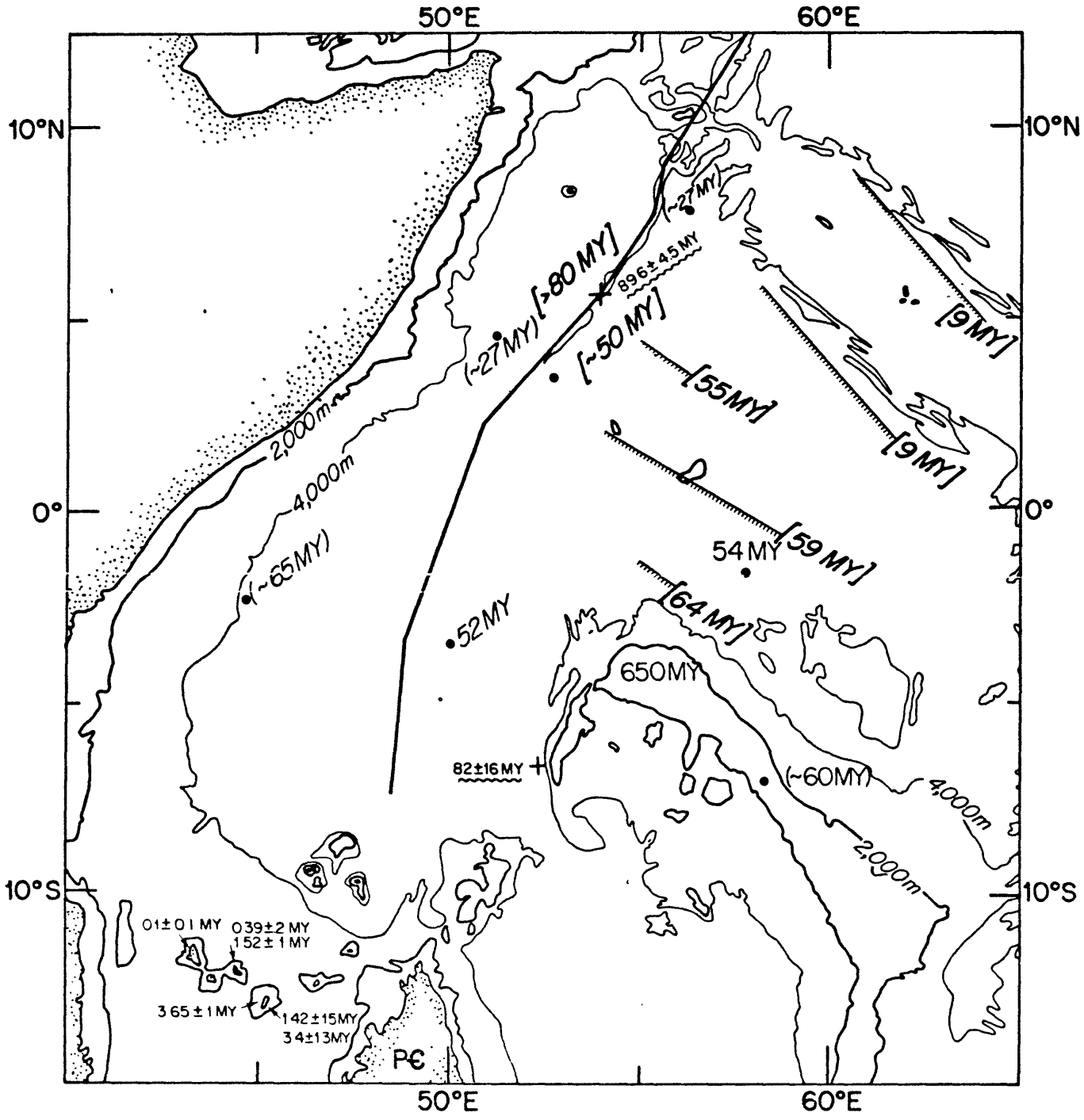
50°E
60°E
10°N
0°
10°S
(~27MY)
[>80 MY]
896±45MY
[~50 MY]
[55MY]
[9MY]
2,000m
4,000m
(~65MY)
54 MY
[59 MY]
52MY
[64 MY]
650MY
82±16MY
(~60MY)
01±01 MY
039±2 MY
152±1 MY
365±1 MY
142±15MY
34±13MY
Pε

241, according to Simpson and Schlich, et al. (1972), indicates a minimum age of approximately 100 m.y. to the west of the lineation while to the east site 240 shows basal sediments of Eocene age which together indicate an age difference of at least 40 m.y. across the lineation.

Other age determinations in the area (figure 16) tend to confirm the interpretation that the ridge and its buried extension separate sea floor of different ages. To the north age elevation calculations indicate that basement age to the west of the fracture zone is in excess of 80 m.y., while that to the east is around 50 m.y. which is confirmed by anomalies 23 and 25 as shown by McKenzie and Sclater (1971). However, in the same area Bunce et al. (1967) give a potassium argon date for basalt dredged from the ridge crest of 89.6 ± 4.5 m.y. but at such great depth in the sea the accuracy of the dating method (Wasserburg and Hayden, 1955) may be in doubt.

In the southern Somali Basin those areas that have been dated show a variety of ages consistent with more than one deformation event. The continental areas, the Seychelles and Madagascar, have Cambrian or older materials in some areas (Baker and Miller, 1963; Pepper and Everhart, 1963). The Comores are predominantly Pliocene and Pleistocene (Hajash and

Armstrong, 1972). To the east potassium-argon dating on basalt from the wall of the Amirante Trench indicates an age of 82 ± 16 m.y. (Fisher et al., 1968).

Fracture Zone Constraints on Plate Motion

Due to the lack of readily identifiable magnetic anomaly sequences in the Somali Basin, its structural history has eluded previous analysis. However, constraints on plate motion and therefore the evolution of the area may be established by the trend and morphology of the lineament and their relationship to the geometric properties of plate tectonics.

Bathymetric (Matthews, 1966), seismic (Bunce, et al., 1967), and data presented here on the trend of the fracture zone have been compiled in figure 11. If the location and extent of the fracture zone are related to the opening of the Indian Ocean, then the termination of the fracture zone should indicate those portions of crust that were previously adjacent, and if spreading has been uniform and symmetric then those portions of crust should be equidistant from the present spreading center. In addition for these constraints to hold, the initial fracture zone terminations must be preserved. While it cannot be demonstrated that all these criteria are met on the basis of available

data, it is instructive to compare the length of fracture zone branches to determine if they are compatible with these concepts and the main features of the basin. The elevated portion of Chain Ridge extends about 1000 kms southwestward from the Carlsberg. With the buried scarp included, the total extrapolated distance to 7.5°S is more than 2310 kms (figure 17). If it continues to the northern tip of Madagascar its total length will be in excess of 2700 kms and if either boundary fault for Madagascar was part of the same feature the total length would be far greater. The northeastward trending branch of Owen Fracture Zone extends as a topographic feature for 1440 kms or on the basis of magnetic data (McKenzie and Sclater, 1971) 1675 kms where it joins what has been tentatively identified as a spreading center. An extension of Owen Fracture Zone has been proposed along a fault that has been mapped on land to the Hindu Kush (Matthews, 1966) which would add approximately 800 kms to the total length of the fracture zone. While the exact structural relationships at the distant ends of the fracture zone remain to be determined there is a significant difference between the length of the two branches. This discrepancy in branch lengths indicates a simple sea floor spreading model does not incorporate all the

Figure 17.

Fracture zone branch lengths. Location of the fracture zone determined by this paper and Laughton (1966) bathymetry with the trend drawn along peaks. Circle with cross indicates previously mapped maximum southern topographic extent. Fault trends simplified from Nowroozi (1971) at the north end and Pepper and Everhart (1963) in Madagascar.

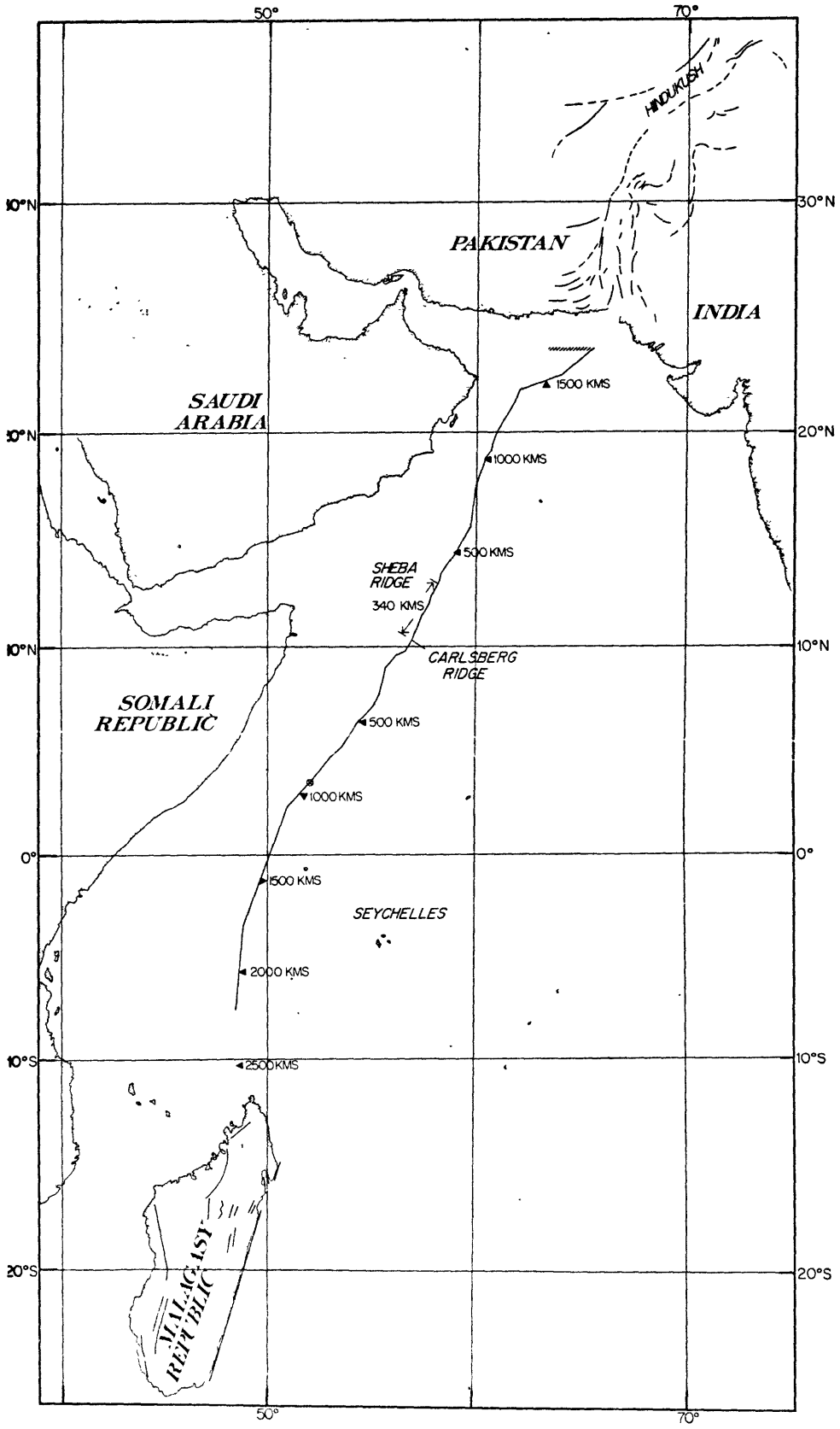
50°
70°
HINDUKUSH
30°N
20°N
10°N
0°
10°S
20°S
PAKISTAN
INDIA
SAUDI ARABIA
1500 KMS
1000 KMS
500 KMS
SHEBA RIDGE
340 KMS
CARLSBERG RIDGE
SOMALI REPUBLIC
500 KMS
1000 KMS
1500 KMS
SEYCHELLES
2000 KMS
2500 KMS
MALAGASY REPUBLIC

observations.

Fracture zone models that incorporate various observed morphologies provide some additional information for this area. In the Menard and Chase (1970) terminology Chain Ridge is a combination scarp and great ridge in the northern sector while in the southern sector it is primarily a buried scarp. In all cases this scarp faces toward Africa. Le Pichon and Hayes (1971) assume that the main elevation of a fracture zone is due to the shear along plate boundaries. In addition Le Pichon and Hayes (1971) were able to assign some variation in morphology to the shear between crust with different properties and origins. However, as the northern sector of Chain Ridge is the most highly elevated their criteria when directly applied here would imply that it is a high standing ridge caused by continent-continent shear. While microcontinents may exist in the western Somali Basin it is unlikely that the conditions for the Le Pichon and Hayes (1971) model are met. The elevation of the ridge is more likely due to variations in the nature of the shearing process along the length of the fracture zone rather than the variation in the properties of the materials on either side of it.

Sea Floor Age and Fracture Zone Trend Constraints on Proposed Continental Reconstructions

Using the information previously developed on sea floor and fracture zone trends the proposed continental reconstructions for the area may be examined. The reconstruction consistent with the new data presented here will indicate possible pre-Cenozoic evolution patterns for the basin.

In figure 18 the earliest attempts to reconstruct Gondwana-land (Wegner, 1929; DuToit, 1937) relied on matching similar geologic histories for the different land masses. The Wegener upper Carboniferous reconstruction (270-320 m.y.) does not show Madagascar but indicates a small seaway along the east coast of Africa. Major ocean intrusion in the area occurred during the Eocene due to the northwestward motion of India (Wegener, 1929). DuToit (1937) shows the south end of Madagascar opposite the African Coast at 10°S and a small sea in the western Somali Basin throughout the Mesozoic. Heirtzler and Burroughs (1971) on the basis of geophysical data from the Mozambique Channel also favor a southward migration for Madagascar. These reconstructions imply a pre-Cenozoic seaway in the western Somali Basin with the southward migration of Madagascar. Constraints of the new data favor the pre-Cenozoic Western Somali Basin seaway but limit

Figure 18.

Proposed Indian Ocean Reconstructions.

A. Wegener (1929)
B. DuToit (1937)
C. Tarling (1971)
D. Dietz and Holden (1970)
E. Smith and Hallam (1970)

A

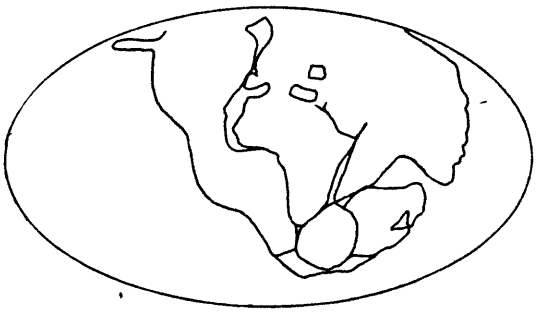

B

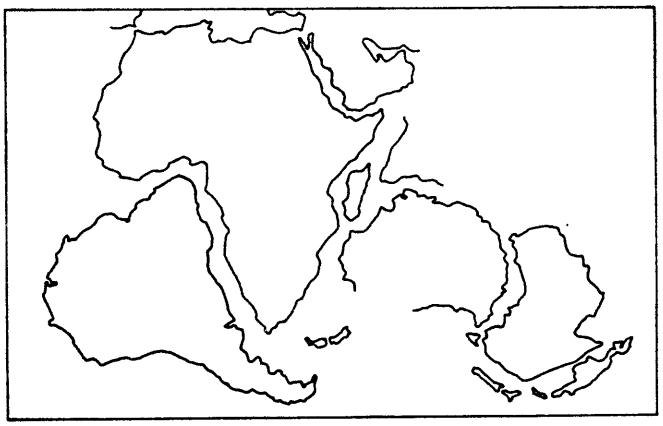

C

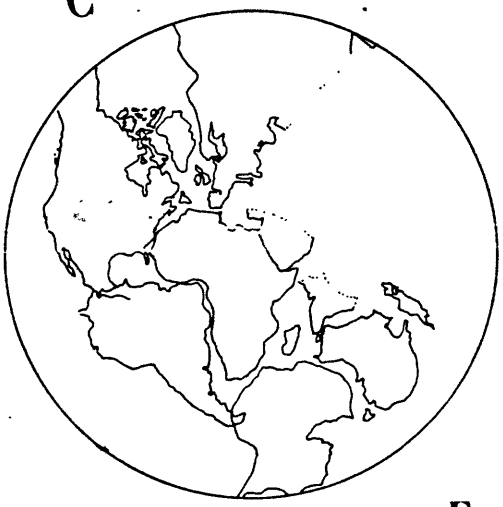

D

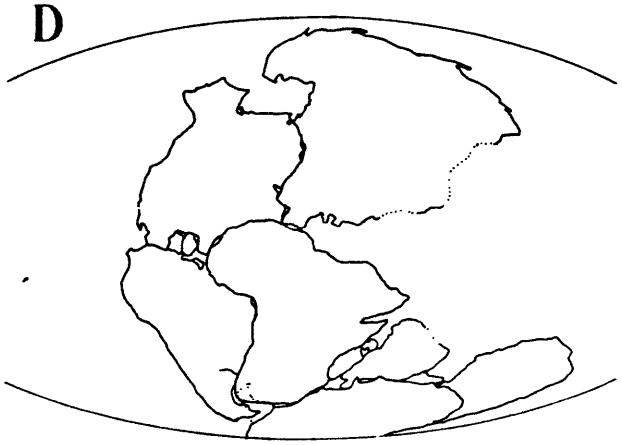

E

the southward motion of Madagascar.

This constraint of at least Mesozoic sea floor ages for the Western Somali Basin is supported by the Tarling (1971) work based on paleomagnetic polar wandering data and geological information. Sea floor in the area could be 250-300 m.y. old (Tarling, 1971). Dietz and Holden (1970) favor initial continental separation at 180 m.y. with an active spreading center paralleling the coast. The extent of the fracture zone and its relation to pre-Cenozoic crust precludes the Dietz and Holden (1970) mechanism for Mesozoic sea floor in the area but supports the Tarling (1971) concept of a "minor proto-Indian Ocean" for the area.

The Smith and Hallam (1970) computer fit for the 500 m contour indicates the present day Western Somali Basin corresponded with the location of Madagascar and India until the break-up of Gondwanaland during the upper Cretaceous. Sowerbutts (1972) has used the Smith and Hallam reconstruction to relate Cretaceous development in the East African rifts with the south-eastward movement of continents out of the present day Somali Basin area. Sea floor age and fracture zone trend information presented earlier exclude this evolutionary history because the

sea floor in the Western Somali Basin is older than permitted by this interpretation and because the proposed Sowerbutts (1972) rifting direction would cross the fracture zone trend.

In summary, the Wegener (1929) and DuToit (1937) data may not contradict the new data presented here but the Dietz and Holden (1970) and Smith and Hallam (1970) reconstructions clearly do and are not acceptable. Thus, the Tarling (1971) Gondwanaland configuration fits best with this data as it permits the trend and age difference associated with the fracture zone to be conserved.

MODEL FOR SOMALI BASIN EVOLUTION

New data presented here and results previously presented in the literature form three methods for constraining plate motion as treated in the discussion. These constraints are the basis of a Somali Basin evolution model. The buried extension of Chain Ridge borders Mesozoic sea floor to the west. The present day Carlsberg Ridge is terminated at its north end in the Owen Fracture Zone. Therefore, it is likely that the Early Cenozoic Carlsberg Ridge as shown by Fisher et al., 1971 terminated in a zone of shearing presently marked by the buried extension of Chain Ridge. The trend of the fracture zone may therefore be used to locate the continents that border its terminations from the time of Gondwanaland to the present.

Figure 19A represents the proposed initiation of spreading in the eastern Somali Basin area. Continent locations are controlled by the fracture zone location as well as the Tarling (1971) reconstruction. The western Somali Basin which was at this time a branch of the Tethys is underlain by material with an oceanic basement velocity (Francis et al., 1966; Schlich et al., 1972) and, therefore, may represent much older sea floor related to spreading that resulted in the formation of the Tethys.

Figure 19.

Schematic evolution of the Somali Basin. Africa is assumed fixed while India's hypothetical position is controlled only by the trend of a single fracture zone.

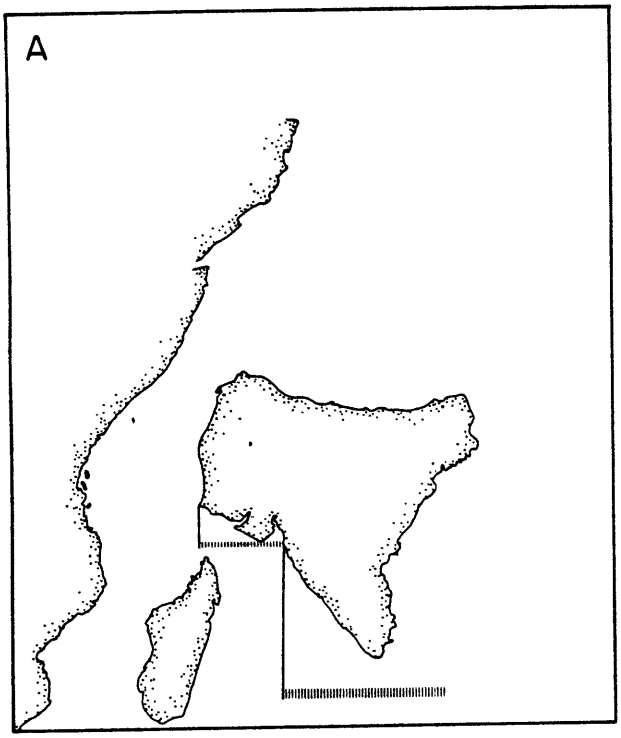
A

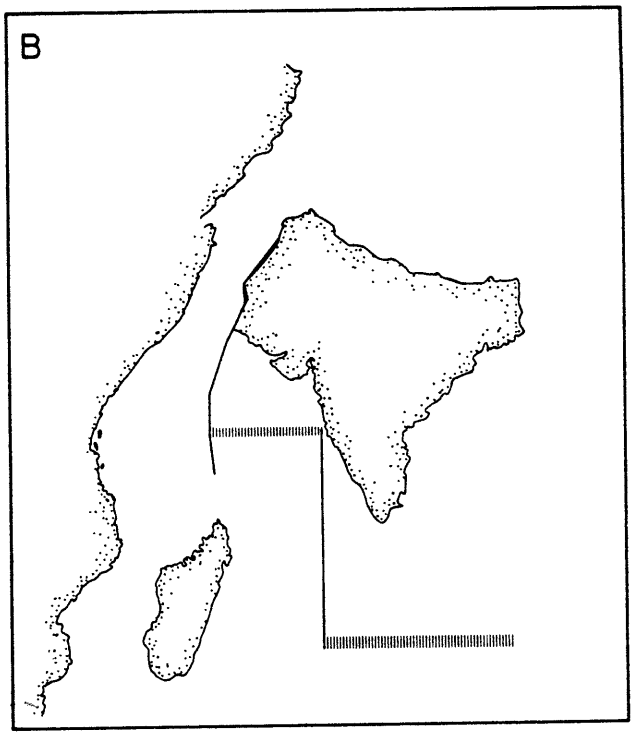
B

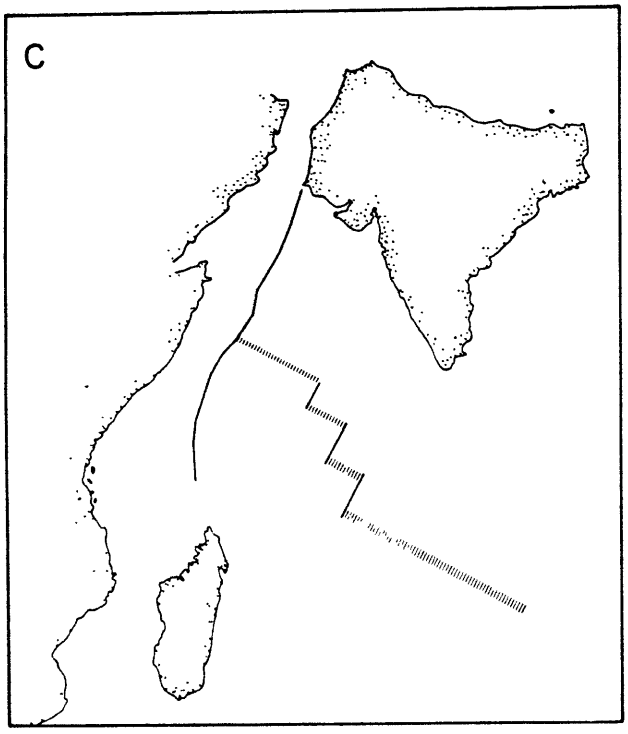
C

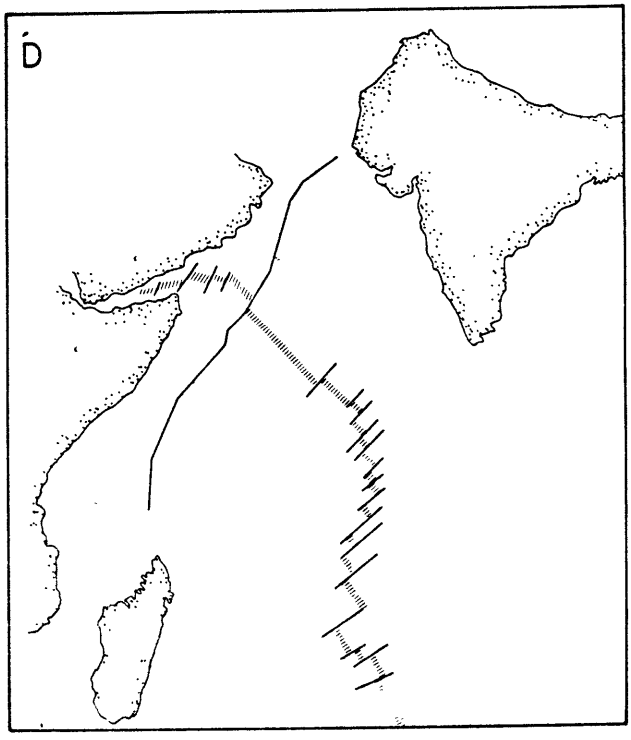
D

The Western Somali Basin could have been a small area of the Tethys underlain by oceanic crust, surrounded by continents, rapidly sedimenting, and subsiding. Under those conditions it would have been transitional ocean to continent crust as described by Menard (1967).

The maximum mapped southern extent of the fracture zone (7.5°S) is south of the Seychelles microcontinent (4.5°S). Three possibilities arise from this observation and the model's interpretation of the mechanisms responsible for basin evolution. First, the southernmost portions of the fracture zone could be aligned with and therefore indistinguishable from another similar basement fracture and therefore the Carlsberg would have always been north of the Seychelles. Second, the Seychelles could have moved north at some time after the initial formation of the scarp. Third, the spreading axis could have jumped in such a manner that it isolated the Seychelles.

Extensions of the fracture zone beyond 7.5°S may also indicate several interesting possibilities for the structural history of that area. The fracture zone may be related to any of three linear features on Madagascar. They are the eastern boundary fault (Pepper and Everhart, 1963), a fault along the western boundary of the island (Gregory, 1920; Pepper and Everhart,

1963), or the trend of the northeast facing coast of Madagascar as evidenced by contours in the Fisher et al., 1968 bathymetry. Any or all of these features may be related to deformation processes other than those associated with Owen Fracture Zone. However, it is unlikely that the fracture zone would terminate north of the Madagascar region so it is reasonable to speculate on the structures its extension would imply. If it extends to the western boundary fault of Madagascar then the faulting would clearly be related to processes other than the termination of a spreading center (the present day Carlsberg) in an extensive fault as the continental material (Madagascar) would be in between the two. A change in trend of the fracture zone would align it with the northeast facing coast of Madagascar and then if the spreading center is to remain orthogonal to the fracture zone an even greater migration totaling approximately 90° in the trend of the spreading center is implied. Finally, if the eastern boundary fault of Madagascar is to be an extension of the fracture zone as can be implied from others extrapolations (Heezen and Tharp, 1969; Fisher et al., 1968) then the fracture zone must be transformed eastward perhaps by a small spreading center trending east-west and located north of Madagascar. Specific determination of the proposed ancient spreading center's relationship to the Seychelles and the fracture zone's trend in the

Madagascar area awaits further geophysical surveys of the southern Somali and northern Mascarene Basins.

Figure 19B represents the early stages of Gondwanaland dispersal in the Western Somali Basin area. The buried scarp which is an extension of the fracture zone indicates a predominantly northward trend for the motion of India with respect to Madagascar and Africa for this initial episode. A similar trend for India's motion during early dispersal has been indicated by McKenzie and Sclater (1971) from the direction of the Chagos Fracture Zone and these indications of north-south motion may have been contemporaneous during the early Cenozoic.

During Stage B, the lineament was composed of an inactive scarp south of the spreading center and a zone of active shearing north of the spreading center and extending, perhaps to the northern border of India. Thus, the transform fault sector of the fracture zone would have connected a spreading center with a zone of subduction or crustal shortening between India and Asia in the Tethys.

Figure 19C represents the conditions resulting in the formation of the more northeasterly trending section of the fracture zone which coincides with the elevated portions of Chain Ridge. At this time the formation of the Mid-Indian Ridge from the original north-south Chagos Fracture Zone resulted in the Carlsberg Ridge trending northwest-southeast. Thus, the adjustment in spreading direction which resulted in Mid-Indian Ridge formation (McKenzie and Sclater, 1971) may have also resulted in the change of fracture zone trend and morphology observed north of 3.5°S. The change from pure strike slip motion along what is now the Mid-Indian Ridge to spreading could have resulted in a component of overthrusting which might be responsible for the elevation of basement forming Chain Ridge.

Although a change in the trend of the fracture zone has occurred in Stage C the shear is along a fault connecting a zone of spreading with a zone of subduction as in Stage B.

Figure 19D represents the final major structural event in the evolution of the fracture zone. The opening of the Gulf of Aden at Sheba Ridge during the Miocene (Fisher and Bunce et al., 1972) resulted in a major rearrangement in plate boundaries. The northeast-southwest trend of the fracture zone is maintained

but due to the initiation of a new spreading center to the north a ridge-ridge transform fault is the most active zone of shearing. Differential motion along the northeastern branch is possible as noted by McKenzie and Sclater (1971), if there is a difference in the rates of spreading north and south of the fracture zone.

The model demonstrates that fracture zone trend and morphology, age of the sea floor, and continental reconstructions form a set of constraints from which the evolution of the Somali Basin area may be developed. In so doing at least three major phases of fracture zone development may also be demonstrated. First, the disparity in fracture zone branch lengths as well as deformation at its terminations indicates possible structural change related to the fracture zone occurred in these predominantly continental areas. Second, one phase of fracture zone development in the deep sea occurred when it was connecting a spreading center with a zone of subduction. And third, the other phase of oceanic fracture zone development occurred when the active portion of the fracture zone connected two ridges.

CONCLUSIONS

Geophysical observations and interpretations in the Somali Basin area lead to conclusions about the main fracture zone, the basins that border it and possible development schemes for the region. The southwestern extension of Owen Fracture Zone consists of a northeast-southwest trending elevated portion known as Chain Ridge and a buried scarp which is an extension of it that runs more north-south to the vicinity of Madagascar (7.5°S). It may align with and be related to any of three faults associated with Madagascar. The major change in trend and morphology of the fracture zone appears related to changes in the style of basin evolution.

Regional depth to basement and sediment thickness show a great increase from the eastern basin to the western basin and when age-elevation and other methods of determining sea floor age are used the western basin is at least 30-40 m.y. older than the eastern and possibly much older than that. Seismic refraction measurements show at least part of the western basin to be floored by oceanic crust which could have developed during the formation of the Tethys while extensive Mesozoic sedimentation in this sea nearly surrounded by continents resulted in the

formation of a crustal section similar to the oceanic-continental section shown by Menard (1967).

The trend and morphology of the fracture zone, sea floor age, and proposed reconstructions form constraints on an evolutionary model of the area. The early Cenozoic Carlsberg Ridge terminated in the north-south trending scarp that borders Chain Ridge and defines the initial northward component of India's movement away from the Western Somali Basin. In a subsequent phase of evolution, the ridge-trench nature of the fracture zone was maintained but formation of the Mid-Indian Ridge coincided with a more northeasterly trend for the fracture zone and the formation of Chain Ridge. A final stage of development occurred after the Miocene formation of Sheba Ridge during which the northeasterly trend was maintained but the main shear along the fracture zone was along a ridge-ridge sector.

Finally, the study of possible continent to continent fracture zones leads to general properties of them which may be useful elsewhere. Under certain conditions a fracture zone's relationship to continents and its branch length limit possible basin evolution schemes and control reconstruction fits. One lineament may have several structural histories with, in some cases, the different chronologic episodes represented by different

trends and morphologies along strike. Because fracture zones transect abyssal plains which lie far from spreading centers and often have poor magnetic records, they place constraints on early ocean basin evolution and in many areas may form the only direct structural link between continental margins and present day spreading centers.

III NEOGENE SEDIMENTATION IN THE SOMALI BASIN AND THE INITIATION OF MONSOON CIRCULATION

INTRODUCTION

Previous paleooceanographic studies have utilized paleontologic, sedimentologic, and plate tectonic principles to infer the past physical and chemical features of the oceans through their related biological and geological records. Expansion of this method of studying earth history into new geographic areas and earth processes is inevitable. Indeed, the possibility of examining any hypothesis about a paleooceanographic phenomenon by utilizing the constraints imposed by several basic fields of inquiry means that not only may the specific phenomena be examined in detail but also through comparison of interpretations refinements in the parent scientific fields may be developed.

This section will develop a model of Neogene sedimentation in the Somali Basin which relates the observed increase in sedimentation rates to the initiation of monsoon atmospheric flow through associated high sea surface productivity due to upwelling. As background some previous paleooceanographic studies will be reviewed and the characteristics of northwestern Indian Ocean atmospheric systems will be presented. Sedimentation rate determinations and hypotheses for their variation will then form the

basis for evaluating paleooceanographic processes.

Past paleooceanographic studies illustrate the great diversity of methods that have been employed. Biogeographic distributions at sea with a stable continent ocean configuration have been used to predict past ocean currents (Fell, 1967). However, biogeographic distributions have also been even more successfully used to elaborate on continental configurations by analyzing terrestrial faunas (McKenna, 1973) or to determine the paleooceanographic features themselves in the mobile continent-ocean framework (Berggren and Hollister, 1974). Past variation in the carbonate system (Berger, 1973; Lohmann, 1974) and the location of equatorial productivity with respect to plate movement (Heezen et al., 1973) have also delineated major paleooceanographic changes within the plate tectonic framework. The effects of ocean evolution have also been noted in calcareous nannoplankton diversities which increase at times of major epicontinental seas (Haq, 1973). Initial model studies are the only attempts to give a physical explanation for the observed effects (Luyendyk et al., 1972). Thus, most work to date has involved the observation of the changes and more physical explanations for the causes of change may greatly enhance understanding of the processes.

This study concentrates on a substantially different paleooceanographic phenomenon, the effects that major plate motions can have on atmospheric flow. Therefore, it both describes paleooceanographic change through the deep sea sediment record and infers the cause in terms of the past atmospheric circulation.

CIRCULATION SYSTEMS

The primary features of ocean circulation in the Somali Basin are all affected by seasonally reversing monsoons. The atmospheric circulation is primarily a result of a varying insolation pattern over the northwestern part of India where seasonally alternating high and low pressure systems develop. In winter in the northern hemisphere the land is cold in northern India and Pakistan and the resulting surface pressure is high (1016 mb) as shown in figure 20 (Ramage et al., 1972). The result is an outflow of air toward the ocean with sea level velocities of ~ 10 knots. In the summer this same land area is warm; surface pressures are lower (995 mb) and an inflow of air from the ocean at 15-20 knots occurs (figure 20). This inflow is aided by contrasting high pressure areas in southern Africa and at 67E, 37S (1024 mb) in the southern Indian Ocean.

Figure 20.

Wind direction and sea level pressure, January and July, western Indian Ocean simplified from Ramage et al., 1972.

WINDS AND SEA LEVEL PRESSURE

JANUARY

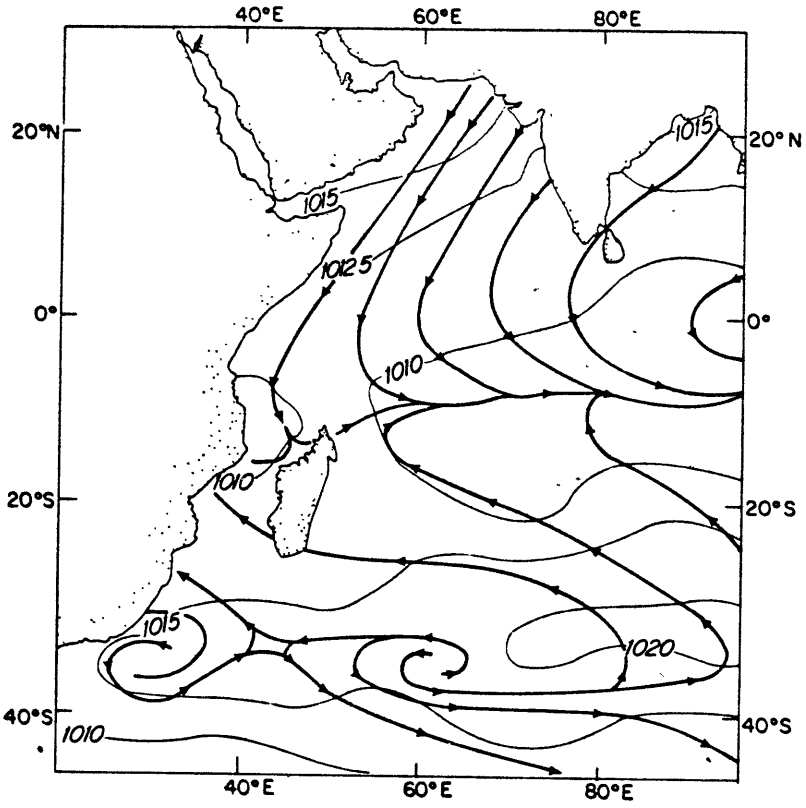

JULY

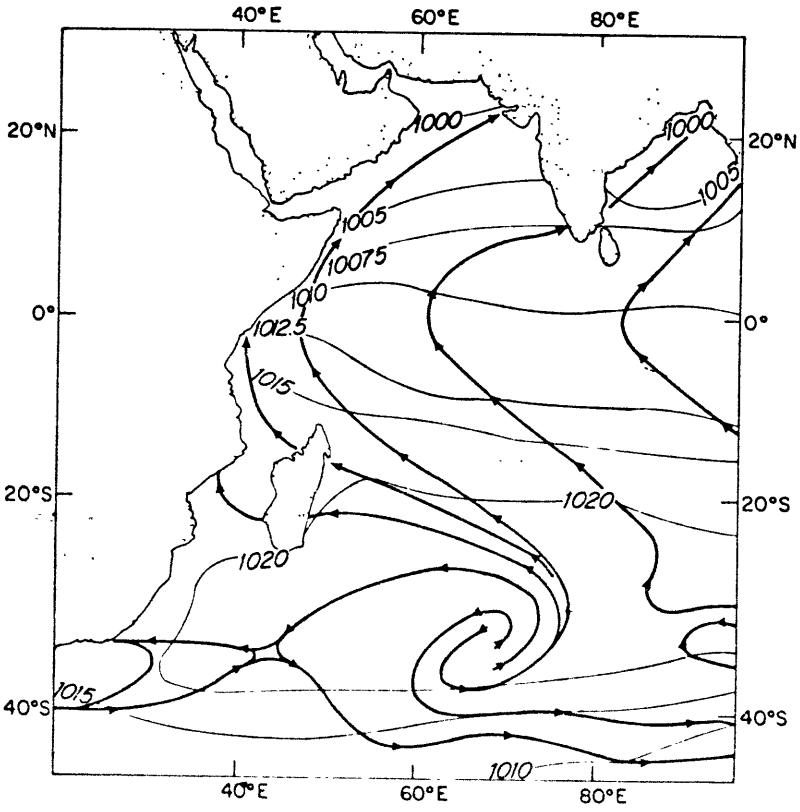

Monsoon circulations are forced by contrasts in thermal properties between continents and oceans (Simpson, 1921). Although no simple complete theoretical treatment of them is available (Holton, 1972) a model proposed by Sankar-Rao and Saltzman (1969) relies only on the effects of ocean continent heating contrasts and shows many features normally observed. Thus, a simple analysis of the heating contrast which is due to the differing thermal capacities of the surfaces is extremely important for the physical interpretation of the monsoon circulation. The Sankar-Rao and Saltzman (1969) model heats areas proportional to the difference between the mean low level air temperature and ground surface temperature. Over the ocean an empirical heat balance equation in langleys per day may be expressed as:

where $Q_{st} = Q_s - Q_r - Q_b - Q_e - Q_h$

Q_{st} = net heat balance at surface

Q_s = rate of incoming short wave radiation modified by cloud cover (insolation)

Q_r = rate of radiation reflection at surface

Q_b = rate of emission of back radiation

Q_e = rate of cooling from evaporation

Q_h = sensible heat loss to atmosphere

and over the ocean Q_{eff} the effective radiation at the sea surface,

$$Q_{eff} = Q_s - Q_r - Q_b$$

is equal in magnitude to Q_e and an order of magnitude larger than Q_h (Ramage, 1971). In the Indian Ocean the heat equivalent of the total radiational energy added per unit time and area is 233 ly da^{-1} of which 211 ly da^{-1} are removed in latent heat of evaporation and 19 ly da^{-1} are removed as sensible heat transferred to the atmosphere (Budyko et al., 1962).

However, on lands bordering the northwestern Indian Ocean the observed predominantly dry climates (Landsberg et al., 1963) imply significant changes for some terms in the heat balance equation. If Q_s is assumed equal for land and sea Q_b which is a function of absolute temperature to the fourth power will be nearly equal for each. Q_r will vary as the albedo of the surfaces which for water at a solar altitude of $\geq 35°$ is 7% whereas vegetation, 20%, or sand 4% (Eagleson, 1970) reflect much more shortwave radiation. Q_e over land is dependent on the soil type, depth to the water table, and amount and character of vegetation which causes it to be highly variable. In areas where the water table is below the limits of capillary action evaporation ceases which excludes

increasing the moisture in the air except through transpiration when the water table is deeper than 1.3 m (Berry et al., 1945). As evapotranspiration in arid lands is considered small, evaporation over the sea could be much greater because of the depression of the water table (Berry et al., 1945). Thus, if the net heat balance at the surface, Q_{st}, is to be equivalent over land and sea the terms in the heat balance equation indicate a considerably higher sensible heat loss to the atmosphere over the land than over the ocean due to the variation in evaporation between the two. This variation which exceeds the effects of albedo differences accounts for the heating and low pressure formation over India which is a primary driving force of the summer monsoon.

CHRONOLOGY OF FINAL STAGES OF BASIN EVOLUTION

The structural development of the area as synthesized in the model (figure 19) results in two major changes. The central portion of the Tethys Ocean is bisected by the northward motion of India and Africa, and the remaining areas, the Mediterranean Sea and Indian Ocean, are isolated. Bordering continents change position with respect to one another resulting in a substantially different relationship of land to land and land to sea.

The Gondwanaland reconstructions (figure 18) indicate the extent of the pre-Cenozoic Tethys while the fracture zone trend (figure 17) controls the geometric development of the present basin. As indicated the western Somali Basin was an arm of the Tethys which remained ocean throughout the destruction of the Tethys. The eastern Somali Basin was formed by sea floor spreading during the Cenozoic and caused the northward migration and eventual collision of India with Asia.

Terrestrial faunas may be used to establish that time when convergence of the Asian and Indian continental areas had resulted in substantial land connections. Mammalian migration between India and Asia as postulated by McKenna (1973) has not been specified due to lack of adequate assemblage information. However, mammalian migration between Africa and Asia has been determined at 18 m.y., Early Miocene, (van Couvering, 1974, personal communication) which indicates that bifurcation of the Tethys occurred by that time. To the east Powell and Conaghan (1973) indicate on the basis of stratigraphic sections on land that collision between India and a proto-Tibetan land mass occurred prior to Middle Eocene, but crustal fracture within India (Late Eocene-Oligocene) and underthrusting and consequent

uplift (Miocene-Recent) were later. Thus, in spite of brief incursions of paralic and non-marine conditions in the Paleogene, marine influences were not completely removed from northern India until Middle Miocene (Wadia, 1966; Powell and Conaghan, 1973). In summary the structural evolution of the Somali Basin has profound implications for events to the north. The initial division of the Tethys into two separate oceanic areas and dessication of the northern India-Pakistan area was complete by the later part of the Middle Miocene.

DETERMINATION OF NEOGENE SEDIMENTATION RATES

To examine the effects of structural change on oceanographic evolution the sediment type and accumulation rates for four Somali Basin Deep Sea Drilling Sites have been determined (figure 21). A total of 95 samples was examined to develop the Neogene nannofossil biostratigraphic zonation at each location. Sampling intervals were determined by initial reports (Fisher and Bunce et al., 1972; Simpson and Schlich et al., 1972) as well as the location of cores within the drilled section. In only one location, site 236, did continuous coring provide an uninterrupted section. Smear slides of untreated subsamples of the section were prepared for viewing at 1250 x in phase contrast light. Table 1 shows the distribution of calcareous

Figure 21.

Location of sampled Deep Sea Drilling Program sites in the Somali Basin.

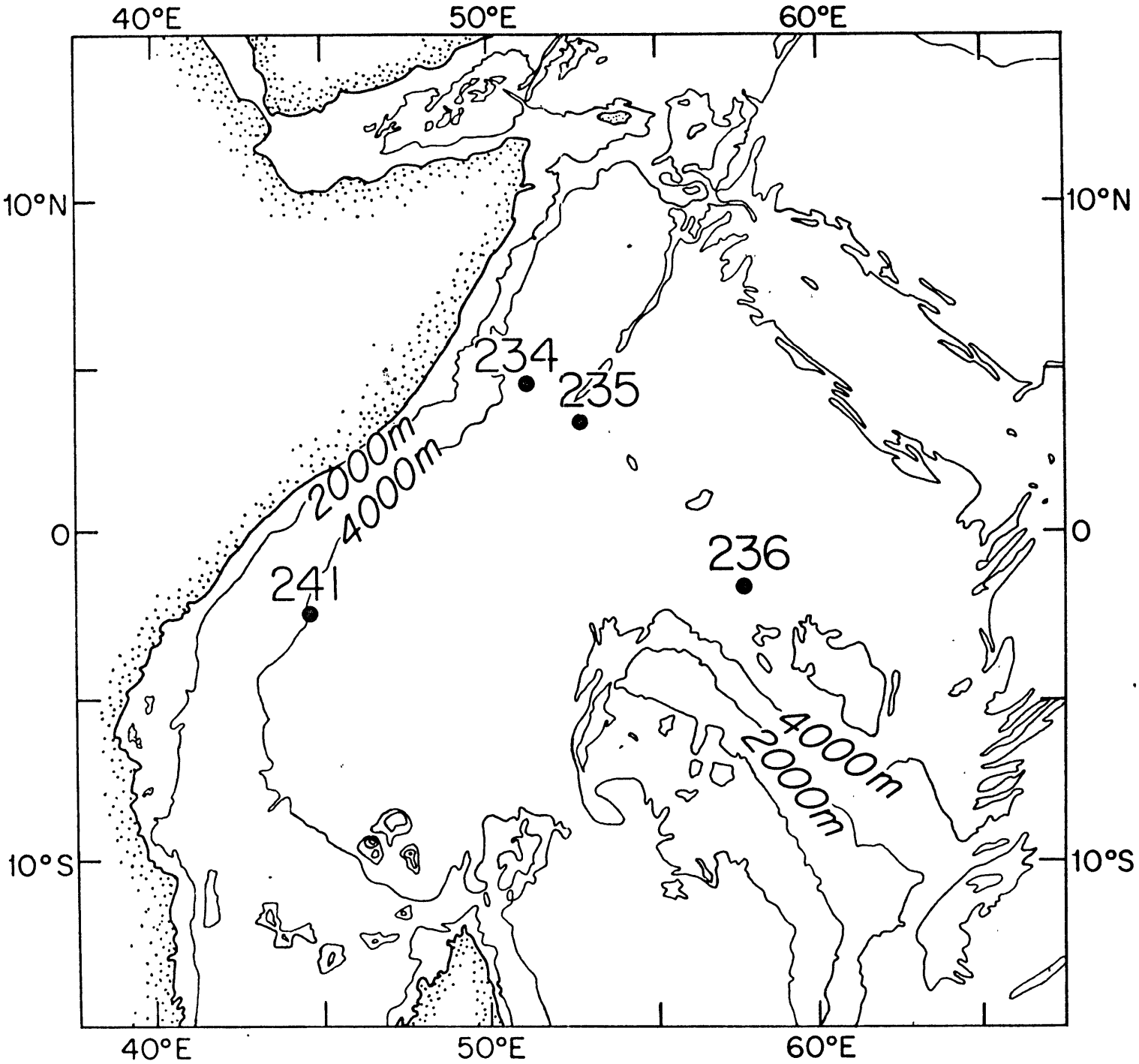
40°E
50°E
60°E
10°N
0
10°S
234
235
236
241
2000m
4000m
4000m
2000m

TABLE 1

Martini (1971) Nannofossil Zonation of Somali Basin Sediments. Numbers in Columns Indicate Core-Section Which Are Assigned to the Zones to Left. (cc = Core Catcher)

Nannofossil zones	Site 234	Site 235
E. huxleyi G. oceanica P. lacunosa		4-3,2-3,1-5,1-1
D. brouweri D. pentaradiatus D. surculus R. pseudoumbilica D. asymmetricus	1-2,1-1	9-1,7-3,6cc,5-1
C. rugosus		9-2
C. tricorniculatus		
D. quinqueramus	1-5,1-4	12-3,11-3,11-1,10-2,10-1
D. calcaris	3-1,2-4	
D. hamatus	5-1	13-1
C. coalitus D. kugleri		14cc,14-2
D. exilis	6-1	
S. heteromorphous		15-4,15-1
H. ampliaperta		
S. belemnos		
D. druggi		
T. carinatus	11-1,10-3,9-1	
S. ciperoensis		

TABLE 1
(continued)

	Site 236	Site 241
E. huxleyi	3cc,3-2,3-1, 2-1,1-1	5-5,4-1,3-6,3-1,2-5, 1-5,1-1
G. oceanica		
P. lacunosa		
D. brouweri	4-2,4-1	8-1,8-4,6-1
D. pentaradiatus		
D. surculus		
R. pseudoumbilica		
D. asymmetricus		
C. rugosus		
C. tricorniculatus	5-1,4-3	
D. quinqueramus	14-1,13-5,12-5, 12-1,10-1,8-1, 6-5,6-2	11-3,10-3,9-2
D. calcaris	15-6,15-3,15-1	
D. hamatus		
C. coalitus		
D. kugleri		
D. exilis		
S. heteromorphous	17-6,16-6	
H. ampliaperta		
S. belemnos		
D. druggi		
T. carinatus		16-1,15-3
S. ciperoensis	20-2,19-3	16-2

nannoplankton and biostratigraphic zonation based on the standard zonation scheme of Martini (1971). The results of the nannofossil biostratigraphic zonation have been converted to absolute time by comparison with the Neogene time-scale suggested by Berggren (1974). The chronostratigraphy of the sites has been plotted on the scale of total penetration for each site along with nannofossil preservation (figure 22). Those data allow the sediment accumulation rate for each time interval to be calculated (Table 2) and plotted (figure 23).

In figure 23 the sediment accumulation rate shows a general increase between the early Miocene and the Recent. In all cases, present deposition rates exceed early Neogene rates. During the middle Miocene all sites show increasing rates. During late Miocene time sites 235 and 236 remain constant while 234 and 241 increase rapidly. Site 241 decreases in the Pliocene while the others remain level or increase. All sites show late Pleistocene increases.

Figure 22.

Nannofossil chronostratigraphy and occurrence in Somali Basin Deep Sea Drilling sites 234, 235, 236, and 241. The nannofossil biostratigraphy according to the Martini (1971) zonation was determined as shown and the zones were converted to absolute time using the Berggren (1974) correlation.

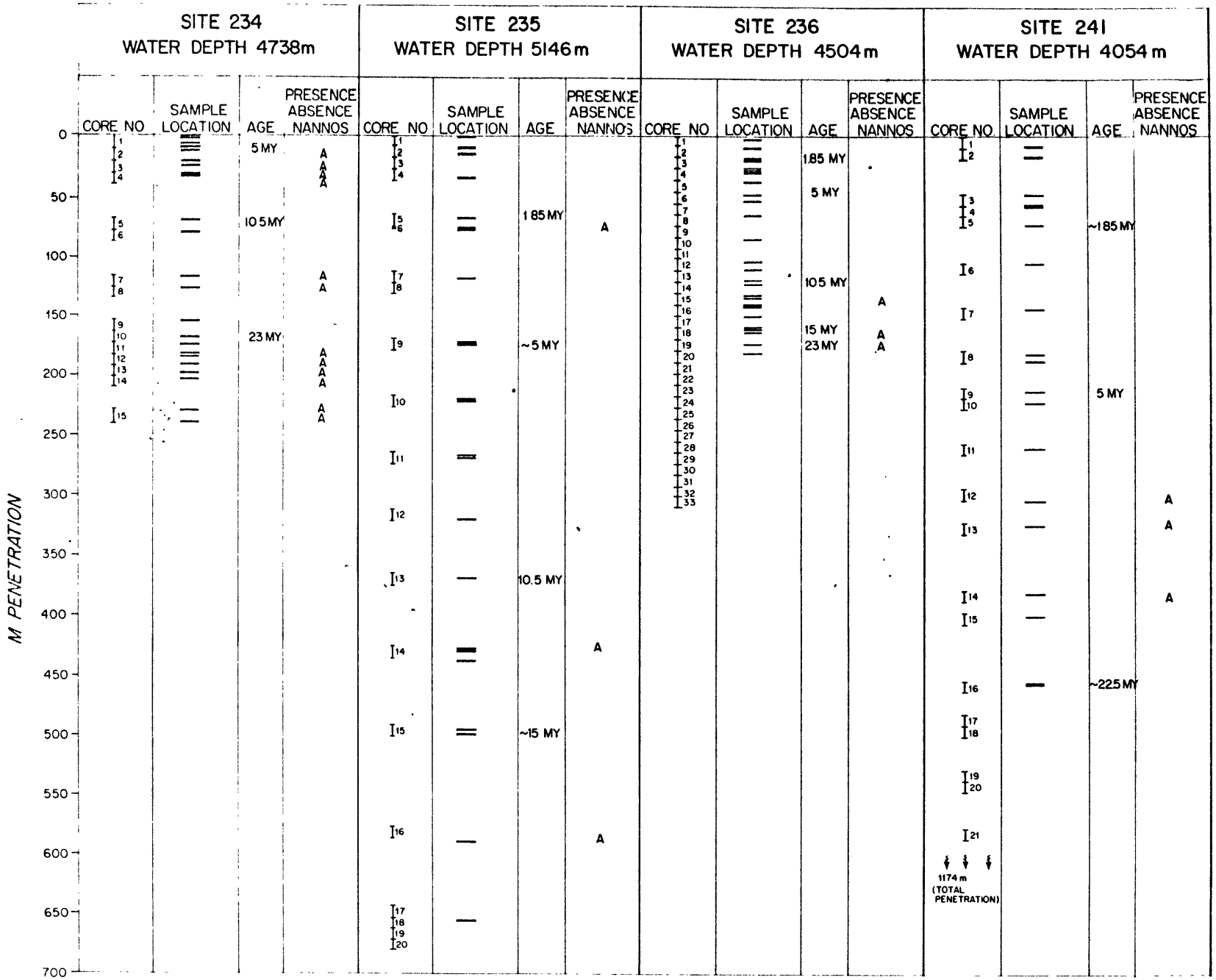
SITE 234
WATER DEPTH 4738m
SITE 235
WATER DEPTH 5146m
SITE 236
WATER DEPTH 4504m
SITE 241
WATER DEPTH 4054m
CORE NO
SAMPLE LOCATION
AGE
PRESENCE ABSENCE NANNOS
M PENETRATION
0
50
100
150
200
250
300
350
400
450
500
550
600
650
700
5 MY
10.5 MY
23 MY
1.85 MY
~5 MY
10.5 MY
~15 MY
1.85 MY
5 MY
10.5 MY
15 MY
23 MY
~1.85 MY
5 MY
~22.5 MY
1174 m
(TOTAL PENETRATION)

TABLE 2

Somali Basin Neogene Sedimentation Rate Determinations

DSDP Sites	Core Number	Late Quaternary Piston Cores Rate m/m.y.	Pleistocene Thickness m / Rate m/m.y.	Pliocene Thickness m / Rate m/m.y.
234	34	45	nd	nd
235	32	48	67 / 36.2	106 / 33.6
236	36	<34*	18 / 9.7	29 / 9.2
241	59 59	<31+ >50	72 / 38.9	140 / 44.4

* Average of Appendix II & III results for Core 36

+ Appendix III

TABLE 2 continued

Somali Basin Neogene Sedimentation Rate Determination

Upper Miocene	Middle Miocene	Lower Miocene
Thickness m / Rate m/my	Thickness m / Rate m/my	Thickness m / Rate m/my
64 / 11.8	←	97 / 7.8 →
196 / 33.8	131 / 29.1	
71 / 12.9	40 / 8.8	16 / 2
←	244 / 13.9	→

Figure 23.

Sedimentation rate plotted with respect to age for the western Indian Ocean sites 234, 235, 236, and 241. Rates as determined in Table 2 are plotted in the middle of the time interval they represent.

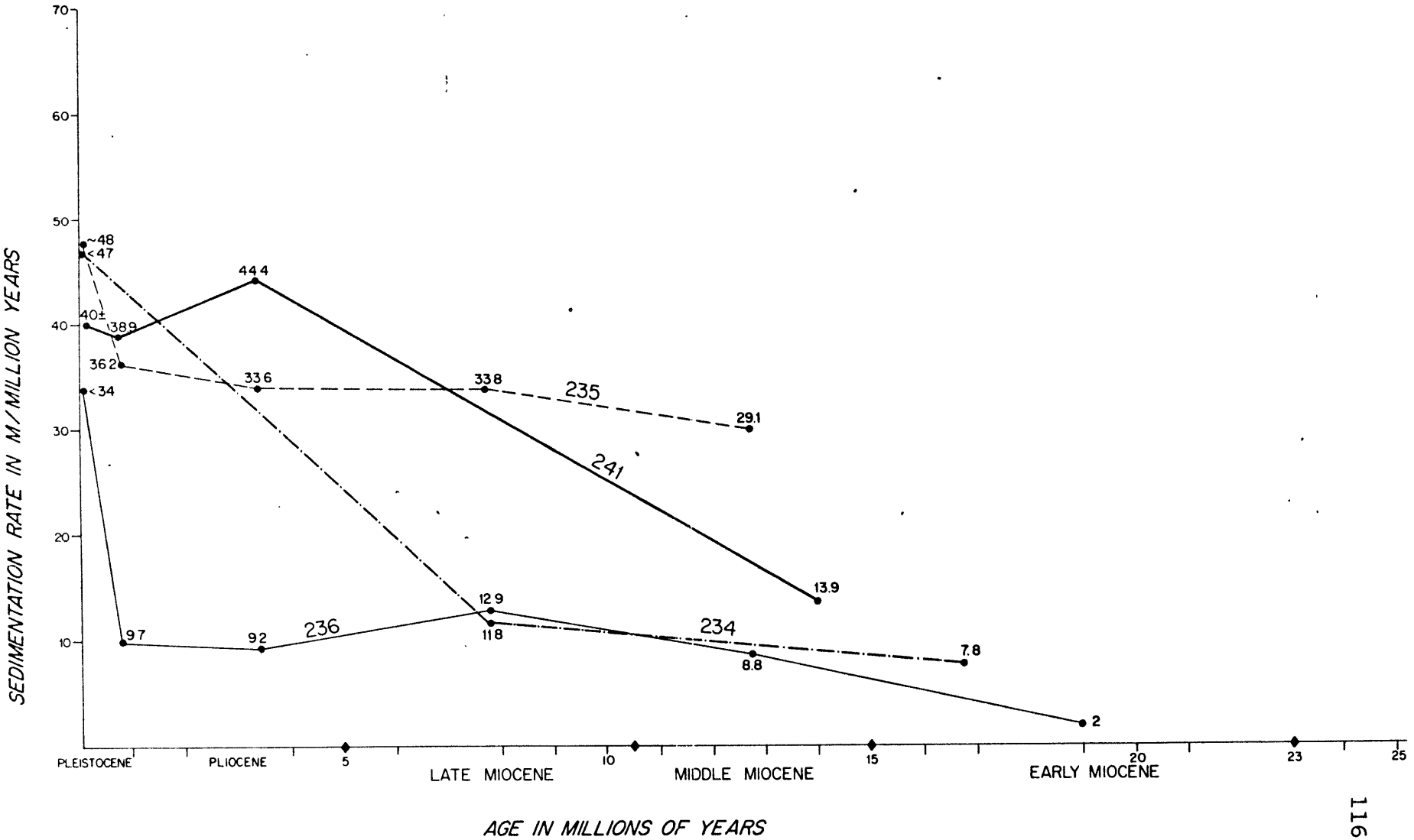
SEDIMENTATION RATE IN M/MILLION YEARS
70
60
50
40
30
20
10
~48
<47
40±
444
389
362
336
338
235
29.1
<34
241
13.9
129
97
92
236
118
234
7.8
8.8
2
PLEISTOCENE
PLIOCENE
5
LATE MIOCENE
10
MIDDLE MIOCENE
15
EARLY MIOCENE
20
23
25
AGE IN MILLIONS OF YEARS

CAUSES OF SEDIMENTATION RATE VARIATION

Pelagic deposition in the deep sea results in sedimentation rates that often vary from 1 to 10 m/m.y. (Menard, 1964). Higher accumulation rates have been observed under areas of high productivity (Hays, et al., 1969) and in areas adjacent to continents. In general, as a basin becomes larger through sea floor spreading a greater number of sites should show reduced sedimentation rates as the locations become more remote from land and deeper. In addition the subsidence of the sea floor often brings larger areas into the depth of significant carbonate dissolution resulting in decreased sediment accumulation rates.

Late Quaternary sediment accumulation rates have been determined through radiocarbon and nannofossil biostratigraphic age determinations on piston core material (Appendices II and III). In the northwestern Somali Basin Recent sediment accumulations are somewhat higher (54 m/m.y.) than those in the equatorial areas ($\sim$ 45 m/m.y.). In both cases the rate is higher than that generally associated with deep sea pelagic sedimentation in a major ocean basin.

Therefore, general conceptions of sediment accumulation as mentioned above do not fit the pattern in the Somali Basin. In the Somali Basin the general trend is toward a greater accumulation of sediment through time as the basin becomes both deeper and larger (figure 23). This increase in pelagic sediment accumulation can only occur if a new source of sediments develops or if a process hindering the accumulation of sediments abates. The latter may be checked by examination of figure 22 for the sedimentation rates in the nannofossil free sections of the cores. If dissolution predominates the general trend should show a pattern of accumulation variation through time that reflects primarily the deepening of each site and secondarily the variation in the CCD. However, the general trend in figure 23 is of greater accumulation through time rather than less.

To test the former hypothesis of a new source of sediment supply several possibilities must be considered. As noted earlier the main episode of Himalayan uplift occurred during the mid-Miocene and could have caused a substantial increase of terrigenous sedimentation that would affect the general pattern of basin sediment evolution. The western Somali Basin would be cut off from such sedimentation by both the Carlsberg and Chain

Ridge. However, with variation in morphology of the plate boundaries some sediment could get into the area. Indeed this appears to be the case for site 235 which is east of Chain Ridge where the Miocene sedimentation rate is uniformly higher than elsewhere.

Increased biogenic productivity is the remaining new source. If the increased sedimentation rate is due to the effects of a greatly increased biogenic input.then: (1) this biogenic material should be recognized in the sedimentary section; (2) a new source of biogenic material from the surface waters must be postulated; (3) physical oceanographic conditions must have changed to make the surface water productivity increase possible.

Examination of figure 22 allows a qualitative evaluation of the effects of the nannofossil carbonate component on increased post mid-Miocene sedimentation rates. As previously noted dissolution is not primarily responsible for the sedimentation rate variations. Although turbidite deposition had been proposed for the basin (Ewing et al., 1969) initial descriptions of the drilling sites (Fisher and Bunce et al., 1972) as well as sediment properties observed in these samples indicate such processes are not significant. Thus, the increased sediment

accumulations must be due to greatly enhanced biogenic input of which the nannofossil component is a part.

As the greater sediment accumulation continues to the present time the new source of biogenic material in the surface waters implied by the greater sediment accumulation rates must be observable in today's ocean. This source is the extensive upwelling occurring in the northwestern Indian Ocean which results in an annual productivity for the area of about twice the average rate for the world ocean (Ryther, et al., 1966). Thus, sediment accumulation rate data indicate significant upwelling may have begun in the Indian Ocean during the mid-Miocene to Pliocene.

To determine whether the variations indicated by the sediment record are substantiated the land sea configuration and the forces responsible for present day circulations must be examined. As previously noted land sections in India indicate the final marine regression occurred during middle Miocene. The tectonic evolution of the area resulted in the transformation of a previously ocean area to a continental area. The ensuing variation in the thermal properties of the surface initiated the land-sea heating contrast presented earlier. Greater warming could then occur in the lower atmosphere over India causing the characteristic circulation. Contemporaneously the basin reached

approximately its present configuration. Thus, with a major element forcing present monsoon flow, the Indian summer heat low, the upwelling system could have been initiated in Middle to upper Miocene on the basis of independent physical, stratigraphic and plate tectonic evidence which supports the interpretations drawn of the basis of the deep sea sedimentary record alone.

SUMMARY AND CONCLUSIONS

The Neogene sedimentation record has been examined in four northwestern Indian Ocean Deep Sea Drilling sites. Nannofossil biostratigraphic zonations of each site have been converted to absolute time and sediment accumulation rates were determined. All sites have significant Neogene sedimentation rate increases to 15-50 m/m.y. which on average are considerably higher than normal pelagic sedimentation rates.

Examination of the lithology of the sediments as well as the preservation of the calcareous nannofossils indicates the dramatic increase in sedimentation rates may be due to increased biogenic productivity in the surface waters. Present day surface productivity in the northwestern Indian Ocean is approximately twice that of the world average (Ryther et al., 1966) due to

upwelling and is reflected by high later Quaternary sedimentation rates. The initiation of monsoon conditions which cause the high productivity may be specified by determining when high rates of sedimentation were first observed. Data from these sites indicate an Upper Miocene to Pliocene initiation for the main monsoon flow, associated upwelling, and high rates of sedimentation.

Once the chronology of the change in the circulation systems has been specified through the geologic record the effects of significant changes in the structural history of the basin may be considered with respect to the components forcing the atmospheric and oceanic circulations. The heating contrast between continent and ocean which is related to the thermal properties of the surface is a primary driving force for the monsoon. However, during the early Cenozoic the relationship of land and sea in the area was sufficiently different to preclude such a mechanism. Examination of the oceanic and continental structural records for the area demonstrates that marine influences were not removed from northern India until middle Miocene (Powell and Conaghan, 1973). Thus physical conditions in the atmosphere necessary for monsoon flow may have been met by middle Miocene while the predominant ocean circulation and

productivity effects recorded in marine sediments indicate an Upper Miocene to Pliocene initiation.

IV LATE QUATERNARY SEDIMENTATION AND OCEANOGRAPHIC VARIABILITY

INTRODUCTION

Previous Work

Deep sea sediment studies provide an extensive and detailed record of past oceanographic and climatic conditions for the last several hundred thousand years. Because of the variety of carbonate lithologies and the sensitivity of each to various oceanographic and climatic parameters the carbonate component of pelagic sediments has been studied extensively in the Atlantic and Pacific oceans. This section will present analyses of carbonate sediments from Somali Basin and will infer from the variation in specific sediment properties changes in the bottom and surface water conditions.

After an initial period of descriptive studies the understanding of pelagic sediments was greatly expanded by Arrhenius (1952) who studied equatorial Pacific sediments and was able to relate carbonate amount and lithology to climatic cycles by assuming that decreased total carbonate reflected decreased productivity during interglacials. In a more recent study of the equatorial Pacific Hays et al. 1969 used magnetic

stratigraphy, paleontologic analyses, and total calcium carbonate to demonstrate that the last carbonate maximum is correlative with the Wisconsin glaciation and therefore by extrapolation there were probably eight major glacial fluctuations during the last 700,000 years.

In the Atlantic Ericson et al. (1961) determined past climatic fluctuation through variations in the Foraminifera fauna and Ericson (1970) compared this with results from the Pacific which indicated to him that warm surface waters in the Pacific were at least partly synchronous with cool Atlantic waters. In other Caribbean work Emiliani (1961, 1966) has equated oxygen isotope variation in the carbonate fraction with sea surface paleotemperature ignoring the fractionation due to ice formation. Broecker and van Donk (1970) treated this further factor in the oxygen isotope record and indicated the Emiliani (1966) isotopic fluctuations represented the latter part of the Pleistocene only. Shackleton and Opdyke (1973) used magnetic stratigraphy and the assumption of uniform sedimentation rate to determine the chronology of an equatorial Pacific oxygen isotope curve. Their results indicate ages for the boundaries slightly greater than those of Broecker and

van Donk (1970).

Recent work in the Atlantic (McIntyre et al., 1972) has extended to mapping the geographical extent of various foraminifera and coccolith assemblages to determine surface water conditions over a large area of the North Atlantic during the Pleistocene. Variation between left-coiled Globigerina pachyderina (cold) and abundant fine carbonate led them to develop a model in which high latitude glacials are carbonate minima; intermediate latitudes have two carbonate maxima due to coccolith productivity zone migration; and a single carbonate maxima occurs at the equator. Quantitative temperature variation through time is currently being determined through relating present sea surface conditions to fossil assemblages through factor analysis (Imbrie and Kipp, 1971) and sea surface temperature for 18,000 yrs BP has been determined (McIntyre, 1974).

Cooke (1973) has reviewed the main Pleistocene chronologies and noted the disparity between the original oxygen isotope curve of Emiliani (1966), a later more extensively dated curve (Rona and Emiliani, 1969) and the chronology developed by Broecker and van Donk (1970). While the Emiliani curve originally placed the four main glacial stages in the last 500,000 years Ericson and

Wollin (1968), Broecker and van Donk (1970), and Ruddiman (1971) all indicate the four major glacial stages occur during a 2 m.y. time period. As more dates and climate fluctuation data become available the long time scale receives more support.

Dissolution, terrigenous dilution, and sea surface productivity variations may each be related to climatic change. In considering Atlantic sedimentation rates Broecker, et al. (1958) were able to demonstrate that a decrease in the deposition rates of carbonate and clay fractions occurred at 11,000 years BP in core A 180-74 (0°03'S, 24°10'W) with the rate of coccolith sedimentation decreased by a factor of approximately 2. Thus, in some areas intervals of high carbonate sedimentation in spite of terrigenous dilution equate with cold surface waters. However, in a later model based on chemical reasoning and core data, Broecker (1971) found the total rate of $CaCO_3$ accumulation in the equatorial regions of all oceans is constant but coarse foraminiferal carbonate is lower during Atlantic glacials but higher during Pacific glacials. The fine component is almost uniform (Broecker, 1971) through time. In addition examination of a limited number of accumulation rates implies greater solution during glacials (Broecker, 1971). Berger (1973) has

considered the effects of carbonate dissolution which he asserts are intensified during interglacials which removes the need for involving productivity variations to account for total carbonate amounts.

In contrast to the Atlantic and Pacific Oceans the Indian Ocean carbonate record and its relation to climatic change have not been investigated in comparable detail. Initial northwestern Indian Ocean studies were undertaken during major, often world-wide expeditions and concentrated primarily on descriptions of morphology (Wiseman and Seymour Sewell, 1937) and sediment type (Murray, 1899, 1909); Stubbings (1939a, b) and Schott (1939). The Swedish Deep Sea Expedition (1947-48) concluded this phase of exploration with description of the carbonate sequence of northwestern Indian Ocean cores (Olausson, 1960). Research connected with the International Indian Ocean Expedition during the 1960's resulted in a general surface sediment description prepared by Bezrukov (1964), and specific components were treated in more detail: carbonate (Wiseman, 1965); clay minerals (Griffin, et al., 1968; Goldberg and Griffin, 1970; Biscaye, 1965; and total sediment thickness based on seismic data (Ewing, et al., 1969). In addition, general sediment studies

concentrating on specific areas such as the northwestern Indian Ocean (Konta, 1968) or Arabian Sea (Stewart, et al., 1965) and the shelf off Somalia (Müller, 1966, 1967) have been completed.

Paleontologic studies of the major microfossil groups such as Radiolaria (Nigrini, 1967), diatoms (Kolbe, 1956) and Foraminifera (Conolly, 1967; Frerichs, 1968; Be and Tolderlund, 1971) provide some of the necessary background data for climatic studies. Previous climatological inferences have been drawn from Indian Ocean sediments. Philippi (1912) related the disappearance of tropical Foraminifera and appearance of red clay as being due to cooling of water temperatures. Stubbings (1939) examined the ratio Globigerina bulloides, implying cooler waters to Globorotalia menardii, indicating warmer waters and in a 132 cm core in the southern Somali Basin he found four high values indicating to him cooler periods. Through a detailed analysis of two central Indian Ocean cores rich in Foraminifera Oba (1967) was able to infer an alteration in surface water temperatures. In addition he found that high total carbonate in the equatorial areas was deposited during glacial ages. Olausson et al. (1971) treat the Somali Basin area in greater detail and use the variation in the carbonate contribution of different size fractions

to consider variations in sea surface currents. Vincent (1972) examined Foraminifera faunas from several southwestern Indian Ocean locations and in cores free of margin sedimentation processes was able to see faunal changes which indicated a Pleistocene-Holocene sea surface temperature change of 5°C or less.

Descriptive Physical Oceanography of the Somali Basin Area

The Indian Ocean differs from other oceans in some respects due to its special geographic configuration. First, the Somali Basin is landlocked to the north which effectively excludes any north-south circulation driven by Arctic water. Second, the Somali Basin has sill depths which preclude significant present day Antarctic Bottom Water circulation (Warren, 1974). Third, the geographic arrangement of ocean and continent and their contrasting thermal properties together with seasonal fluctuations in solar radiation results in reversal of winds and surface currents over much of the Somali Basin. These three factors are predominantly responsible for the large scale aspects of the circulation in the area; these include the monsoon current system, the equatorial current systems, and bottom currents.

The southwest monsoon atmospheric and oceanic circulation system predominates during the summer months, May to September. During that time a high pressure area in the South Central Indian Ocean and a low pressure area over northern India are responsible for the atmospheric circulation which in turn drives the near surface oceanic circulation.

Water mass properties and dynamic topography delineate the features of the southwest monsoon. In figure 24 sea surface temperature for July 1963 (Wyrtki, 1971) is shown. Although the details vary from year to year the general nature of the phenomenon remains, and upwelling along the coast of East Africa is represented by cooler waters (25°C and less) while the central portion of the ocean has waters above 28°C. A wedge of warm surface water may be seen entering from the Gulf of Aden-Red Sea area which is common for this month (Warren, Stommel, and Swallow, 1966). Dynamic topography of the area (Bruce, 1968; Düing, 1970) reveals a complex series of cyclonic and anticyclonic cells with associated flow patterns. Thus, the Somali Current does not separate from the coast simply but rather in a complex circular flow.

Figure 24.

Western Indian Ocean sea surface temperature in January and July 1963. Isotherms are contoured at 1°C intervals based on Wyrtki (1971).

SEA SURFACE TEMPERATURE
JANUARY 1963

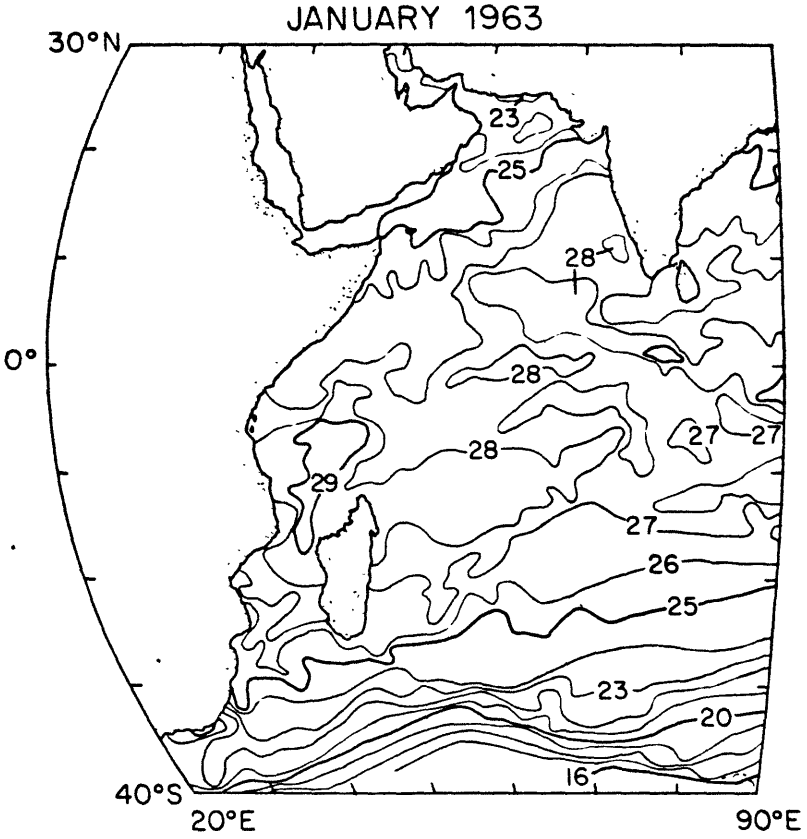

SEA SURFACE TEMPERATURE
JULY 1963

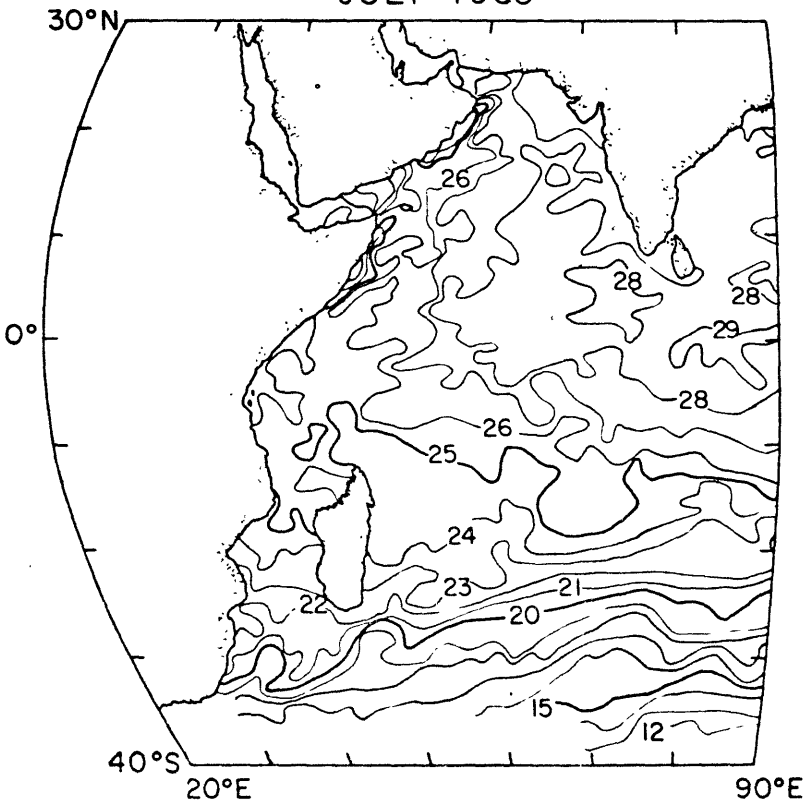

The velocity and transport of the Somali Current have been discussed by several authors including Swallow and Bruce (1966), and Bruce (1969; 1970; 1973). During 1964 the Somali Current (0-200 m) increased in width between 0° - 8°N, had a speed exceeding 200 cm/sec and turned east near 9°N (Swallow and Bruce, 1966). The departure of the current from the coast results in a variable pattern of upwelling related to the currents. For example, in August 1970 separate regions of upwelling at 6°N and 10°N, each associated with separate seaward turning branches of the current, were observed (Bruce, 1973). Subsequently the two branches merged.

During the northeast monsoon, from November to March, sea surface temperature shows very gentle horizontal gradients and no upwelling in the northern Somali Basin (figure 24b). Currents associated with this northeast monsoon system may reflect continuation of the summer circulation although at greater depth (Bruce and Volkmann, 1969).

Equatorial circulation in the Indian Ocean shows many features in common with the Pacific but it is subjected to a seasonal reversal of atmospheric circulation. Near surface equatorial circulation systems are generally composed of westward

flowing north equatorial currents at ~ 10°N, an eastward flowing north equatorial counter current at 5° - 10°N, a westward flowing south equatorial current 5°N to 5°S with an eastward flowing subsurface equatorial undercurrent imbedded in it, a westward flowing intermediate equatorial current below this system (5°N to 5°S, > 250 m) and an eastward flowing south equatorial countercurrent at approximately 10°S to 15°S (Philander, 1973). Variable atmospheric conditions over the Indian Ocean modify this typically Pacific Ocean scheme.

During the northeast monsoon the relatively shallow surface drift flows south along the coast of Somalia and turns east along the equator, with the countercurrent flowing on both sides of the equator during November and December (Wyrtki, 1973). But during January-April the countercurrent is entirely south of the equator with its southern boundary near 10°S (Wyrtki, 1973). In March 1964 at 58°E the eastward flowing equatorial undercurrent was observed at an average speed of 100 cm/sec below the westward flowing surface currents which have a transport of 40 million m^3/sec. At 61°E in March 1963 the undercurrent had a maximum velocity of 30 - 80 cm/sec (Taft and Knauss, 1967) which Swallow (1967) has related to the variation in wind stress.

However, during the southwest monsoon major changes in circulation in the northern Indian Ocean have large effects on the equatorial current pattern. In July when the Somali Current is strongest, all flow north of the equator is eastward with the countercurrent shifted north and joined to the monsoon current while the south equatorial current strengthens in its location (Wyrtki, 1973). Taft and Knauss (1967) were unable to observe the equatorial undercurrent during the southwest monsoon of 1963. Swallow (1967) found early in the southwest monsoon an undercurrent was present. However, Bruce (1973) reported that during August a westward component existed from the equator to 5°N while the eastward flowing undercurrent when observed was at 1 - 2°S. Thus the undercurrent was considerably diminished (transport east 5 x 10^6 m^3/sec) and its axis was shifted south (Bruce, 1973).

In analogy with the Pacific the extent of upwelling associated with the Indian Ocean equatorial currents may be considered. At the outset three factors must be acknowledged. First, a complete physical explanation of upwelling systems incorporating all their variability is not available. Second, in the physical sense upwelling implies vertical velocities

which although they have not been adequately measured are usually inferred from water mass characteristics. And third, upwelling in the biological sense implies an increased availability of nutrients in the photic zone and the productivity associated with it. The sedimentary record being even farther removed records certain facets of the increased productivity. Cromwell (1953) and Stommel (1960) describe divergent surface flow on the equator due to westward wind stress with 0 Coriolis force at the equator but poleward transport in regions away from the equator where Coriolis force increases. Such a mechanism could explain equatorial upwelling in the Indian Ocean during one-half of the year. Reports of upwelling in the equatorial Indian Ocean are not detailed although most investigators find some indication of it occurring under present conditions (Knauss and Taft, 1964). However, at the coast of Africa the divergence of the south equatorial current during the southwest monsoon results in upwelling as part of the current joins the Somali Current while the rest turns south (Duncan, 1970).

The Somali Basin is isolated from bottom waters in adjacent basins by the Carlsberg Ridge on the north. To the south and east the mid-Indian ridge and Mascarene Plateau form a barrier. Directly south the Mozambique Channel is quite shallow but just northeast of Madagascar the Amirante Trench deepens to over 4 kms. The sills in the trench area (9°30'S, 54°15'E and 9°15'S, 53°15'E) although not adequately mapped appear too shallow (4200 - 4400 m and 4000 - 4200 m) to permit the deepest few hundred meters of Mascarene basin water to enter (Warren, 1974). The bottom potential temperature minimum in the southern Somali Basin is 0.82°C which corresponds with the 3900 m isotherm at 12°S in the Mascarene Basin. Bottom water current velocities east of Madagascar of 6-7 cm/sec (Warren, 1971) are therefore not expected in the Somali Basin.

Primary Productivity in the Somali Basin Area

Primary productivity in the Somali Basin has long been recognized as a function of circulation and its seasonal variability. However, due to the large area and complications introduced by carbon assimilation measurement detailed measurements allowing seasonal mapping have not been completed. Ryther and Menzel (1965) measured nutrients in the post-southwest

monsoon season and found nutrient concentration in the central Arabian Sea (nitrate 56.2 ug A/l) about twice that of the Sargasso Sea (29.0 ug A/l) in the North Atlantic. In spite of its high productivity the system is quite fragile as Ryther and Menzel (1965) demonstrated that the standing crop of organisms represents approximately one day of primary productivity.

Primay productivity maps (Ryther, et al., 1966; Kabanova, 1968) and discussions (Krey, 1973) note areas of high production. Ryther, et al (1966), although not including seasonal variability (figure 25), were able to demonstrate high productivity north of the South Equatorial Current. The Somali coast shows high productivity associated with the upwelling of nutrient rich deeper waters. Mean daily production (0.35 gC/m^2) is about twice the average ocean value but production values vary within two orders of magnitude (Ryther, et al., 1966).

Phytoplankton in the Somali Basin area has been predicted by Krey (1973) and sampled in isolated areas by Zernova and Ivanov (1964) and Thorrington-Smith (1971). In the most recent study Thorrington-Smith (1971) was able to recognize four phyto-hydrographic regions in the equatorial area from 60° - 70°E, some of which are specifically related to the equatorial

Figure 25.

Western Indian Ocean sea surface productivity measured in grams of carbon assimilated per m^2 per day as shown in Ryther et al., 1966.

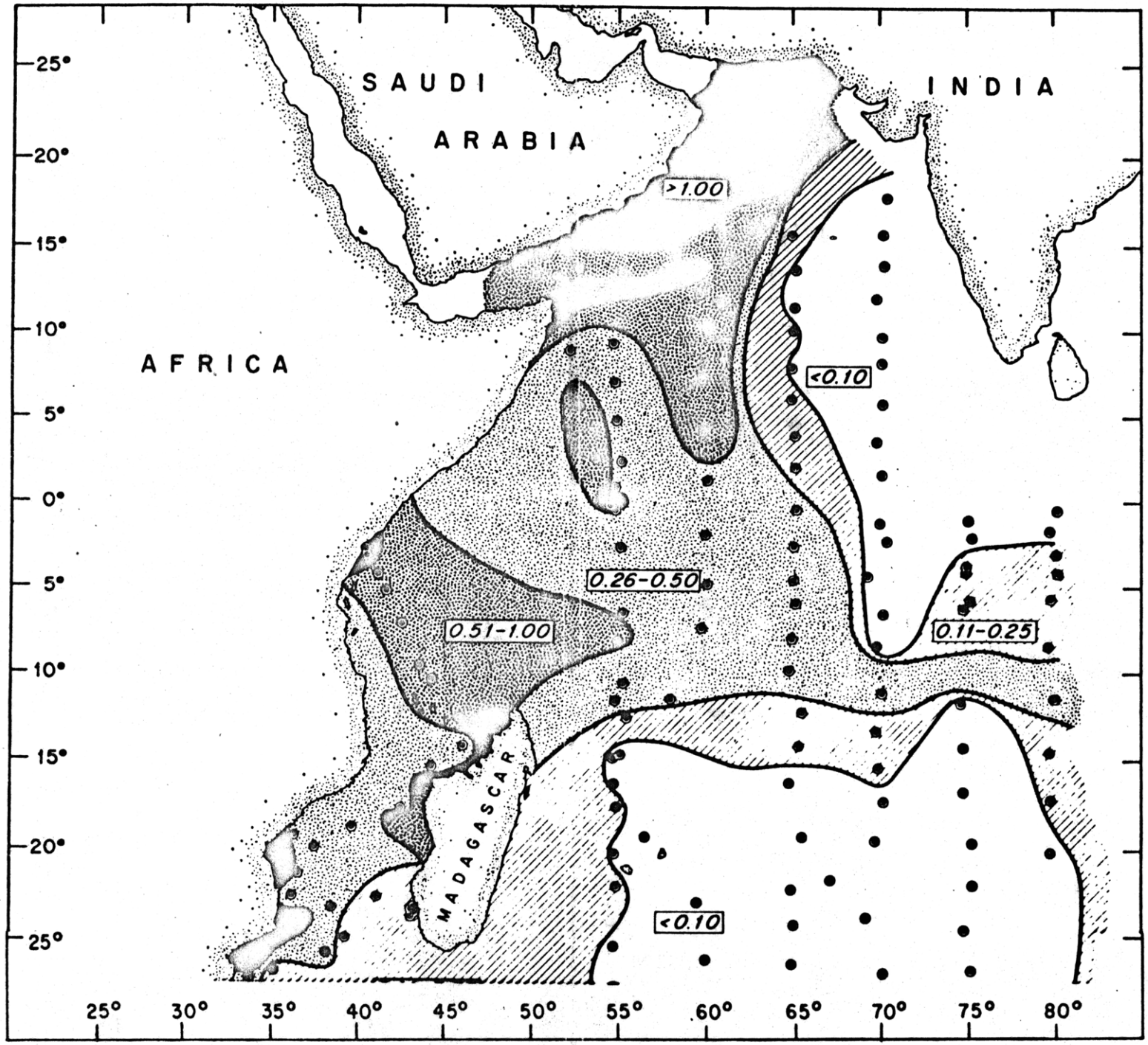
SAUDI
ARABIA
INDIA
AFRICA
MADAGASCAR
>1.00
<0.10
0.26-0.50
0.51-1.00
0.11-0.25
<0.10
25°
20°
15°
10°
5°
0°
5°
10°
15°
20°
25°
25°
30°
35°
40°
45°
50°
55°
60°
65°
70°
75°
80°

undercurrent.

Zooplankton communities have been related to divergence zones, poor divergence zones, and stable stratification zones in the surface waters (Timonin, 1971). Of the zooplankton, foraminifera have received the most attention in plankton tow work. Be and Tolderlund (1971) mapped occurrences of foraminifera in Indian Ocean surface waters but did not consider seasonal variability. Globigerina bulloides occurred in great numbers just south of the horn of Africa presumably associated with upwelling there.

Zobel (1971) in a more detailed study of plankton tows near the Somali coast during the northeast monsoon found, "The absolute abundance of foraminifera is dependent on the presence of upwelling water." (p. 1333) and the species distribution is influenced by horizontal mixing of surface water. She maps distributions of Globigerinoids sacculifer, G. ruber, Globorotalia cultrata, Globigerinella siphonifera which occur in amounts greater than 30% along the Somali coast. G. bulloides is shown to occur up to 30% in the more active upwelling areas along the coast of India.

In summary both total productivity and occurrence of some specific organisms reflect the predominant physical oceanographic features of the Somali Basin. Upwelling areas unique in the world's oceans mark the Somali Basin. Total productivity twice the world average is found there. Diatoms generally appear more prevalent in upwelling areas (Krey, 1973) and the distribution of G. bulloides is almost exclusively limited to such areas (Be and Tolderlund, 1971; and Zobel, 1971) while total productivity of foraminifera increases in upwelling areas (Zobel, 1971).

OBJECTIVES

The objective of this section is to examine the late Quaternary carbonate record of the Somali Basin and infer the principal oceanographic and climatic processes responsible for it.

This final step in the combined analysis of the structural and sedimentological evolution of the Somali Basin will therefore concentrate on present conditions in the ocean, their sediment record, recent variability indicated by the sediment record, and the mechanisms responsible. Whereas, on a time scale of structural evolution the sediment record was determined by the evolution of large scale ocean features, the shorter late

Quaternary carbonate record may reflect changes in the main ocean features. The method of study and data collected will be discussed in the next section. This forms a basis for understanding the major processes whose fluctuation in turn is the foundation of paleooceanographic and paleoclimatic change which are discussed in the final section.

METHOD OF STUDY

Eighteen cores from the Somali Basin (figure 26) were sampled and smear slides were prepared and examined under the light microscope. Visual estimations of the various components were tabulated and displayed as variation down core (Appendix I). This information coupled with core descriptions forms the basis of lithologic variability observed in the cores.

Selected cores were treated in more detail and nannofossil variability down core was established in the light microscope as a general index of temperature variability (Appendix IV). Radiocarbon analyses were obtained from 5 cores which had been sampled on the basis of preliminary nannofossil age determinations and published literature in the area (Appendix III). This information on 18 cores from the area was supplemented by published data from 10 Swedish Deep Sea Expedition cores in the Somali Basin (Olausson, 1960).

Figure 26.

Core locations in the Somali Basin area. Core numbers > 100 indicate samples taken on the Swedish Deep Sea Expedition, Olausson (1960). Other numbers refer to cores described in detail in Appendix I.

CORE LOCATIONS

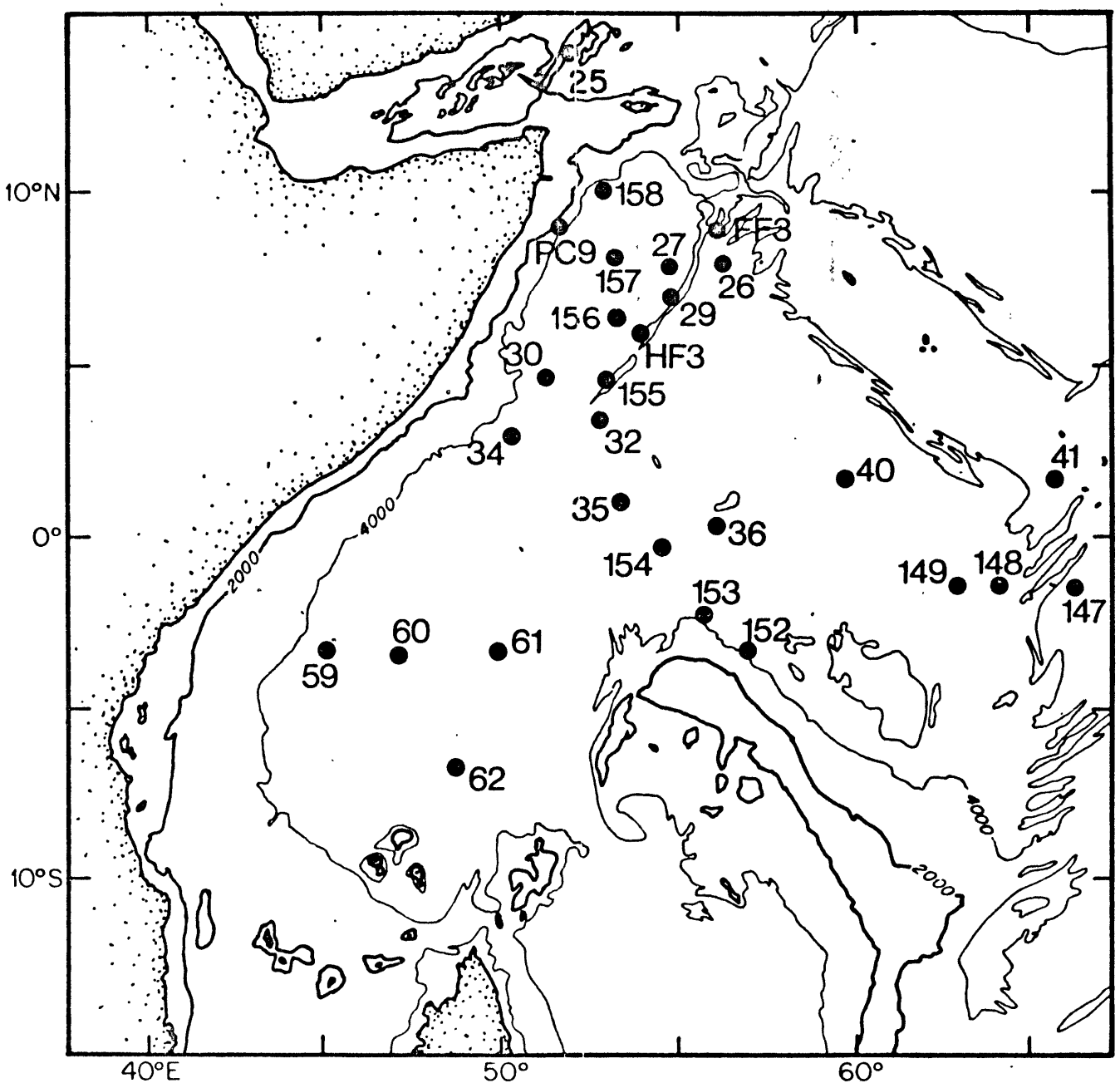

CORE LITHOLOGY

Carbonate Content of the Somali Basin Cores

The carbonate content from a total of 28 cores in the Somali Basin area was used to interpret the sediment record from the area. In spite of water depths equal to or greater than 5000 m only very few cores display sections that are free from nannofossil and foraminfera carbonate.

In the 18 cores described in Appendix I, carbonate content has been visually estimated through the foraminifera and nannofossil components visible in the smear slides. This method, which estimates amount from observed cross section areas, is sensitive for low carbonate values but as carbonate increases its discrimatory power is reduced. Cores 40, 61, and 25 show substantial intervals that are free of carbonate; other cores display considerably lowered values in some sections (Appendix I).

Chemical determination of total carbonate was reported on 10 Swedish Deep Sea Expedition Cores from the Somali Basin (Olausson, 1960). However, the cause of the variability was never discussed. Throughout the basin average total carbonate values of 40% to 50% or more are common. Some curves notably

core 154 show carbonate values of less than 10% in conjunction with sharp increases.

Lithologic Variability of Late Quaternary Somali Basin Sediments

The main components of Somali Basin sediments and their qualitative variability are shown in Appendix I. Inorganic components include detrital grains, micronodules, zeolites, volcanic shards, and clay minerals. Detrital grains and clay minerals are more common and amount to about 10% of each sample by visual estimate. A few cores - 25, 60, and the lower part of 61 - exhibit very high percentages of sand and silt size detrital grains. In core 25 which is from the Alula Fartak Trench the source of the high detrital content is most likely Saudi Arabia. Cores 60 and 61 in the southern Somali Basin are probably influenced by river input in the Cape Delgado area (10°S in East Africa) and subsequent gravity transport of the material.

The siliceous component of the sediments includes all non-crystalline silica from diatoms, radiolaria and sponges. Although these components were visually estimated separately, they are presented as a sum in the curves for each core.

The calcareous material has been divided into foraminifera and nannofossils which usually represent coarse and fine fraction carbonates respectively. Observations of coarse carbonate in other oceans have been an important part in interpreting variability in late Quaternary ocean processes which may be related to climatic change. W. Schott (1935) was the first to note fluctuation in coarse foraminiferal carbonate in Atlantic sediments and he related it to glacial-interglacial variations. Arrhenius (p. 57, 1952) found increases in foraminiferal concentrations in the equatorial Pacific sediments which he attributed to lower temperature surface waters and upwelling. Emiliani (1955) found a correlation between the coarse carbonate fraction (> 62u) and oxygen isotope curves which was subsequently treated in more detail by Broecker (1971). Broecker's (1971) analysis of three Atlantic cores indicates that the coarse fraction (> 64 or > 75 u) carbonate accumulates at a higher rate during interglacials (p. 256) while total carbonate remains nearly constant. Pacific cores indicate the converse (Broecker, 1971, p. 256; Arrhenius, 1952) with foraminiferal shells being deposited at a higher rate during glacials. Broecker (1971, p. 261) infers from accumulation rate data that more dissolution occurred in all

oceans during interglacials than glacials and that increased coarse relative to fine carbonate in Pacific glacials reflects greater interglacial dissolution there. Berger (1973) reaffirmed these indications of greater interglacial dissolution. Olausson (1971) has shown that an appreciable change in foraminifera per unit volume of sediment reflects a change in supply or dissolution which he asserts (p. 377) could be caused by climatic variations. In summary, observations of the variation in coarse carbonate have formed the basis of a substantial understanding of late Quaternary sedimentation in the Atlantic and Pacific Oceans even though some details of interpretation are in dispute. Therefore, observation of the coarse carbonate fraction in the Indian Ocean may reasonably be expected to be of importance.

In the past sieving has been used to determine the amount of coarse material but because this fraction may contain siliceous material (Arrhenius, 1952) and the calcareous foraminiferal tests are subject to physical degradation or dissolution (Broecker, 1971) they as well as the juvenile forms may be in the fine fraction which would introduce an error. Point-counting would substantially reduce these errors in identifying the amount of foraminiferal carbonate in a given sample at the cost of greatly

increasing the time for analysis. Visual estimates of the percentage of the field of view occupied by foraminiferal carbonate provided a reasonable compromise between accuracy and speed which enables large numbers of samples to be considered giving a wide geographic and stratigraphic coverage.

In Appendix I over 500 samples from 18 different cores were analyzed using this method. As successive samples from an individual core were examined a commonly recurrent pattern of absence and then presence usually not exceeding a few tens of percent was noted. As the observed variation is primarily of a presence-absence nature the methodology should quite accurately reflect the sedimentary record. As variations in coarse carbonate proved helpful elsewhere, an index to indicate in which Somali Basin cores the enrichment in coarse carbonate occurs more frequently was devised. Each peak in the foraminiferal carbonate curve was counted for a given core and standardized with respect to the length of the core (Table 3). Thus, if sedimentation rates do not vary too greatly throughout the basin these numbers provide a measure of how frequently the process is occurring at the different core locations. The chronology of and cause for the carbonate lithologic variation will be treated in following sections.

TABLE 3

Frequency of Foram Enrichment Per Unit Length of Core

Core Number	Water Depth Corr m	Core Length Cm	Total Number Foram Beds	Beds/m
25	5329	570	0	0
26	4680	1142	5	.44
27	5102	1146	8	.70
29	5106	1156	10	.86
30	5049	1106	5	.45
32	5123	959	3	.31
34	5004	895	5	.56
35	5101	1053	12	1.14
36	4576	866	6	.69
40	5426	599	2	.33
41	3433	511	8	1.57
59	4444	850	8	.94
60	4832	815	2	.25
61	4897	1005	1	.10
62	4425	973	8	.82
HF3	5099	580	4	.69
FF3	4001	106	2	1.89
PC9	3985	875	10	1.14

CORE BIOSTRATIGRAPHY AND SEDIMENTATION RATES

Late Quaternary Nannofossil Assemblage Variation

In Appendix IV an approximate index for paleotemperature assessment is discussed. The approach indicated by that method which employs a ratio of *Gephyrocapsa spp.* plus *Emiliania huxleyi* versus all other nannofossils will be applied to Somali Basin sediments.

Core 62 at the north end of the Mozambique Channel was sampled at a 10 cm interval to 150 cm. In each sample 300 individuals were observed and the ratio calculated as shown in Table 4. Present day sea surface temperature in that area (6°46'S) varies between 25-26°C in July to over 28°C in December (Wyrtki, 1972) and the surface sediment sample showed a ratio of 6.15. The ratio down to 150 cm in that core (figure 27) fluctuates from less than 4 to over 10 but remains within the equatorial temperature-ratio domain indicating sea surface temperature in that area remained about 26° to 29°C for the interval sampled.

Core PC9 located in the upwelling area near the horn of Africa at 8°59'N was also sampled to a depth of 460 cm and the ratio was calculated (Table 4). At the sediment surface the

TABLE 4

Core 62 Nannofossil Ratios

Level in CM	G.Spp + E. huxleyi	Other	G/O	Level in CM	G.Spp. + E. huxleyi	Other	G/O
0	258	42	6.2	60	177	133	1.3
10	263	37	7.1	80	132	181	.7
20	265	35	7.6	100	140	178	.8
30	268	32	8.4	120	152	161	.9
40	246	54	4.6	140	111	202	.5
50	255	44	5.8	160	162	150	1.1
60	235	64	3.7	180	147	154	.9
70	278	22	12.6	200	130	170	.8
80	244	56	4.4	220	109	192	.6
90	257	43	6.0	240	84	249	.3
100	262	37	7.1	260	136	169	.8
110	262	39	6.7	280	91	250	.4
120	233	67	3.5	300	175	144	1.2
130	231	69	3.4	320	136	172	.8
140	269	30	8.7	340	151	165	.9
150	272	25	9.7	380	115	195	.6
	CORE PC9			400	118	199	.6
0	141	174	.8	420	169	150	1.1
10	142	160	.9	440	150	150	1.0
20	138	177	.8	460	173	144	1.2
40	177	161	1.1				

Figure 27.

Ratio of *Gephyrocapsa spp.* + *Emiliania huxleyi* to other nannofossil species in cores PC 9 and 62. (See Appendix IV for description of method.)

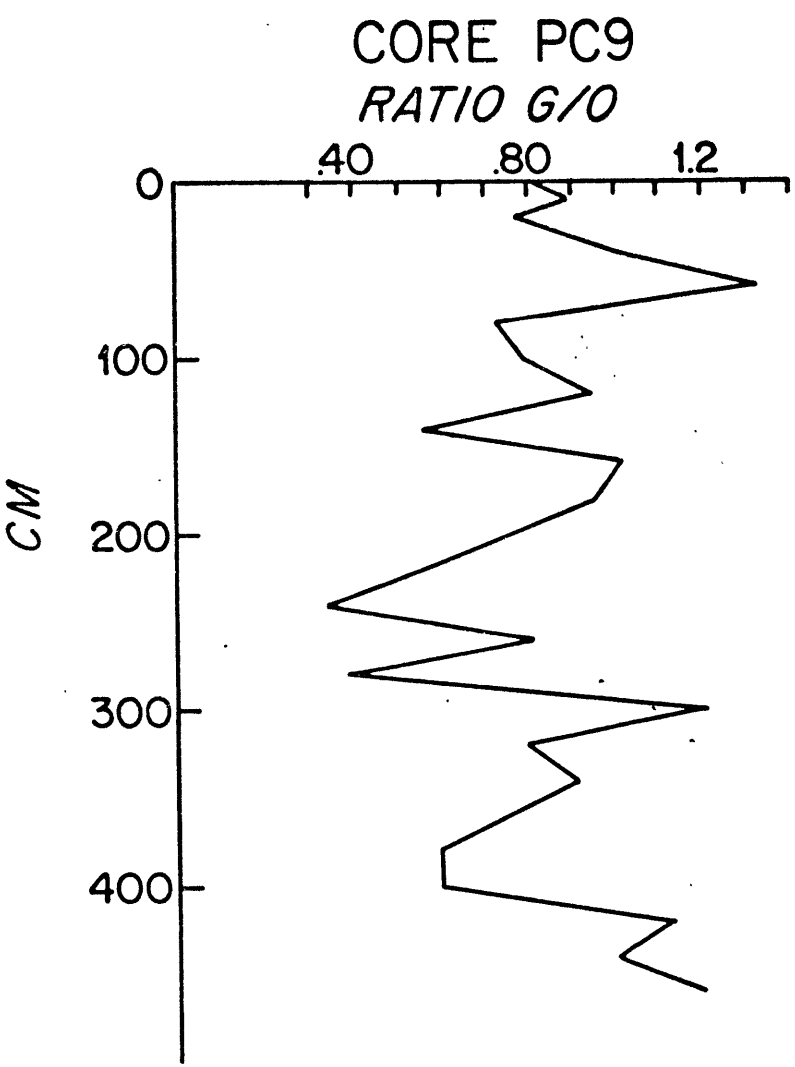
CORE PC9
RATIO G/O
.40
.80
1.2
0
100
200
300
400
CM

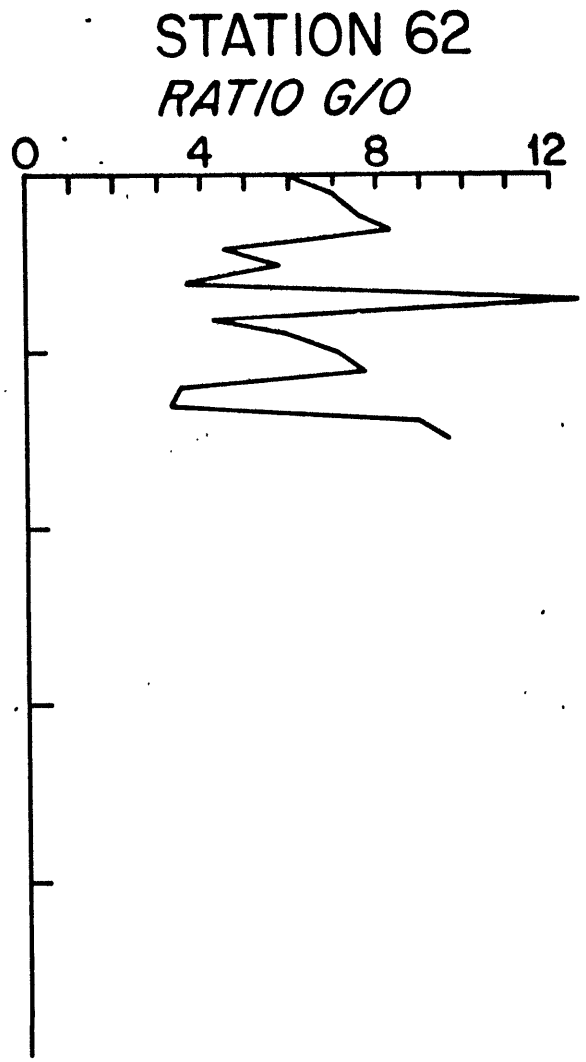
STATION 62
RATIO G/O
0
4
8
12

ratio is 0.81 and averaged sea surface temperature in the area varies from 24° - 25°C in July to around 26°C in December (Wyrtki, 1971). Thus, present conditions place PC9 in the sensitive area of the Pacific ratio curve (see Appendix, Figure 44, 9°N) where the value is rising rapidly consistent with high equatorial temperature. However, in the same area a slight temperature decrease would result in the ratio remaining below 1.0. Considering these factors indicated in the Pacific curve, Core PC9 shows continuous relatively cool temperatures for its latitude throughout the sampled interval.

Sediment Ages and Sedimentation Rates

The variation in total carbonate and its lithology throughout the Somali Basin and the mechanisms responsible can be related to an absolute chronology through age dating appropriate sediments. Table 5 is a summary of Appendices II and III which contain dates for various sediment horizons. Although in most cases exact dates are not given, the resulting minimum or maximum given allows comparison of the sedimentation rate.

The geographical variation in sedimentation rate during the period 0 - 170,000 years is shown in figure 28. Central portions

TABLE 5

Average Sedimentation Rates

Core	Sed. Rate 0-40,000	Sed. Rate 0-170,000	Error
59	<3.1	>5.0	
26	<3.6	<4.6	
27	---	>7.0	
30	<3.0	<6.5	
32	---	4.8	±0.7
34	---	4.5	±0.6
35	---	4.8	±0.4
36	<2.4	<4.5	
41	---	3.2?	±0.4
HF 3	---	4.0	±0.3
PC 9	<5.1	>5.0	

? = good preservation but uncertain identification

Figure 28.

Somali Basin sedimentation rates (cm/1000 years) for the past 170,000 years determined by first occurrence of Emiliani huxleyi (Appendix II).

AVERAGE SEDIMENTATION RATE IN CM/1000 YRS, 0-170,000 YRS

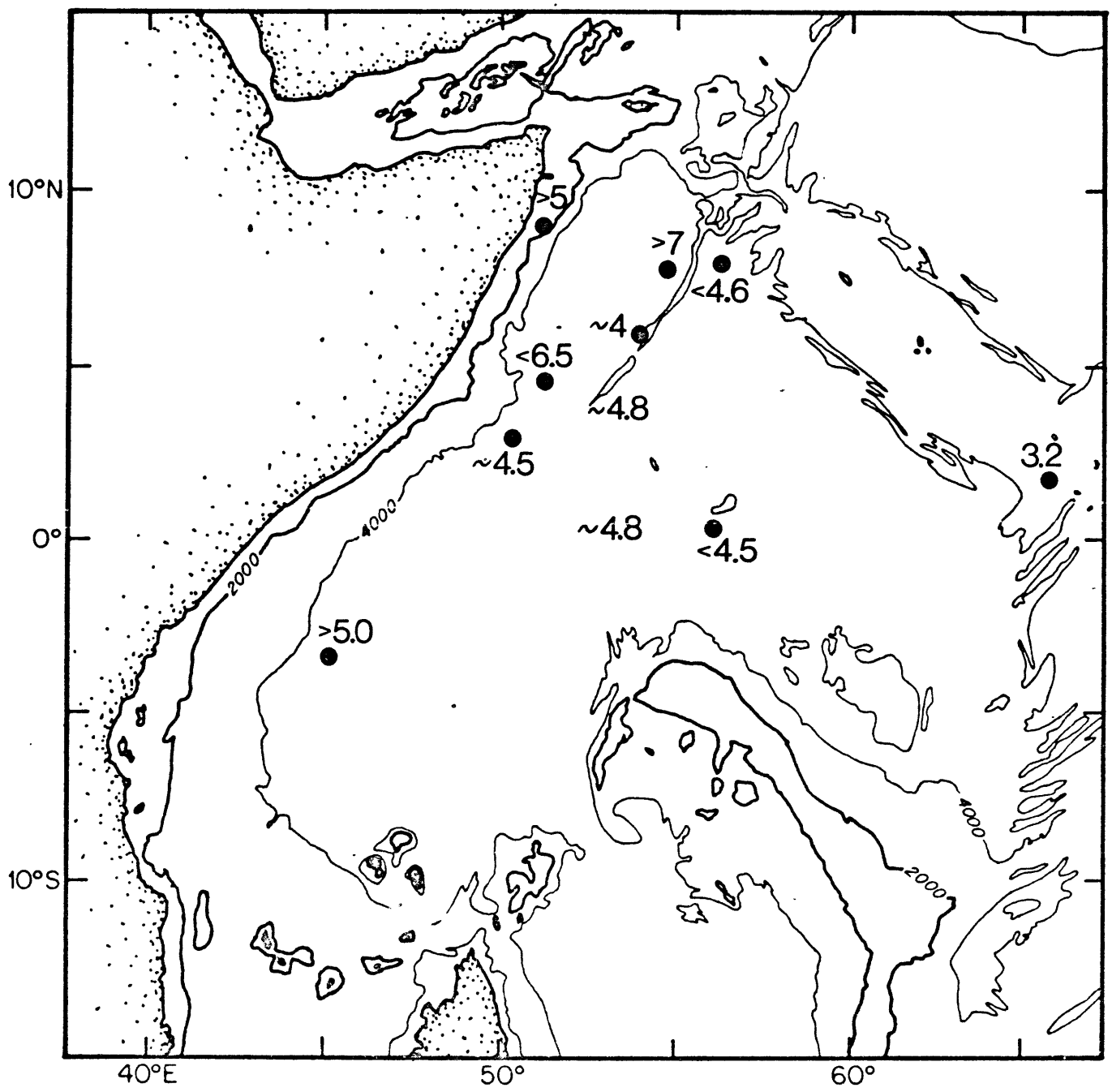

of the basin away from the coast show consistent sedimentation rates of less than 5 cm/1000 years. In the western part of the basin near the equator sedimentation rates exceed 5 cm/1000 years and the entrance to the Mozambique Channel in the southwestern portion of the basin shows a rate that may be as high as 6 cm/1000 years. In the northwestern sector of the basin sedimentation rates in excess of 5 cm/1000 years to over 7 cm/1000 years are recorded. This sector of the basin also exhibits the highest productivity values which may in part be responsible for the increased sedimentation rates.

Table 5 also indicates maximum average sedimentation rate for the period 0 - 40,000 years on the basis of radiocarbon results. Those rates are with the exception of PC9 all less than the rates over the longer time period.

DISCUSSION

Late Quaternary Variation in Carbonate Content and Bottom Water Intrusion

The carbonate content of Somali Basin cores from smear slide and chemical analyses displays two general patterns. There are cores with about 50% or more $CaCO_3$ which show minor fluctuations of total carbonate. In addition a second set of cores displays the same maximum values but also shows much lower minimum values of total carbonate with some carbonate free sections being noted. The total amount and characteristics of the carbonate component of pelagic sediments is commonly used to interpret events in the overlying water masses. Carbonate content may vary due to productivity, dilution, or dissolution. However, conditions in the Somali Basin indicate that dissolution may be the overriding factor and therefore the hypothesis that carbonate values reflect that process will be examined.

Figure 29, a composite plot of core latitude versus depth, shows the Swedish Deep Sea Expedition cores (Olausson, 1960) and those described here (Appendix I). The possible Antarctic Bottom Water sources for the basin are those described by Warren (1974) and the line from the shallowest sill depth separates cores

Figure 29.

Latitude versus water depth of Somali Basin cores. Location of sill is indicated by bars where the flow could enter the basin (Warren, 1974). Below the solid line are cores which have significant sections free of carbonate. The dotted line encloses those cores shown by triangles in which total carbonate regularly varies by greater than 30%. Triangles refer to Swedish Deep Sea Expedition cores (Olausson, 1960) and circles refer to cores in Appendix I.

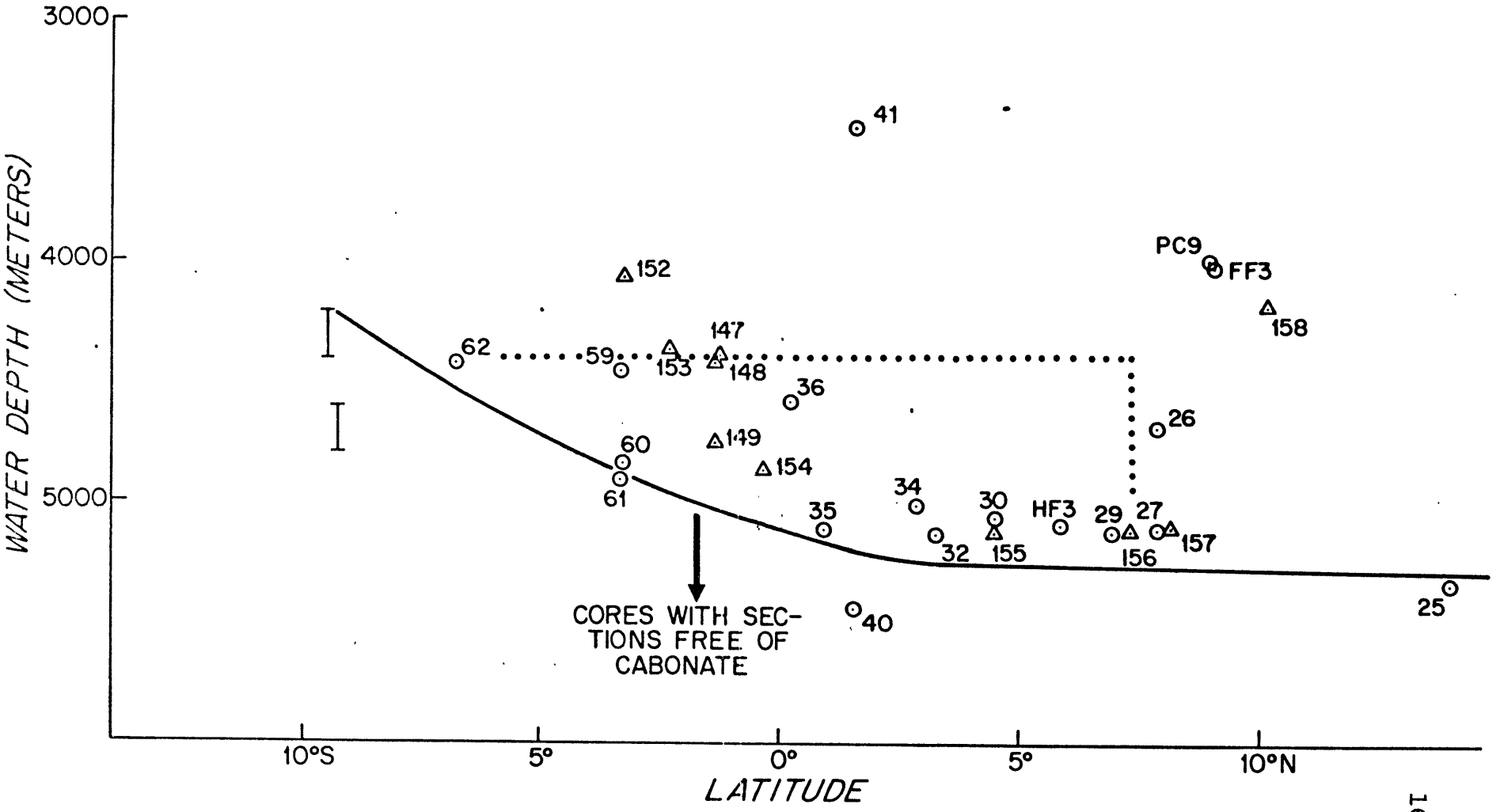
3000
4000
5000
WATER DEPTH (METERS)
41
PC9
FF3
158
152
147
62
59
153
148
36
26
60
149
154
61
34
30
HF3
29
27
157
35
32
155
156
CORES WITH SEC-
TIONS FREE OF
CABONATE
40
25
10°S
5°
0°
5°
10°N
LATITUDE

with continuous carbonate records from those with sections free of carbonate. Although the bathymetry of the area is not known in great detail cores 61 and 40 most likely lie in a single basin that could be influenced by the influx of bottom water. Core 25, which is free of carbonate throughout is from a separate and isolated environment, the Alula Fartak Trench far to the North.

In order to further evaluate the effects of bottom water on Somali Basin sediments the present bottom water and sediment surface conditions must be examined in greater detail. The deep western boundary current flowing northward along Madagascar is largely blocked from entering the Somali Basin by the shallow sill (Warren, 1974). That portion which enters the Somali Basin mixes with overlying waters sufficiently to lose the low bottom temperature of the Madagascar and Mascarene Basins (Warren, 1974). Some transport of bottom water into the basin has been indicated by the occurrence of isolated specimens of the high latitude diatom flora in surface sediments of the southern Somali Basin (Burckle et al., 1974). However, bottom photographs taken in the same area as core 61 show no current derived features which precludes any large magnitude bottom flow (figure 30). Thus, available data indicates present

Figure 30.

Sea bottom photograph at Station 61. Absence of current derived features indicates that if bottom water is entering the basin the rate of flow is low.

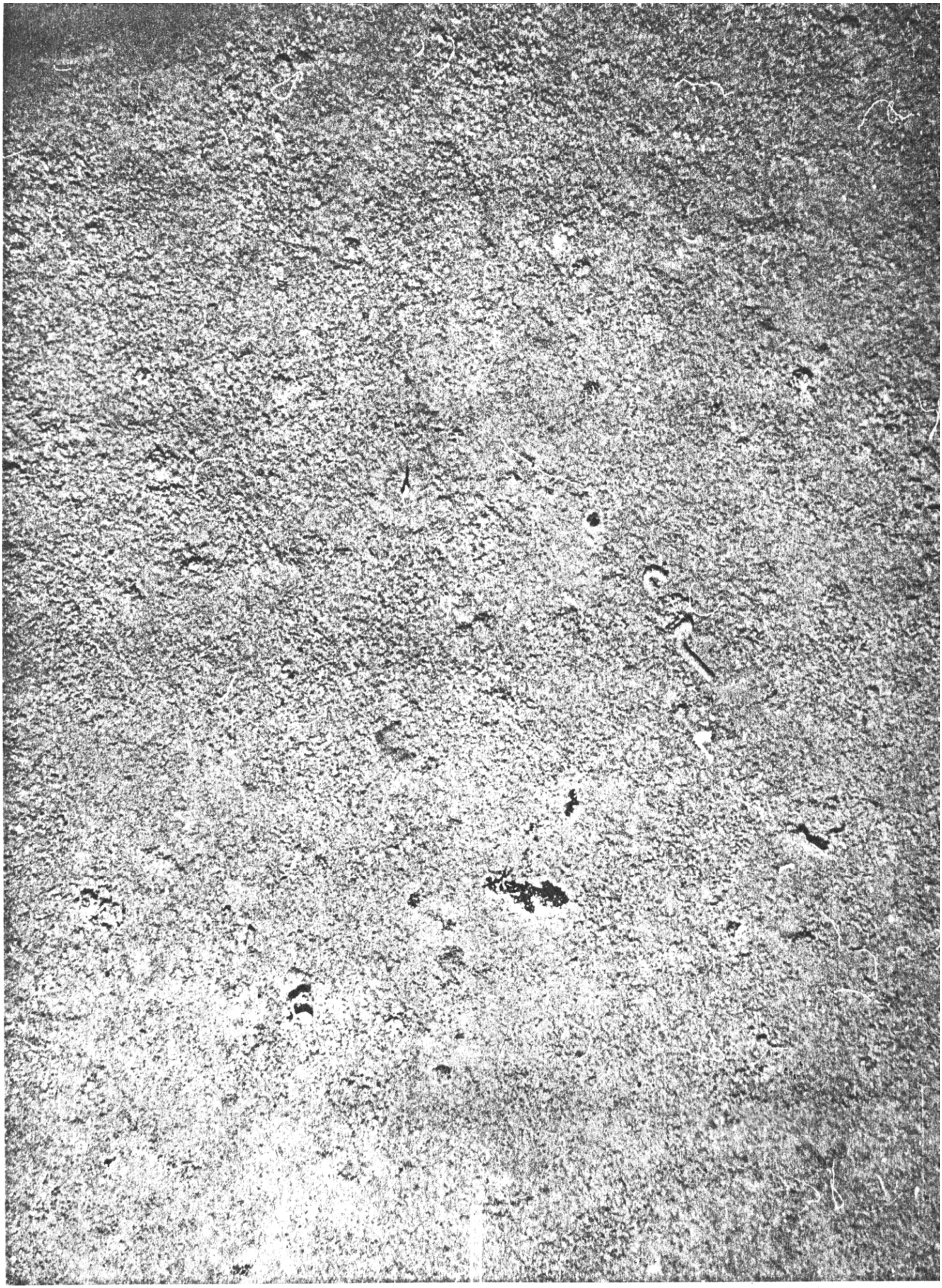

conditions admit limited bottom water transport northward from the Mascarene Basin through a sill which may be at either 4000 - 4200 m or 4200 - 4400 m (Warren, 1974).

In the past a greater supply of bottom water to the Mascarene Basin could have resulted in more of it crossing the sill into the Somali Basin. As increased bottom water activity may be recorded by a reduction in total carbonate the occurrence of carbonate free sections in cores 61 and 40 may form a basis for interpreting Somali Basin sediments. First the other possibilities must be considered. If carbonate cycles are solely due to fluctuations in productivity then absence of carbonate implies a lack of carbonate producing organisms in the surface waters. In addition, as the lack of this productivity would not reasonably be isolated nearby cores should show a similar absence of carbonate. However, continuous carbonate records are found near core 61 (see cores 60 and 62 in Appendix I) and near core 40 (see cores 41 and 36 in Appendix I). Likewise terrigenous or siliceous dilution could not explain total absence of carbonate as even a large relative contribution could not eliminate all carbonate. The third possible explanation for the lack of carbonate in certain sectors of cores 40 and 61 is dissolution exceeding supply due to increased bottom water flow

northward into the Somali Basin. Such increased bottom water activity would affect the deeper portions of the basin as well as those closer to the source of bottom water. Both these considerations are met as demonstrated in figure 29 which shows cores with carbonate free sections as being the deepest in the basin.

Only a trace of nannofossil carbonate was found in 4897 m at the sediment water interface of core 61. However, other cores further north in the basin and up to 200 m deeper (figure 29) contain carbonate at the surface (core 32 in Appendix I, for example). Core 40, although deeper, is farther from the source of bottom water and may be isolated by topographic barriers and therefore contains a greater amount of carbonate in present surface sediments.

Past increases in the total amount of bottom water may have caused significant dissolution in cores in the Somali Basin which apart from productivity or dilution variations should affect the deepest cores the most. The effected cores should, as noted earlier, have large fluctuations in total pelagic carbonate while those well above should be unaffected by dissolution and maintain relatively high total carbonate throughout. To test this hypothesis 10 cores from the Somali Basin for

which total carbonate has been determined will be examined (Olausson, 1960). Figure 31 a and b shows respectively West to East and South to North transects of cores with the core tops plotted according to water depth as shown to the left. Cores 148, 149, 154, 155, and possibly 156 all exhibit cyclic variation in total carbonate with maxima greater than 50% and near zero minima. Dependent upon the total carbonate amount that is chosen to indicate presence or absence of bottom water, these cores, even though carbonate does not fall to zero, may be used to indicate substantial influxes of late Quaternary bottom water into the basin. Hollister et al. (1974) found carbonate under present day Antarctic Bottom Water in the Samoan Passage which indicates substantial presence of bottom water does not necessarily remove all carbonate. The shallowest core with substantial carbonate decreases (148 at 4405 m) establishes the upper bathymetric limit of possible bottom water influence during the sampled interval. However, core 156 and core 157 occur 600 m deeper in the northern limits of the basin. There core 157 displays almost no fluctuation in total carbonate while core 156 displays minor total carbonate variations. Their lack of dissolution cycles may be explained by considering the effects of enhanced productivity in the northern Somali Basin.

Figure 31.

Total carbonate contents of Swedish Deep Sea Expedition cores (Olausson, 1960). Core top corresponds to depth at which core was taken. See Figure 26 for location of cores. Figure 31a represents a west to east section. Figure 31b represents a south to north section.

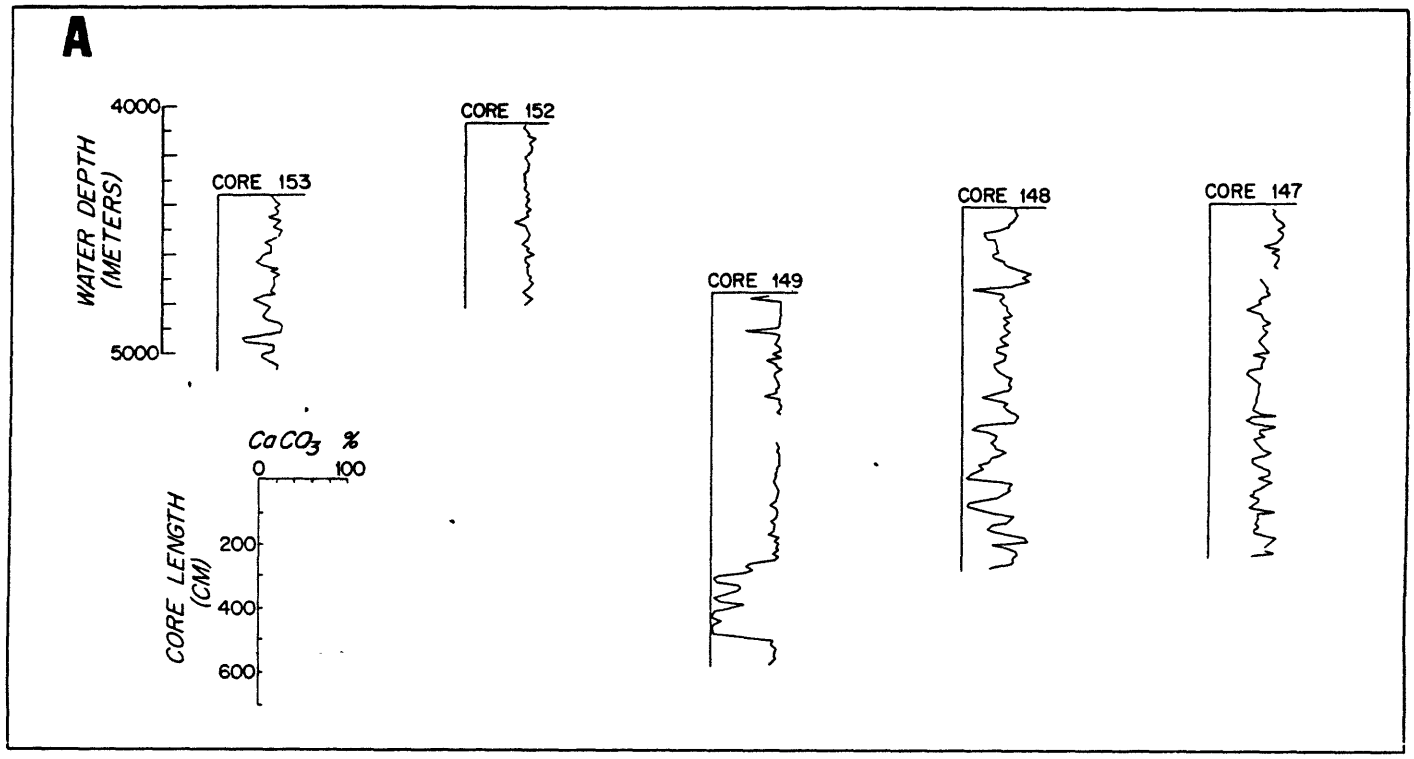
A
4000
WATER DEPTH (METERS)
5000
CORE 153
CORE 152
CORE 149
CORE 148
CORE 147
CaCO3 %
0
100
CORE LENGTH (CM)
200
400
600

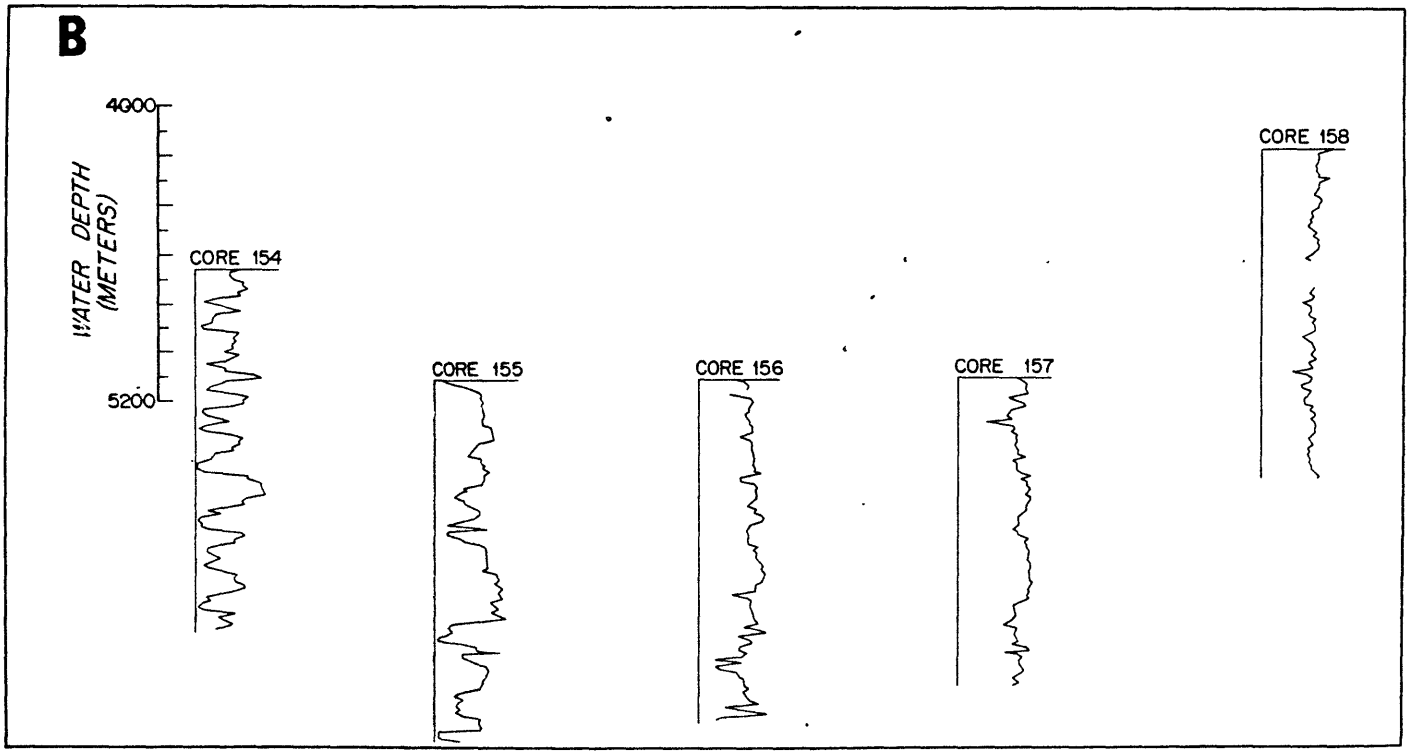
B
4000
WATER DEPTH (METERS)
5200
CORE 154
CORE 155
CORE 156
CORE 157
CORE 158

Analogous to equatorial Pacific observations (Arrhenius, 1952) high productivity off the coast of Somalia (Ryther et al., 1966) may have suppressed the effects of dissolution.

In summary, the dissolution effects related to increased bottom water during the Pleistocene have extended over most of the basin as shown in figure 32 and resulted in an approximately 800 m elevation of dissolution effects from 5200 m to 4400 m. High surface water productivity in the north has obscured the effect of dissolution there. These cycles in dissolution are related to increased bottom water flow which is the primary controlling factor for Somali Basin carbonate cycles.

Late Quaternary Variation in Carbonate Lithology

Examination of the smear slide analyses of cores presented in Appendix I demonstrates a discontinuous sequence of foraminifera deposition is common at most sites. Previous Indian Ocean studies (Stubbings, 1939; Oba, 1967; Olausson et al., 1971) have concentrated on the foraminifera fraction of the sediments to determine past oceanographic conditions. Therefore, this section will examine the probable causes for foraminifera

Figure 32.

Area of Somali Basin (shaded) where dissolution cycles are inferred from variation of total carbonate in Swedish Deep Sea Expedition cores (see figures 26, 31). Hydrographic work and postulated sill depths suggest that at most the upper portions of Mascarene Basin bottom water flows into the Somali Basin today (Warren, 1974).

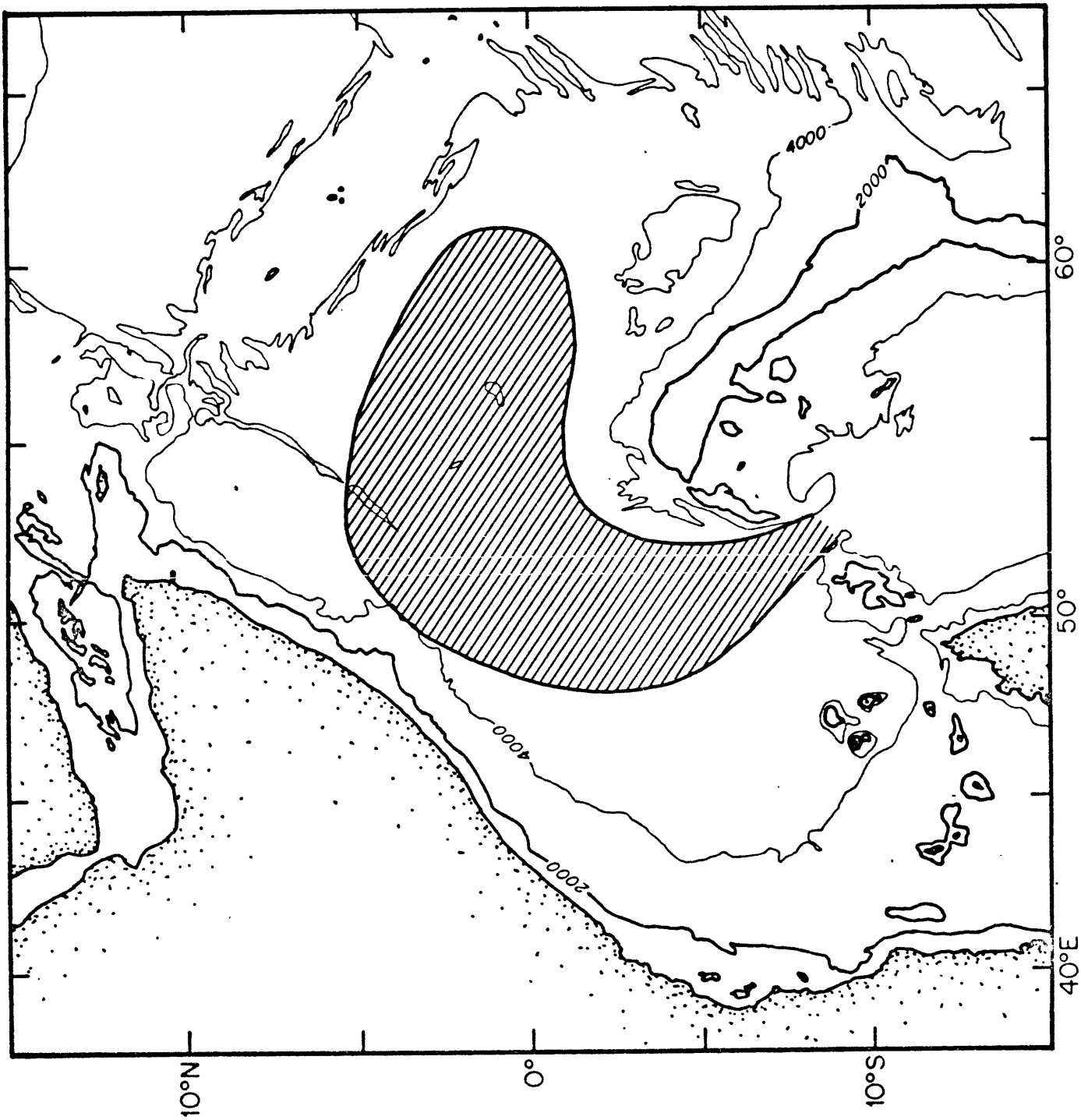
4000
2000
4000
2000
60°
50°
40°E
10°N
0°
10°S

enrichment in the sediments which could be due to selective dissolution, gravitational sedimentary processes, or variations in supply from the sea surface. Before determining the cause of these foraminifera layers in the sediments the following must be established: First, the determinations as shown in Appendix I rely primarily on presence-absence analysis in the smear slides and not on comparisons of many visually estimated percentages. Second, the foram layer frequency derived in and of itself is only a measure used to indicate in which areas the process occurs more often. Third, the method does not require any further assumptions be made but rather tests the available frequency data against the parameters associated with the processes that could control them.

Dissolution has been shown to affect the total carbonate content of many cores in the basin and therefore might be expected to control the occurrence of foraminiferal tests. If so, shallow water cores should display the greatest number of foraminiferal tests while in deep water almost all foraminifera should be absent. Accordingly figure 33 which shows the frequency of foram bed occurrence versus water depth should display a linear trend. The great variability in frequency from 0.1 to

Figure 33.

Frequency of Foraminifera test occurrence versus water depth in the Somali Basin.

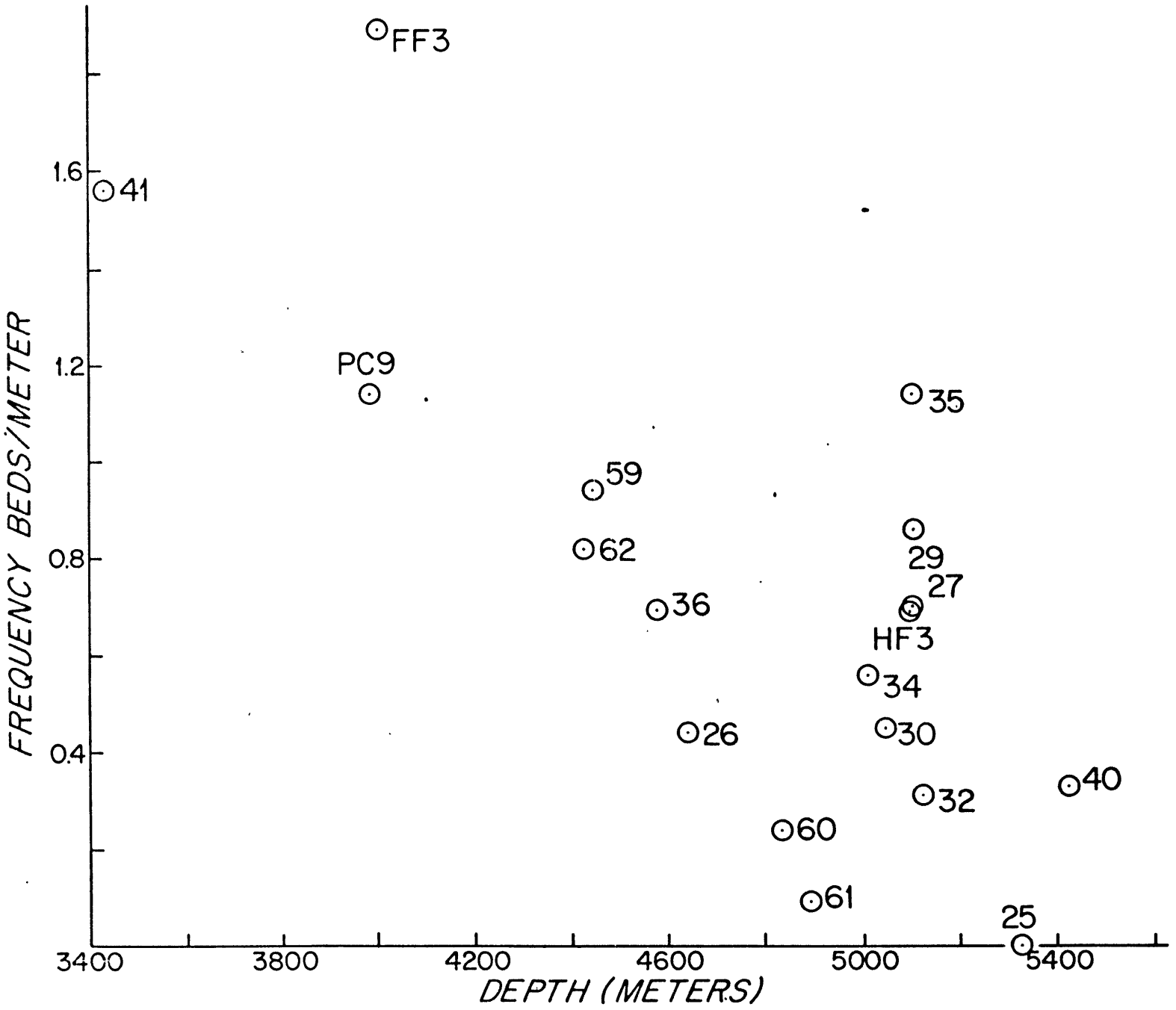
FF3
41
PC9
35
59
62
29
27
36
HF3
34
26
30
40
32
60
61
25
1.6
1.2
0.8
0.4
3400
3800
4200
4600
5000
5400
FREQUENCY BEDS/METER
DEPTH (METERS)

1.0 bed/m in the deeper water (5100 m) indicates that although dissolution may have an affect on the occurrence of forams it is not the predominant factor in these Somali Basin sediments.

Similarly if gravitational sedimentary processes such as slumping or turbidites are responsible for small scale formation of beds then a causative relationship between topography and occurrence should result. Large scale gravitational sedimentation processes should be visible in the cores as coarse grained terrigenous material or sharp contacts between distinctively different lithologic units but such features occur only rarely and can thus account for only a very small fraction of the total number of beds. Similarly graded beds, another sign of redeposition, were not macroscopically visible. A general index of sea bottom morphology was determined by drawing a circle of 1° latitude around each core and the number of 500 m contours up slope from the core for that area was determined. In figure 34 if gravitational processes predominate a linear relationship between foraminiferal test occurrence and a measure of the necessary topography for down-slope movement should emerge. However, the lack of that correlation indicates that on the basis

Figure 34.

Frequency of Foraminifera test occurrence versus sea bottom topography.

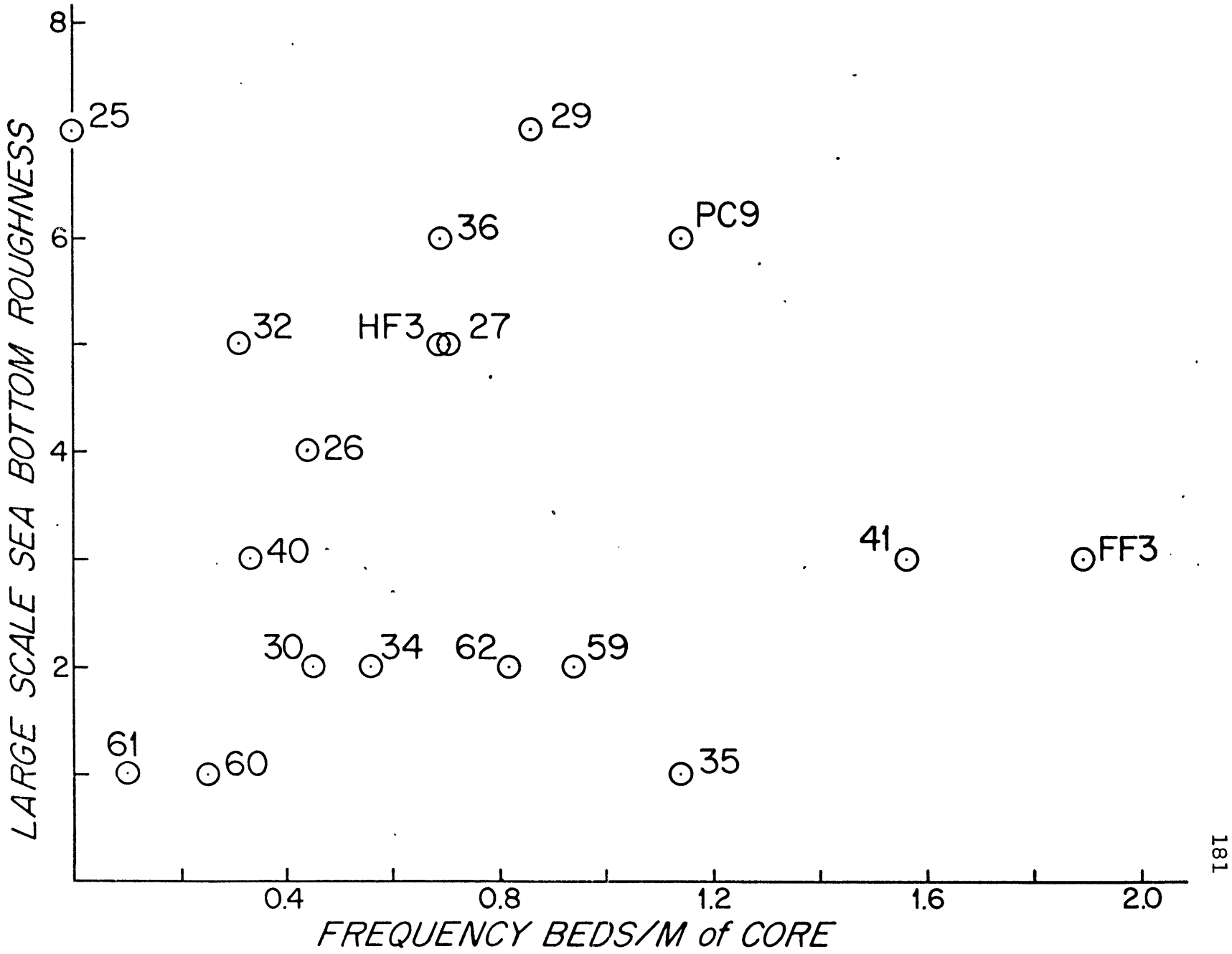
LARGE SCALE SEA BOTTOM ROUGHNESS
8
6
4
2
25
29
36
PC9
32
HF3
27
26
40
41
FF3
30
34
62
59
61
60
35
0.4
0.8
1.2
1.6
2.0
FREQUENCY BEDS/M of CORE

of this data gravitational sedimentation processes alone are not responsible.

Relationship between Carbonate Lithology and Upwelling

If foraminiferal test occurrence is related to variation in surface water productivity then present areas of productivity and general late Quaternary productivity should show some similarities assuming the variation induced by glacial and interglacial conditions in the area is a matter of degree and not kind. Studies of the surface water assemblage of Foraminifera in the northwestern Indian Ocean have shown anomalous occurrence of Globigerina bulloides near the equator off the Somali Coast (Zobel, 1971). Thus, if G. bulloides only flourishes in these near equatorial latitudes because of upwelling then its occurrence should coincide with other indications of upwelling during the late Pleistocene. Data from core 156 (Olausson et al., 1971) allows a test of this hypothesis by permitting a comparison of total foraminifera number with percent G. bulloides in the same samples. As shown in figure 35 every foram increase in the core has a corresponding increase in G. bulloides indicating a high degree of correlation between total foraminifera number and an indicator organism for upwelling. In two cases

Figure 35.

Globigerina bulloides and total number of pelagic Foraminifera in core 156 (Olausson, 1960).

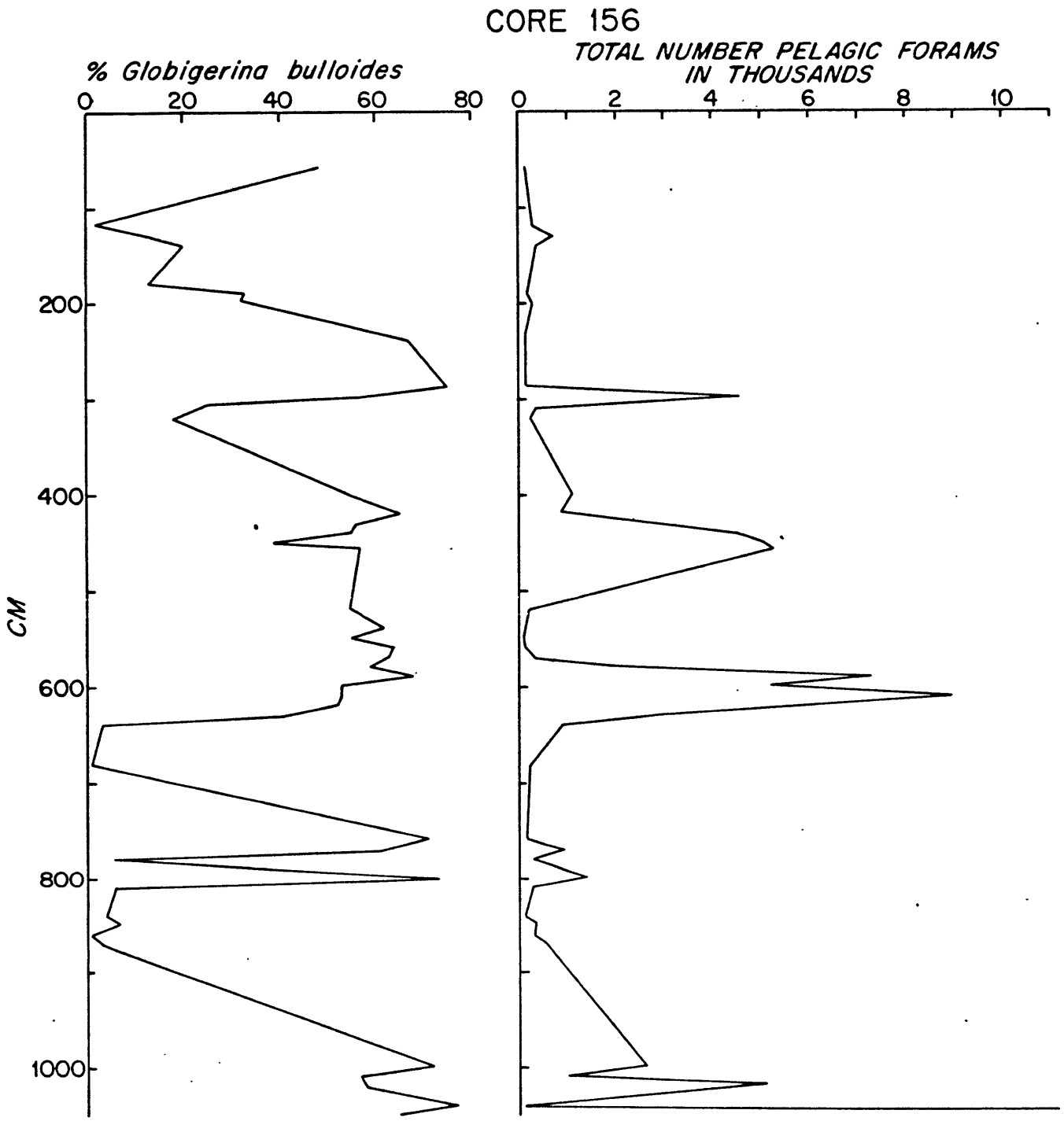
CORE 156
% Globigerina bulloides
0
20
40
60
80
TOTAL NUMBER PELAGIC FORAMS
IN THOUSANDS
0
2
4
6
8
10
CM
200
400
600
800
1000

60 cm and 525 cm to 757 cm a high percentage of G. bulloides is not matched with a high total foraminifera number. However, this relationship of G. bulloides to areas of upwelling makes it and possibly other foraminifera species highly unreliable as climatic indicators under such conditions unless the possible changes in the upwelling system are considered. G. bulloides most commonly indicates water temperatures of 5-10°C (Bé and Tolderlund, 1971) which is at least 10°C cooler than was observed during either monsoon in 1963 (figure 24). This cooling of surface waters coincidental with increased numbers of foraminiferas must reflect increased upwelling as near equatorial glacial conditions in other oceans resulted in temperature decreases of less than 2°C (McIntyre, 1974).

Figure 36 shows the distribution of foraminiferal beds per m core and the distribution of productivity under present conditions is shown in figure 25. The high frequencies off the coast of Somalia and in the equatorial regions are similar to high productivity under present conditions at each of these locations (figure 25). As total foraminifera numbers in present surface waters and upwelling are highly correlated in the northwestern Indian Ocean (Zobel, 1971) the correlation of high productivity and upwelling should follow.

Figure 36.

Frequency of Foraminiferal test occurrence per meter of core in the Somali Basin.

FORAMINIFERA ENRICHMENTS PER METER OF CORE

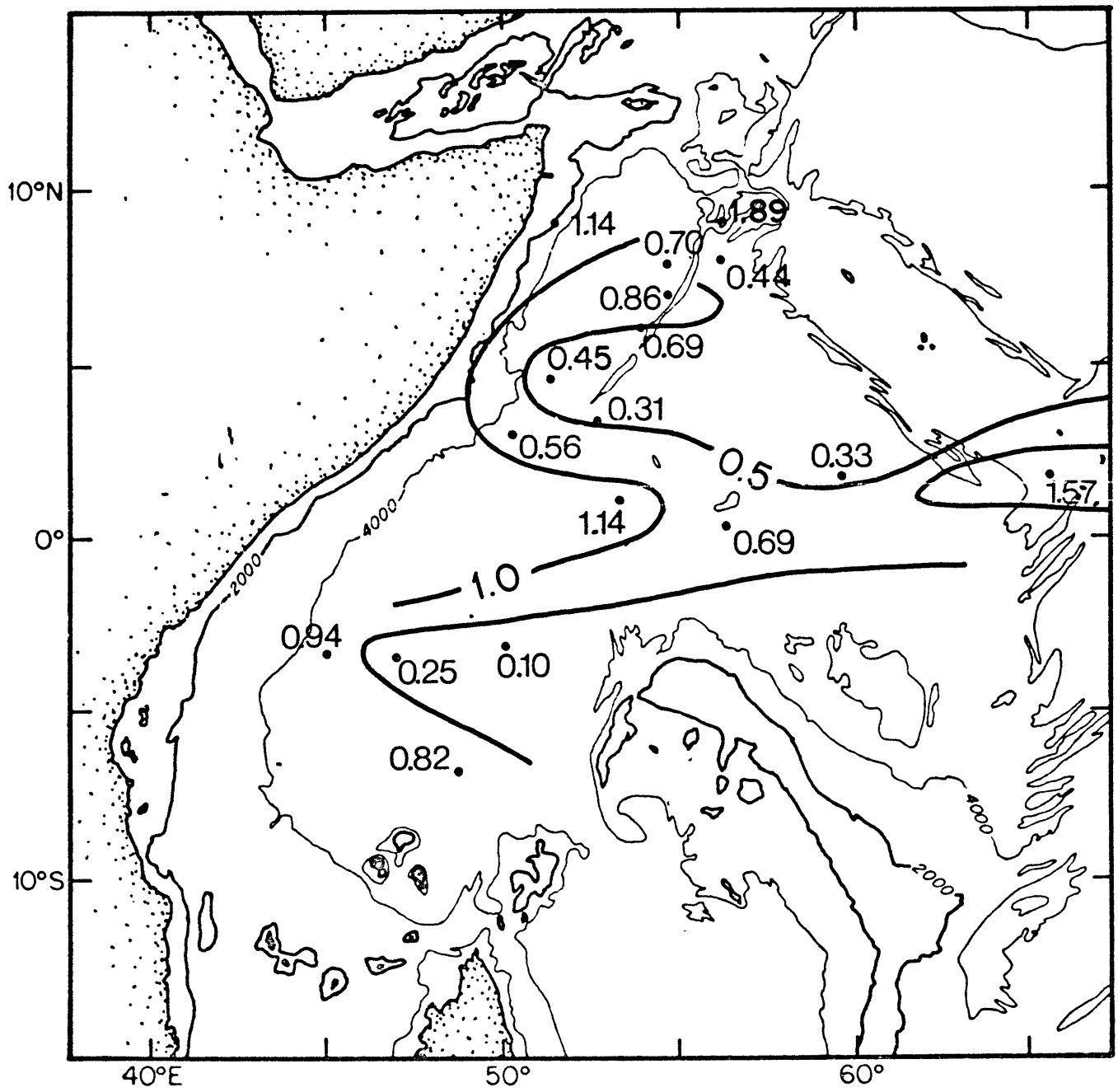

On the basis of the patterns shown the high present day upwelling off the coast of Somalia coincides with a frequency of 1 bed/m or more. Equatorial upwelling may have been more predominant in the past as a high frequency is present there but only partially supported by present day productivity values. In the southern part of the basin the divergence in the South Equatorial Current is not clearly indicated by the foraminiferal frequency but this may reflect an insufficient number of cores in the area. In summary, Somali Coast upwelling appears to have predominated during the late Quaternary to present while equatorial upwelling was more significant during the late Quaternary. Thus, in the Somali Basin these indications of cooler surface waters are primarily due to upwelling and may therefore more accurately indicate wind stress at the sea surface.

The Somali Basin Paleooceanographic Record and Climatic Change

Previous investigations of climatic change as described in the introduction to this section have generally interpreted the carbonate record in pelagic sediments and its dilution, dissolution, and changes in supply as being univariant with

respect to climatic phases. Consequently, the terms glacial and interglacial have been attached to an increase or decrease in each of these factors affecting the carbonates and discussion has centered upon which causes are significant in different areas and at different climatic phases. However, data from the Somali Basin suggests that dilution, change in supply, and dissolution may not vary in simple fashion with respect to time and each other. Therefore, the assessment of climatic change should be developed on the basis of distinct components.

The record of total carbonate in the Somali Basin exemplifies one process, dissolution, that reflects climatic variables. As indicated by dissolution in cores 148, 149, 154, and 155 the quantity of bottom water entering the basin through time has varied. To the extent that the rate of bottom water formation controls the rate of its entry into the Somali Basin the record of dissolution reflects conditions at the site of bottom water formation thousands of miles away rather than the northwestern Indian Ocean Pleistocene climate. Thus, that record may not be representative of fluctuations in local surface conditions. For those the record of sea surface temperature and upwelling in cores above the zone of dissolution provide more information. The nannofossil-temperature record of core 62

in the southern Somali Basin (figure 27) spans over 29,000 years when age is determined by approximations from nearby cores 59 and 63 (Appendix II). By analogy with present conditions the nannofossil record indicates a maintenance of the equatorial temperature regime of 26°C to 29°C over the time interval. A similar temperature record at core PC-9 in the northern Somali Basin covers 0 - 92,000 years as determined by approximate sedimentation rates for that core (Appendices II and III). Present summer sea surface temperature conditions (figure 27) range as low as 22°C due to the upwelling. The sediment surface nannofossil ratio of 0.8 reflects this anomalous cool condition which is the equivalent of the flora found at 35°N in the Pacific as determined by Okada and Honjo (1973) and tabulated here (Appendix IV). Fluctuations in the ratio of between 0.4 and 1.4 for the past 90,000 years reflect maintenance of 22 - 24°C conditions which in turn indicates continual upwelling at this latitude through the time period. In addition, the lithologic record of foraminifera enrichment is consistent with the upwelling interpretation.

In summary, the most significant Pleistocene fluctuations recorded in deep Somali Basin sediments reflect bottom water processes that may be occurring far from the local area. A

shallower water core in the basin indicates local sea surface temperature remained relatively constant south of the equator. Upwelling to the north was intensified and spread over a greater area according to the foraminiferal record but no significant temperature changes were observed in the present day upwelling area.

SUMMARY AND CONCLUSIONS

The late Quaternary record of Somali Basin sedimentation has been examined using data from 28 piston cores. Of these smear slide descriptions for 18 coress are presented in Appendix I while total carbonate determinations on 10 other cores are presented in Olausson (1960). The nannofossil assemblage in some of the cores was examined for its climatic and chronostratigraphic record. Maximum ages for five cores were obtained using radiocarbon.

Examination of the sediments revealed several characteristics of the carbonate record for which processes have been determined. The major characteristics are (1) total carbonate absence in certain intervals of those cores from below 5200m;(2) large fluctuations in total carbonate in cores from 5200 to 4400 m except in the northwestern portions of the basin; (3) constant relatively high total carbonate (> 50%) in cores above 4400 m; (4) periodic foram enrichment in layers of cores from all depths. These main characteristics of the carbonate record are caused by (1) bottom water incursions in the Amirante Trench area and subsequent dissolution of carbonates except under the area of extremely high productivity; and (2) upwelling which from plankton tow and surface sediment work has been demonstrated to cause

greater foraminiferal productivity and by inference must have occurred over larger areas of the basin in the past.

By considering effect of the mechanisms responsible for changes in the carbonate record, indications of past climate emerge. On a global scale to the extent that bottom water entry is determined by its rate of formation carbonate dissolution in the Somali Basin indicates climatic conditions at the site of bottom-water formation. On a local scale occurrence of foraminiferal enrichment in sediments over a large area may reflect upwelling in the past covered a larger portion of the basin and as it is presently caused by wind stress a modification of the wind system is implied. Sea surface paleotemperature data from nannofossil assemblages indicate no large scale variation just south of the equator or in the zone of present day upwelling.

Examination of the Somali Basin carbonate record leads to some conclusions about the interpretation of pelagic carbonate records in general. Dilution, dissolution, and supply do not necessarily vary uniformly in response to local climatic conditions as has previously often been assumed (Broecker, 1971 for example). Each reflect a different process in the

ocean which may respond to local or worldwide climatic change at a different rate which excludes the commonly used glacial-interglacial chronology as reviewed in Cooke (1973) for their variations except over large time scales.

V SUMMARY OF RESULTS

The main paleooceanographic processes of the Somali Basin have been studied through examining three areas - structural evolution of the basin, Neogene sedimentation and initiation of monsoons, and Pleistocene sedimentation and recent oceanographic variability. The initiation and variability of large scale oceanic processes can only be considered when the configuration of the basin, the main driving forces for flow, and a means of interpreting the sediment record of the oceanic processes are known.

The southwestern section of Owen Fracture Zone in its Chain Ridge and buried portions extends almost to Madagascar. They are a main constraint on Somali Basin evolution in absence of useable magnetic records to the west of the lineation. Age-elevation and other methods used to determine the age difference across the fracture zone show that the western basin is at least 30-40 m.y. older than the eastern basin and may be considerably older still. The extreme thickness of the sedimentary section to the west of the ridge indicates that the area west of the fracture zone may be transitional crust remaining from the

original formation of the Tethys. A model for evolution of the area is presented in which the trend of the fracture zone controls the termination of the main northern Indian Ocean spreading center as well as the movement of India away from Africa.

Nannofossil biostratigraphic analyses of four deep sea drilling sites in the Somali Basin area have been used to establish Neogene sediment ages and sedimentation rates. All sites show large late Neogene increases in sedimentation rates when Miocene and Recent rates are compared in spite of the fact that the basin is becoming larger and deeper. Increased biogenic productivity in surface waters could best explain the sedimentation rate increase, and therefore as the increased productivity should be related to upwelling and monsoon flow. These sites indicate the main flow was initiated during Late Miocene to Pliocene. That time is shortly after the middle Miocene final marine regression from northern India and probable initiation of the land sea heating contrast that drives monsoon flow.

Examination of the carbonate record in late Quaternary piston cores from the Somali Basin provides data on recent sedimentation rates and oceanographic changes. Dissolution resulting in total carbonate removal in the late Quaternary

occurred below 5200 m while large fluctuations in total carbonate were noted in cores taken from 5200 m to 4400 m except in the northwestern portion of the basin. There high productivity resulted in the continuity of the total carbonate record even at great depth. Sporadic late Quaternary bottom water incursions through the Amirante Trench area may account for the carbonate dissolution. Periodic foraminiferal enrichment has been related to upwelling and its occurrence in greater areas of the basin in the late Quaternary has been indicated. Surface temperature determinations from nannofossil biostratigraphy indicate no large-scale changes in temperature at two locations in the basin.

Paleooceanographic studies include a broad range of disciplines within the earth sciences and as such enable new perspectives on the record of earth history to be developed. These structural and sedimentary studies of the Somali Basin indicate the power of a method which has synthesized elements of the earth's meteorologic, climatic, structural, and oceanographic history through analysis of deep sea sediments in the northwestern Indian Ocean.

BIBLIOGRAPHY

Arrhenius, G., 1952, Sediment cores from the East Pacific, Reports of the Swedish Deep Sea Expedition 1947-1948, Vol. V, Fasc. I.

Baker, B.H. and J.A. Miller, 1963, Geology and geochronology of the Seychelles Islands and structure of the floor of the Arabian Sea, Nature 199: 346-348.

Be, A.W.H., and D.S. Tolderlund, 1971, Distribution and ecology of living planktonic Foraminifera in surface waters of the Atlantic and Indian Oceans in B. M. Funnell and W. R. Riedel, The Micropalaeontology of Oceans, 105-150, Cambridge.

Berger, W.H., 1973, Deep-sea carbonates: Pleistocene dissolution cycles, Jour. of Foram. Res. 3: 187-195.

Berger, W.H., 1973, Cenozoic sedimentation in the Eastern tropical Pacific, Geol. Soc. America Bull., 84: 1941-1954.

Berggren, W.A., 1974, Cenozoic Time Scale: Geological Applications, in W.A. Berggren and J.A. Van Couvering, Paleogeography and Paleobiogeography: Organisms and Continents in time and space, Woods Hole Oceanographic Institution Graduate Education Program Symposium, June 1974.

Berggren, W.A. and C.D. Hollister, 1974, in press, Paleogeography, Paleobiogeography and the History of Circulation in the Atlantic Ocean in W.W. Hay, editor, Geological History of the Ocean Basins, Amer. Assoc. Petrol. Geol.

Berry, F.A., E. Bollay and N.R. Beers, 1945, Handbook of Meteorology, McGraw Hill Book Co., Inc. New York, 1068 p.

Bezrukov, P.L., 1964, Sedimentation in northern and central parts of the Indian Ocean, U.S. Naval Oceanographic Office, Trans. 265, 15 p.

Biscaye, P.E., 1965, Mineralogy and sedimentation of Recent deep-sea clay in the Atlantic Ocean and adjacent seas and oceans, Geol. Soc. Am. 76: 803-832.

Bruce, J.G., 1968, Comparison of near-surface dynamic topography during the two monsoons in the western Indian Ocean, Deep-Sea Res. 15: 665-678.

Bruce, J.G., 1969, A further estimate of maximum transport of the Somali current, Deep-Sea Res. 16: 227-228.

Bruce, J.G., 1970, Notes on the Somali current system during the southwest monsoon, Jour. Geophys. Res. 75: 4170-4173.

Bruce, J.G., 1973, Large-scale variations of the Somali current during the southwest monsoon, 1970, Deep-Sea Res. 20: 837-846.

Bruce, J.G., and G. Volkmann, 1969, Some measurements of current off the Somali coast during the northeast monsoon, Jour. of Geophys. Res. 74: 1958-1967.

Broecker, W.S., 1971, Calcite accumulation rates and glacial to interglacial changes in oceanic mixing in K.K. Turekian ed. Late Cenozoic Glacial Ages, p. 239-265, Yale Univ. Press.

Broecker, W.S., K.K. Turekian and B.C. Heezen, 1958, The relation of deep sea sedimentation rates to variations in climate, Am. Jour. Sci. 256: 503-517.

Broecker, W.S., and J. van Donk, 1970, Insolation changes, ice volumes, and the O^{18} record in deep-sea cores, Review of Geophysics and Space Physics 8: 169-198.

Budyko, M.I., N.A. Efimova, L.I. Zubenok, and L.A. Strokina, 1962, Heat balance of the Earth's surface, Akad. Nauk. USSR, Isv. Ser. Geogr., no. 1, p. 6-16.

Burckle, L.H., K. Venkatarathnam, and J.D. Booth, 1974, Sediment transport by Antarctic Bottom Water in the Western Indian Ocean, EOS 55: 312.

Bukry, D., 1973, Low latitude coccolith biostratigraphic zonation, in Initial Reports of the Deep Sea Drilling Project 15: 685-703.

Bunce, E.T., C.O. Bowin and R.L. Chase, 1966, Preliminary results of the 1964 cruise of R/V CHAIN to the Indian Ocean, Phil. Trans. Roy. Soc. A. 259: 218-226.

Bunce, E.T., M.G. Langseth, R.L. Chase, and M. Ewing, 1967, Structure of the Western Somali Basin, J. Geophys. Res., 72: 2547-2555.

Burroughs, R.H. and E.T. Bunce, 1973, Chain Ridge: Implications for Northwestern Indian Ocean evolution (abstract), EOS 54: 330.

Conolly, J.R., 1967, Postglacial-glacial change in climate in the Indian Ocean, Nature 214: 873-875.

Cooke, H.B.S., 1973, Pleistocene chronology: Long or short?, Quat. Res. 3: 206-220.

Cromwell, T., 1953, Circulation in a meridional plane in the central equatorial Pacific, J. Mar. Res. 12: 196-213.

Dietz, R.S. and J.C. Holden, 1970, Reconstruction of Pangaea: breakup and dispersion of continents, Permian to Present, J. Geophys. Res., 75: 4939-4956.

Drake, C.L., M. Ewing, and G.H. Sutton, 1959, Continental margins and geosynclines: the east coast of North America north of Cape Hatteras in Physics and Chemistry of the Earth: London, Pergamon Press, 3: 110-198.

Düing, W., 1970, The monsoon regime of currents in the Indian Ocean, Int. Indian Ocean Exped. Oceanogr. Mono. 1, 68 p.

Duncan, C.P., 1970, The Agulhas current, Doctoral dissertation, Univ. of Hawaii, 76 p.

DuToit, A.L., 1937, Our Wandering Continents, Oliver and Boyd, Edinburgh.

Eagleson, P.S., 1970, Dynamic Hydrology, McGraw Hill Book Co., New York, 462 p.

Emiliani, C., 1955, Pleistocene temperatures, J. Geol. 63: 538-578.

Emiliani, C., 1961, Cenozoic climatic changes as indicated by stratigraphy and chronology of deep-sea cores of Globigerina ooze facies, Ann. N.Y. Acad. Sci. 95: 521-536.

Emiliani, C., 1966, Paleotemperature analysis of the Caribbean cores P6304-8 and P6304-9, and a generalized temperature curve for the past 425,000 years, Jour. of Geol. 74: 109-126.

Ericson, D.B., 1970, Pleistocene climates in the Atlantic and Pacific Oceans, A comparison based on deep sea sediments, Science, 167: 1483-1485.

Ericson, D.B., M. Ewing, G. Wollin, and B.C. Heezen, 1961, Atlantic deep sea sediment cores, Geol. Soc. Am. 72: 193-286.

Ericson, D.B., and G. Wollin, 1968, Pleistocene climates and chronology in deep-sea sediments, Science 162: 1227-1234.

Ewing, M., S. Eittreim, M. Truchan, and J.I. Ewing, Sediment distribution in the Indian Ocean, Deep-Sea Res. 16: 231-248.

Fell, H.B., 1967, Cretaceous and Tertiary surface currents of the oceans, Oceanogr. Mar. Biol. Ann. Rev. 5: 317-341.

Fisher, R.L., E.T. Bunce, P.J. Cernock, D.C. Clegg, D.S. Cronan, V.V. Damiani, L. Dmitriev, D.J.J. Kinsman, P.H. Roth, J. Thiede, and E.S. Vincent, 1972, Deep Sea Drilling Project in Dodoland, Geotimes, September, 17: 17-21.

Fisher, R.L., C.G. Engel, and T.W.C. Hilde, 1968, Basalts dredged from the Amirante Ridge, Western Indian Ocean, Deep-Sea Res. 15: 521-534.

Fisher, R.L., J.G. Sclater and D.P. McKenzie, 1971, The evolution of the central Indian Ridge, Western Indian Ocean, Bull. Geol. Soc. Am., 82: 553-562.

Francis, T.J.G., D. Davies, and M.N. Hill, 1966, Crustal structure between Kenya and the Seychelles, Phil. Trans. Roy. Soc. A. 259: 240-261.

Frerichs, W.E., 1968, Pleistocene-Recent boundary and Wisconsin glacial biostratigraphy in the northern Indian Ocean, Science 159: 1456-1458.

Gartner, S., 1969, Correlation of Neogene planktonic foraminifer and calcareous nannofossil zones, Trans. Gulf Coast Assoc. Geol. Soc. 19: 585-599.

Gartner, S., 1973, Absolute chronology of the late Neogene calcareous nannofossil succession in the equatorial Pacific, Geol. Soc. Am. 84: 2021-2034.

Geitzenauer, K.R., 1972, The Pleistocene calcareous nannoplankton of the subantarctic Pacific Ocean, Deep-Sea Res. 19: 45-60.

Goldberg, E.D. and J.J. Griffin, 1970, The sediments of the northern Indian Ocean, Deep-Sea Res. 17: 513-537.

Gregory, J.W., 1920, The African Rift Valleys, Geogr. J. 56: 13-47.

Griffin, J.J., H. Windom, and E.D. Goldberg, 1968, The distribution of clay minerals in the world ocean, Deep-Sea Res. 15: 433-459.

Hajash, A. and R.L. Armstrong, 1972, Paleomagnetic and radiometric evidence for the age of the Comores Islands, West Central Indian Ocean, Ea. and Pl. Sci. Let. 16: 231-236.

Haq, B.U., 1973, Transgressions, climatic change and the diversity of calcareous nannoplankton, Marine Geology 15: M25-M30.

Hay, W.W., H.P. Mohler, P.H. Roth, R.R. Schmidt, and J.E. Boudreaux, 1967, Calcareous nannoplankton zonation of the Cenozoic of the Gulf Coast and Caribbean-Antillean area and transoceanic correlation, Gulf Coast Assoc. Geol. Soc. Trans. 17: 428-480.

Hayes, D.E. and M. Ewing, 1970, North Brazilian Ridge and adjacent continental margin, Amer. Assoc. Petrol. Geol. Bull., 54: 2120-2151.

Hays, J.D., T. Saito, N.D. Opdyke, L.H. Burckle, 1969, Pliocene-Pleistocene sediments of the equatorial Pacific: Their paleomagnetic, biostratigraphic, and climatic record, Geol. Soc. Am. 80: 1481-1514.

Heezen, B.C., I.D. MacGregor, H.P. Foreman, G. Forristal, H. Hekel, R. Hesse, R.H. Hoskins, E.J.W. Jones, A. Kaneps, V.A. Krasheninnikov, H. Okada, and M.H. Ruff, 1973, Diachronous deposits: a kinematic interpretation of Post-Jurassic sedimentary sequence on the Pacific Plate, Nature 241: 25-32.

Heezen, B.C. and M. Tharp, 1965, Physiographic diagram of the Indian Ocean, the Red Sea, the South China Sea, the Sulu Sea and the Celebes Sea, Geol. Soc. Am. Inc., New York.

Heirtzler, J.R. and R.H. Burroughs, 1971, Madagascar's paleo-position: new data from the Mozambique Channel, Science 174: 488-490.

Heirtzler, J.R., G.O. Dickson, E.M. Herron, W.C. Pitman, and X. LePichon, 1968, Marine magnetic anomalies, geomagnetic field reversals, and motions of the ocean floor and continents, Jour. Geophys. Res. 73: 2119-2136.

Hess, H.H., 1962, History of ocean basins, in Petrologic Studies, Buddington Volume, 599-620, Geol. Soc. Am., Boulder, Colorado.

Hollister, C.D., D.A. Johnson, and P.F. Lonsdale, 1974, Current controlled abyssal sedimentation: Samoan Passage, Equatorial West Pacific, Jour. Geol. 82: 275-300.

Holton, J.R., 1972, An Introduction to Dynamic Meteorology, Academic Press, New York, 319 p.

Hyndman, R.D., 1973, Evolution of the Labrador Sea, Can. J. Earth Sci. 10: 637-644.

Imbrie, J. and N.G. Kipp, 1971, A new micropaleontological method for quantitative paleoclimatology: Application to a late Pleistocene Caribbean core, in K.K. Turekian editor, Late Cenozoic Glacial Ages, p. 71-181, Yale Univ. Press, New Haven.

Kabanova, Yu. G., 1968, Primary production of the northern part of the Indian Ocean, Oceanology 8: 214-225.

Knauss, J.A. and B.A. Taft, 1964, Equatorial undercurrent of the Indian Ocean, Science 143: 354-356.

Kolbe, R.W., 1957, Diatoms from equatorial Indian Ocean cores, Reports of the Swedish Deep Sea Expedition, 1947-1948, 9 (1): 1-50.

Konta, J., 1968, Petrology of muds from the northwestern region of the Indian Ocean, Woods Hole Oceanogr. Inst. Ref. No. 68-5, 30 p. and figs.

Krey, J., 1973, Primary production in the Indian Ocean, in B. Zeitzschel, editor, Biology of the Indian Ocean, p. 115-126, Springer-Verlag, New York.

Landsberg, H.E., H. Lippmann, K.H. Paffen and C. Troll, 1963, World Maps of Climatology, Springer-Verlag 28 p. and 5 maps.

Laughton, A.S., 1966, The Gulf of Aden, Phil. Trans. Roy. Soc. A. 259: 150-171.

Laughton, A.S., D.H. Matthews, and R.L. Fisher, 1970, The structure of the Indian Ocean in Maxwell, A.E., editor, The Sea, Volume IV, Part II, p. 543-586, Wiley Interscience, New York.

Laughton, A.S., R.B. Whitmarsh, and M.T. Jones, 1971, The evolution of the Gulf of Aden, Phil. Trans. Roy. Soc. A 267: 227-266.

LePichon, X. and D.E. Hayes, 1971, Marginal offsets, fracture zones, and the early opening of the South Atlantic, J. Geophys. Res., 76: 6283-6293.

LePichon, X. and J.R. Heirtzler, 1968, Magnetic anomalies in the Indian Ocean and sea-floor spreading, J. Geophys. Res. 73: 2101-2117.

Lohmann, G.P., 1974, Geographic variations in Cenozoic calcite compensation depth, in W.A. Berggren and J.A. Van Couvering, Paleogeography and Paleobiogeography: Organisms and continents in time and space, Woods Hole Oceanographic Institution Graduate Education Program, Symposium June 1974.

Ludwig, W.J., J.E. Nafe, and C.L. Drake, 1970, Seismic refraction, in The Sea, A.E. Maxwell, editor, Volume IV, Part I, 53-84, Wiley Interscience, New York.

Luyendyk, B.P., D. Forsyth, and J.D. Phillips, 1972, Experimental approach to the paleocirculation of the oceanic surface waters, Geol. Soc. America Bull. 83: 2649-2664.

Martini, E., 1971, Standard Tertiary and Quaternary calcareous nannoplankton zonation in Farinacci, A., editor, Proceedings of the II Planktonic Conf., Rome, Edizioni Tecnoscienza, p. 739-785.

Martini, E. and T. Worsley, 1969, Standard Neogene calcareous nannoplankton zonation, Nature 225: 289-290.

Matthews, D.H., 1963, A major fault scarp under the Arabian Sea displacing the Carlsberg Ridge near Socotra, Nature, 198: 950-952.

Matthews, D.H., 1966, The Owen Fracture Zone and the northern end of the Carlsberg Ridge, Phil. Trans. Roy. Soc. A 259: 172-186.

McElhinny, M.W., 1973, Paleomagnetism and Plate Tectonics, University Press, Cambridge, England 358 p.

McIntyre, A., 1974, World-ocean isotherm map during an ice-age, 18,000 years ago (abstract) EOS 55: 259.

McIntyre, A., and A.W.H. Be, 1967; Modern coccolithophoridae of the Atlantic Ocean, I. Placoliths and Cyrtoliths, Deep-Sea Res. 14: 561-597.

McIntyre, A., A.W.H. Be, and M.B. Roche, 1970, Modern Pacific Coccolithophoridae: a paleontological thermometer, Trans. N.Y. Acad. Sci. 32: 720-731.

McIntyre, A. and R. McIntyre, 1971, Coccolith concentrations and differential solution in oceanic sediments, in B.M. Funnell and W.R. Riedel, editors, The Micropaleontology of the Oceans, p. 253-261.

McIntyre, A., W.F. Ruddiman, and R. Jantzen, 1972, Southward penetrations of the North Atlantic polar front: faunal and floral evidence of large scale surface water mass movements over the last 225,000 years, Deep-Sea Res. 19: 61-77.

McKenna, M.C., 1973, Sweepstakes, filters, corridors, Noah's Arks, and Beached Viking Funeral Ships in Paleogeography in D.H. Tarling and S.K. Runcorn editors Implications of Continental Drift to the Earth Sciences, Vol. I, p. 295-308, Academic Press, New York.

McKenzie, D.P. and R.L. Parker, 1967, The North Pacific: an example of tectonics on a sphere, Nature 216: 1276-1280.

McKenzie, D.P. and J.G. Sclater, 1971, The evolution of the Indian Ocean since the late Cretaceous, Geophys. J.R. Astr. Soc. 25: 437-528.

Menard, H.W., 1964, Marine Geology of the Pacific, McGraw-Hill New York, 271 p.

Menard, H.W., 1967, Transitional types of crust under small ocean basins, J. Geophys. Res., 72: 3061-3074.

Menard, H.W. and T. Atwater, 1968, Changes in the direction of sea-floor spreading, Nature 219: 463-467.

Menard, H.W. and T.E. Chase, 1970, Fracture zones, in The Sea, Vol. IV, Part 1, A.E. Maxwell, editor, 421-444, Wiley Interscience, New York.

Morgan, W.J., 1968, Rises, trenches, great faults and crustal blocks, J. Geophys. Res., 73: 1959-1982.

Müller, G., 1966, Grain size, carbonate content, and carbonate mineralogy of Recent sediments of the Indian Ocean off the eastern coast of Somalia, Die Naturwissenschaften 21: 547-550.

Müller, G., 1967, The H Cl-soluble iron, manganese, and copper contents of Recent Indian Ocean sediments off the eastern coast of Somalia, Mineralium Deposita 2: 54-61.

Murray, J., 1899, On the marine deposits in the Indian, Southern, and Antarctic Oceans, Scot. Geogr. Mag. 5: 405-436.

Murray, J., 1909, On the depths and marine deposits of the Indian Ocean, Rept. Percy Sladen Trust Exped. to the Indian Ocean 1905, II, No. 13, 355-396.

Nigrini, C., 1967, Radiolaria in pelagic sediments from the Indian and Atlantic Oceans, Bull. Scripps Inst. Oceanogr. 11: 1-125.

Nowroozi, A.A., 1971, Seismo-tectonics of the Persian Plateau, Eastern Turkey, Caucasus, and Hindu Kush Regions, Bull. Seismol. Soc. Am. 61: 317-341.

Oba, T., 1967, Planktonic foraminifera from the deep-sea cores of the Indian Ocean, Sci. Rep. Tohoku Univ. 2nd ser. (Geol.) 38: 193-219.

Okada, H. and S. Honjo, 1973, The distribution of oceanic coccolithophorids in the Pacific, Deep-Sea Res. 20: 355-374.

Okada, H. and S. Honjo, 1973, Distribution of coccolithophorids in the North and Equatorial Pacific Ocean: quantitative data on samples collected during Leg 30, Oshoro Maru, 1968 and Leg HK 69-4, Hakuho Maru, 1969, Woods Hole Oceanographic Inst. Tech. Rept. 73-81, 59 p.

Olausson, E., 1960, Description of sediment cores from the Indian Ocean, Reports of the Swedish Deep Sea Exped. 1947-1948, Vol. 9, No. 2: 51-88 and plates.

Olausson, E., B.U. Haq, G.B. Karlsson, and I.U. Olsson, 1971, Evidence in Indian Ocean cores of late Pleistocene changes in oceanic and atmospheric circulation, Geologiska Föreningen i Stockholm Forhandlingar, 93: 51-84.

Pepper, J.F. and G.M. Everhart, 1963, The Indian Ocean: the geology of its bordering lands and the configuration of its floor, U.S. Geol. Survey, Misc. Geol. Investigations I-380, 33 p. and map.

Philander, S.G.H., 1973, Equatorial undercurrent: measurements and theories, Rev. of Geophys. and Space Phys. 11: 513-570.

Philippi, E., 1912, Die grundproben der deutschen. Südpolar expedition in Drygalski, E., Deutsche Südpolar Exped. 1901-1903, Band. 2, Heft 6, p. 431-434.

Pimm, A.C., R.H. Burroughs and E.T. Bunce, 1972, Oligocene sediments near Chain Ridge, northwest Indian Ocean: structural implications, Mar. Geol. 13: M14-M18.

Powell, C. McA. and P.J. Conaghan, 1973, Plate tectonics and the Himalayas, Ea. and Pl. Sci. Let. 20: 1-12.

Ramage, C.S., 1971, Monsoon Meteorology, Academic Press, New York, 296 p.

Ramage, C.S., F.R. Miller, C. Jefferies, 1972, Meteorological Atlas of the International Indian Ocean Expedition, Vol. I The Surface Climate of 1963 and 1964, U.S. Gov't Printing Office, xiii p. and 144 charts.

Rona, E. and C. Emiliani, 1969, Absolute dating of Caribbean cores P6304-8 and P6304-9, Science 163: 66-68.

Ruddiman, W.F., 1971, Pleistocene sedimentation in the equatorial Atlantic: stratigraphy and faunal paleoclimatology, Geol. Soc. Am. 82: 283-302.

Ryther, J.H., J.R. Hall, A.K. Pease, A. Bakun, M.M. Jones, 1966, Primary organic production in relation to the chemistry and hydrography of the Western Indian Ocean, Limnol. and Oceanogr. 2: 371-380.

Ryther, J.H. and D.W. Menzel, 1965, On the production, composition, and distribution of organic matter in the Western Arabian Sea, Deep-Sea Res. 12: 199-209.

Sankar-Rao, M. and B. Saltzman, 1969, On a steady state theory of global monsoons, Tellus 21: 308-330.

Schlich, R., F. Aubertin, J.R. Delteil, L. Leclaire, P. Magnier, L. Montadert, P. Patriet, and P. Valery, 1972, Donnies nouvelles sur le sub-stratum du Bassin de Somalie a' partir d'un profil de sismique reflexion, C.R. Acad. Sc. Paris 275: D1331-1334.

Schott, W., 1935, Die foraminiferen in dem äquatorialen Teil des Atlantischen Ozeans, Wiss. Ergebn. Deutsch. Atlantic Exped. "Meteor" 1925-1927 3: 43-134.

Schott, W., 1939, Deep sea sediments of the Indian Ocean in Trask, P.D. editor, Recent Marine Sediments, p. 396-408, Amer. Assoc. Petrol. Geol.

Schouten, H.P., 1974, Magnetic anomalies over fracture zones in the lower magnetic latitudes of the central North Atlantic (abstract), EOS 55: 232.

Scalter, J.G., R.N. Anderson, and M.L. Bell, 1971, Elevation of ridges and evolution of the Central Eastern Pacific, J. Geophys. Res., 76: 7888-7915.

Shackleton, N.J. and N.D. Opdyke, 1973, Oxygen isotope and paleomagnetic stratigraphy of Equatorial Pacific Core V28-238: Oxygen isotope temperatures and ice volumes on a 10^5 year and 10^6 year scale, Jour. Quat. Res. 3: 39-55.

Simpson, E.S.W., R. Schlich, L. LeClaire, W.A. Girdley, C. Moore, S. White, T.L. Vallier, C. Muller, B. Zobel, J. Sigal, J. Gieskes and B.V. Marshall, 1972, Leg 25 DSDP Western Indian Ocean, Geotimes 17: 21-24.

Simpson, G.C. 1921, The southwest monsoon, Quat. Jour. Roy. Meteorol. Soc. 47: 151-172.

Smith, A.G. and A. Hallam, 1970, The fit of the southern continents, Nature 225: 139-144.

Sowerbutts, W.T.C., 1972, Rifting in eastern Africa and the fragmentation of Gondwanaland, Nature 235: 435-437.

Stewart, R.A., O. Pilkey and B.W. Nelson, 1965, Sediments of the northern Arabian Sea, Marine Geol. 3: 411-427.

Stommel, H., 1960, Wind drift near the equator, Deep-Sea Res. 6: 298-302.

Stubbings, H.G., 1939, The marine deposits of the Arabian Sea, Rep. John Murray Exped. 3: 32-158.

Stubbings, H.G., 1939, Stratification of biological remains in marine deposits, Rep. John Murray Exped. 3: 159-162.

Suess, H.E., 1956, Absolute chronology of the last glaciation, Science 123: 355-357.

Swallow, J.C., 1967, The equatorial undercurrent in the western Indian Ocean. In 1964, Stud. Trop. Oceanogr. Miami 5: 15-36.

Swallow, J.C., and J.G. Bruce, 1966, Current measurements off the Somali Coast during the southwest monsoon of 1964, Deep-Sea Res. 13: 861-888.

Taft, B.A. and J.A. Knauss, 1967, The equatorial undercurrent of the Indian Ocean as observed by the Lusiad expedition, Bull. Scripps Inst. Oceanogr. I.

Talwani, M. and H.G. Kahle, in press, Notes on the free-air gravity map of the Indian Ocean in G. Udintsev, editor, International Indian Ocean Geophysical Atlas.

Tarling, D.H., 1971, Gondwanaland, paleomagnetism and continental drift, Nature 229: 17-21.

Thorrington-Smith, M., 1971, West Indian Ocean phytoplankton: a numerical investigation of phytohydrographic regions and their characteristic phytoplankton association, Mar. Biol. 9: 115-137.

Timonin, A.G., 1971, The structure of plankton communities of the Indian Ocean, Mar. Biol. 9: 281-289.

Van Couvering, J.A., personal communication

Vincent, E.S., 1972, Oceanography and late Quaternary planktonic foraminifera, Southwestern Indian Ocean, Doctoral Dissertation, Univ. of S. Calif. 353 p.

Vine, F.J. and D.H. Matthews, 1963, Magnetic anomalies over ocean ridges, Nature 199: 947-949.

Wadia, D.N., 1966, Geology of India, 3rd ed. revised, English Language Book Society, London 536 p.

Warren, B., 1971, Evidence for a deep Western Boundary Current in the South Indian Ocean, Nature 229: 18-19.

Warren, B., 1974, Deep flow in the Madagascar and Mascarene Basins, Deep-Sea Res. 21: 1-21.

Warren, B., H. Stommel, and J.C. Swallow, 1966, Water masses and patterns of flow in the Somali Basin during the southwest monsoon of 1964, Deep-Sea Res. 13: 825-860.

Wasserburg, G.J. and R.J. Hayden, 1955, A^{40}-K^{40} dating, geochimica et cosmochimica Acta 1: 51-60.

Wegener, A., 1924, The Origins of Continents and Oceans (translated from 3rd German edition) Methuen and Co., Ltd., London, 212 p.

Weser, O.E., 1972, A classification of marine sediments (abstract) Geol. Soc. Am. Spring Meeting Hawaii,

Wilson, J.T., 1965, A new class of faults and their bearing on continental drift, Nature 207: 343-347.

Wiseman, J.D.H., 1965, Calcium and magnesium carbonate in some Indian Ocean sediments in Sears, ed. Progress in Oceanography 3: 373-383.

Wiseman, J.D.H., and R.B. Seymour Sewell, 1937, The floor of the Arabian Sea, Geol. Mag. 74: 219-230.

Wyrtki, K., 1971, Oceanographic atlas of the International Indian Ocean Expedition, U.S. Gov't Printing Office, 531 p.

Wyrtki, K., 1973, Physical oceanography of the Indian Ocean, in B. Zeitzschel, ed., The Biology of the Indian Ocean, p. 18-36, Springer-Verlag, New York.

Zeronova, V., and U.A. Ivanov, 1967, Distribution of net-sampled phytoplankton as effected by hydrological conditions in the North Indian Ocean, U.S. Naval Oceanographic Office, Trans. 331, 14 p.

Zobel, B., 1971, Foraminifera from plankton tows, Arabian Sea: Areal distribution as influenced by ocean water masses in Farinacci, A., ed., Proceedings of the II Plankton Conf., Rome, Edizioni Tecnoscienza, p. 1323-1335.

APPENDIX I

Core Descriptions

The Quaternary sedimentation record in the Somali Basin has been determined principally from 18 piston cores taken in the area (Figure 26 and Table 6). The sediments have been classified under a system proposed by Weser (1972) with slight modification to include descriptive color terms and obvious structural information. In so doing macroscopic observation of the cores has been combined with smear slide analyses to identify sediment types. For each core the results of the smear slide analyses have been compiled as visual estimates of the total percent of the slide containing inorganic material, Foraminifera, nannofossils, and siliceous tests. Inorganic material includes detrital grains, micronodules, zeolites, volcanic shards, and clay. It is primarily composed of silt and clay size mineral grains referred to as lutite. Foraminifera include planktonic and benthonic foraminifera. The very rare occurrences of pteropods are also included in this category to simplify presentation. Nannofossils include all calcareous nannofossils. Siliceous material includes the amorphous silica tests of diatoms, radiolaria, silicoflagellates, and sponge spicules.

TABLE 6

SOMALI BASIN CORES

(Underlined Numbering Used to Avoid Overlap)

Ship	Cruise and Leg	Station	Core	Latitude	Longitude	Water Depth Corr M
CHAIN	100-4	35	25	14°01'N	51°48.2'E	5329
		36	26	7°48'N	56°12.2'E	4680
		37	27	7°46'N	54°46'E	5102
		40	29	6°53.5'N	54°41.2'E	5106
		42	30	4°27.7'N	51°08'E	5049
		44	32	3°13.3'N	52°39.8'E	5123
		46	34	2°52'N	50°13'E	5004
		47	35	0°56.8'N	53°19.8'E	5101
		48	36	0°14.5'N	56°03.5'E	4576
CHAIN	100-5	52	40	1°36'N	59°40'E	5426
		53	41	1°34'N	65°39'E	3433
CHAIN	99-8	59	40	3°24'S	45°00.5'E	4444
		60	41	3°31.2'S	46°59.9'E	4832
		61	42	3°26.6'S	49°49.2'E	4897
		62	43	6°46.4'S	48°41.8'E	4425
CHAIN	43	7	HF 3	5°52'N	53°51'E	5099
ATLANTIS II	15	569	FF 3	8°58.5'N	56°02'E	4001
		558	PC 9	8°59'N	51°44'E	3985

Throughout the text cores are referred to by their core numbers except for cores taken on Chain 99, leg 8 which are noted by their station numbers to avoid an overlap in the core numbering systems. The proper number for each location has been underlined in table 6 and used in figure 26.

Core 25 14°01'N 51°48.2'E 5329 m

0-121 cm Very dark olive, nannofossil bearing, silica rich, terrigenous lutite with layers of coarser material at: 4-15, 34-43, 48-50; and 85-121 cm.

121-570 cm Light olive green, mottled darker, siliceous rich, nanno terrigenous lutite with browner areas at 130, 140, 155, 290, 315 cm.

Core 26 7°48'N 56°12.2'E 4680 m

0-29 cm Brown grading to brownish gray green, lutite bearing, nanno rich, siliceous ooze.

29-122 cm Gray green lutite bearing, nanno rich, siliceous ooze.

122-149 cm Very light gray green, lutite bearing, nanno rich, siliceous ooze with visibly coarsening grain size below 141.

149-534 cm Gray green lutite bearing, siliceous nanno ooze which is foram rich 149-310 cm with sparse black specs 149-205 cm, and slightly darker below 300 cm; dark gray green sections 390-430, 462-482, 505-534 cm.

534-549 cm Off white foram bearing, lutite bearing, nanno siliceous ooze with darker mottled areas.

Figure 37.

Visually estimated percentages of principal components in smear slides from cores 25, 26, 27, and 29.

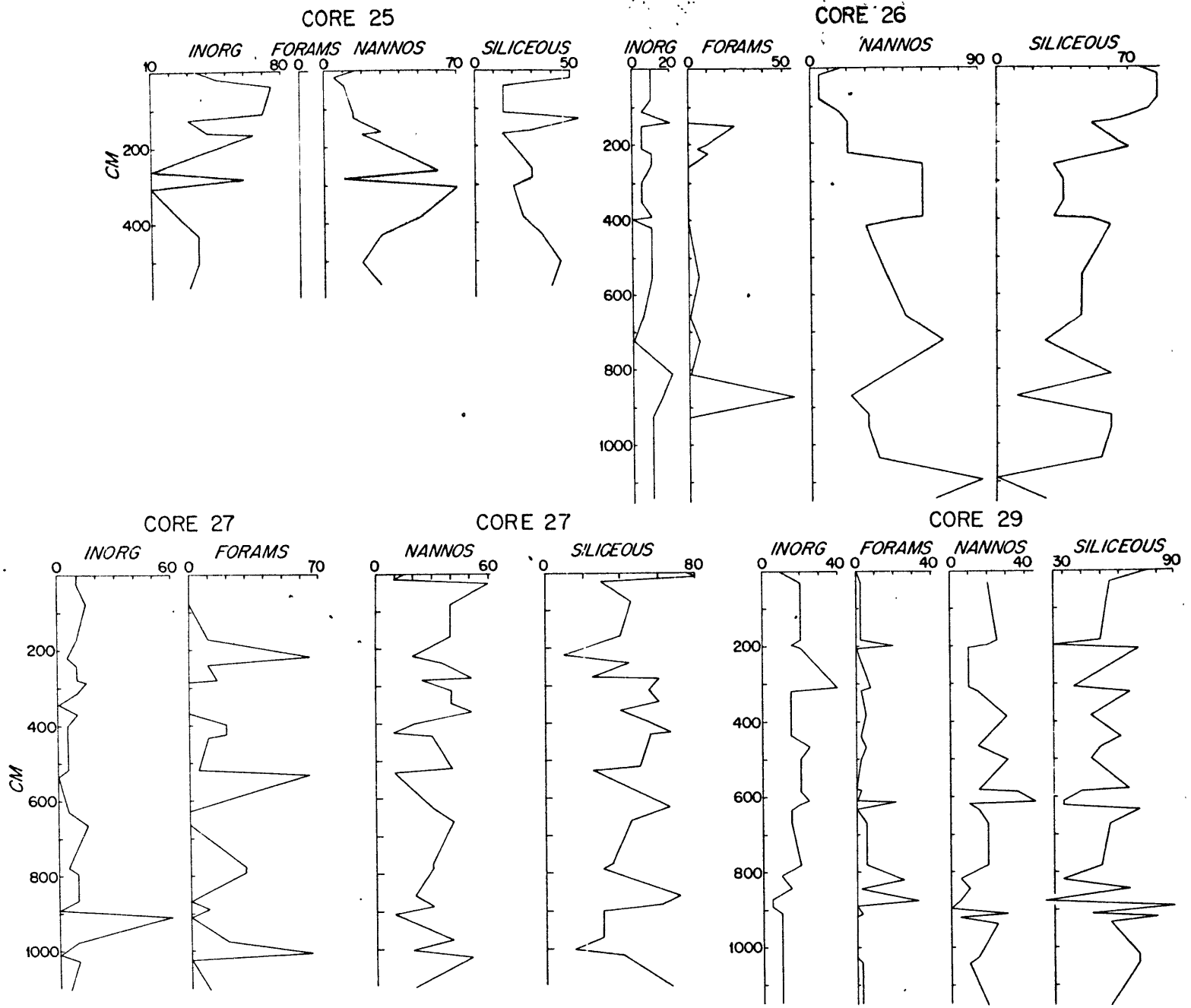
CORE 25
INORG
FORAMS
NANNOS
SILICEOUS
CM
CORE 26
INORG
FORAMS
NANNOS
SILICEOUS
CORE 27
INORG
FORAMS
CORE 27
NANNOS
SILICEOUS
CORE 29
INORG
FORAMS
NANNOS
SILICEOUS
CM

549-800 cm Gray green lutite bearing, micronodule bearing, foram bearing, siliceous nanno ooze with mottling and with darker coloration 585-603, 664-700, 736-748 cm.

800-870 cm Gray green lutite bearing, nanno-foram siliceous ooze with some color lamination 800-810 cm.

870-1086 cm Gray green lutite bearing nanno siliceous ooze with some mottling and olive gray green sections 920-960 and 1030-1047 cm.

1086-1110 cm Off white to light gray green, lutite bearing, nanno ooze with some mottling.

1110-1142 cm Gray green, lutite bearing, silica rich, nanno ooze.

Core 27 7°46'N 54°46'E 5102 m

0-15 cm Brown interlayered with gray, lutite bearing, nanno rich, siliceous ooze.

15-25 cm Very dark gray green, lutite bearing, siliceous-nanno-ooze.

25-175 cm Light and dark gray green, lutite bearing, foram bearing, siliceous nanno ooze.

175-225 cm Gray green, lutite bearing, silica bearing, nanno rich, foram ooze with sharp contacts.

225-246 cm Light and dark gray, lutite bearing, foram bearing, nanno siliceous ooze.

246-283 cm Pale green, lutite bearing, foram rich, silica rich, nanno ooze.

283-319 cm Gray mixed with olive lutite bearing, nanno siliceous ooze.

319-350 cm Pale green nanno siliceous ooze.

350-372 cm Olive lutite bearing, siliceous nanno ooze.

372-406 cm Pale green, lutite bearing, foram rich, nanno rich, siliceous ooze.

406-454 cm Gray grading to olive, lutite bearing, foram rich, nanno siliceous ooze; visibily coarser 434-443 cm with abrupt bottom contact, and olive below with angular basal contact.

454-526 cm Pale green, lutite bearing, foram bearing, nanno siliceous ooze.

526-539 cm Pale green, nanno bearing, siliceous rich, foram ooze with sharp contacts.

539-632 cm Light olive, grading to gray and olive, grading to dark olive, grading to light gray, and to pale green, lutite bearing, nanno siliceous ooze.

632-673 cm Olive lutite bearing, nanno siliceous ooze.

673-778 cm Dark pale green lutite bearing, nanno siliceous ooze.

778-803 cm Pale green lutite bearing, nanno siliceous foram ooze with sharp basal contact.

803-872 cm Olive lutite bearing, nanno rich, siliceous ooze.

872-894 cm Foram bearing, nanno siliceous ooze.

894-917 cm Olive nanno bearing, siliceous terrigenous lutite.

917-983 cm Gray with olive grading to pale green below 929, lutite bearing, foram rich, siliceous nanno ooze.

983-1008 cm Pale green silica rich, nanno rich, foram ooze.

1008-1028 cm Olive grading to gray, lutite bearing, siliceous nanno ooze.

1028-1106 cm Pale green, lutite bearing, foram bearing, nanno rich, siliceous ooze.

1106-1146 cm Pale green silica bearing, nanno bearing, foram ooze.

Core 29 6°53.5'N 54°41.2'E 5106 m

0-9 cm Brown and gray green lutite bearing, nanno rich, siliceous ooze.

9-196 cm Pale gray green lutite rich, nanno rich, foram bearing to foram siliceous ooze coarser 87-196 cm with abrupt basal contact.

196-313 cm Light and dark gray, grading to light gray and olive, grading to light olive, lutite rich, foram rich, nanno rich, siliceous ooze.

313-468 cm Pale green foram bearing, lutite rich, nanno rich, siliceous ooze with coarser material 455-468 cm.

468-508 cm Light olive to gray below 489 cm foram bearing, lutite rich, nanno siliceous ooze.

508-584 cm Olive and gray lutite rich, nanno rich, siliceous ooze.

584-622 cm Pale gray green lutite rich, nanno siliceous ooze with siliceous foram ooze 616-622 cm terminated by abrupt bottom contact.

622-651 cm Olive lutite bearing, nanno rich, siliceous ooze.

651-821 cm Pale green foram bearing, lutite rich, nanno rich, siliceous ooze with nanno bearing lutite rich siliceous foram ooze 798-821 cm having abrupt basal contact.

821-850 cm Olive foram bearing, nanno bearing, lutite rich, siliceous ooze.

850-878 cm Pale green nanno bearing, lutite bearing, siliceous rich, foram ooze with sharp contacts.

878-895 cm Dark olive lutite bearing, siliceous ooze.

895-911 cm Pale green foram bearing, lutite rich, nanno siliceous ooze.

911-928 cm Very dark olive gray, nanno bearing, lutite rich, siliceous ooze.

928-939 cm Gray and mottled dark olive gray, lutite rich, nanno siliceous ooze.

939-1043 cm Pale green foram bearing, nanno bearing, lutite rich, siliceous ooze.

1043-1156 cm Olive and gray grading to pale green at 1060 cm foram bearing, lutite rich, nanno rich, siliceous ooze.

Core 30 4°27.7'N 51°08'E 5049 m

0-3 cm	Brown lutite bearing, siliceous nanno ooze.
3-57 cm	Gray green lutite rich, silica rich, nanno ooze.
57-90 cm	Pale green lutite rich, foram rich, nanno siliceous ooze.
90-146 cm	Very light green lutite bearing, micronodule bearing, silica rich, foram nanno ooze.
146-160 cm	Very dark gray green, lutite rich, siliceous nanno ooze.
160-226 cm	Gray lutite bearing, siliceous rich, foram nanno ooze.
226-265 cm	Pale green lutite rich, nanno rich, siliceous ooze with black and gray mottling.
265-320 cm	Pale green lutite rich, nanno rich, siliceous ooze.
320-350 cm	Gray lutite bearing, silica rich, nanno ooze.
350-412 cm	Mottled gray green foram bearing, lutite bearing, siliceous nanno ooze.
412-489 cm	Dark green to olive nanno lutite siliceous ooze with black specs.

Figure 38.

Visually estimated percentages of principal components in smear slides from cores 30, 32, 34, and 35.

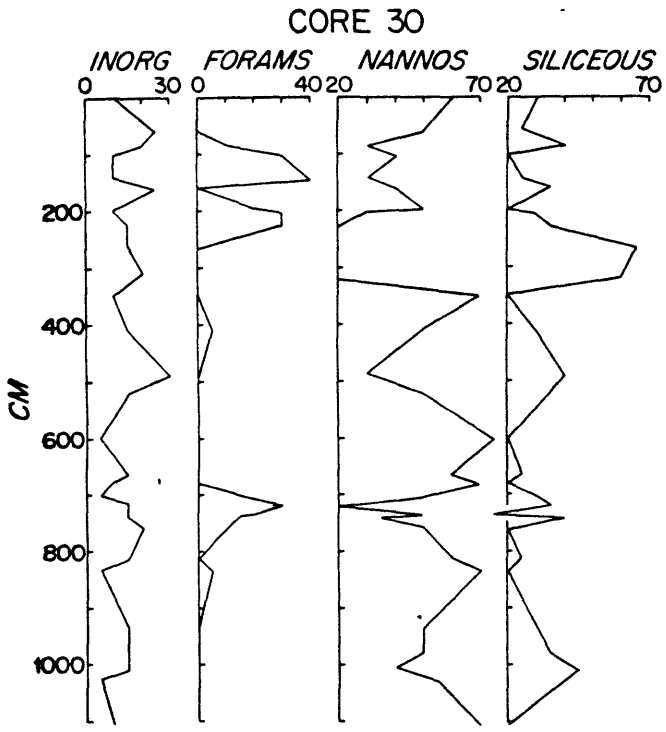
CORE 30
INORG
FORAMS
NANNOS
SILICEOUS
0
30
0
40
20
70
20
70
CM
200
400
600
800
1000

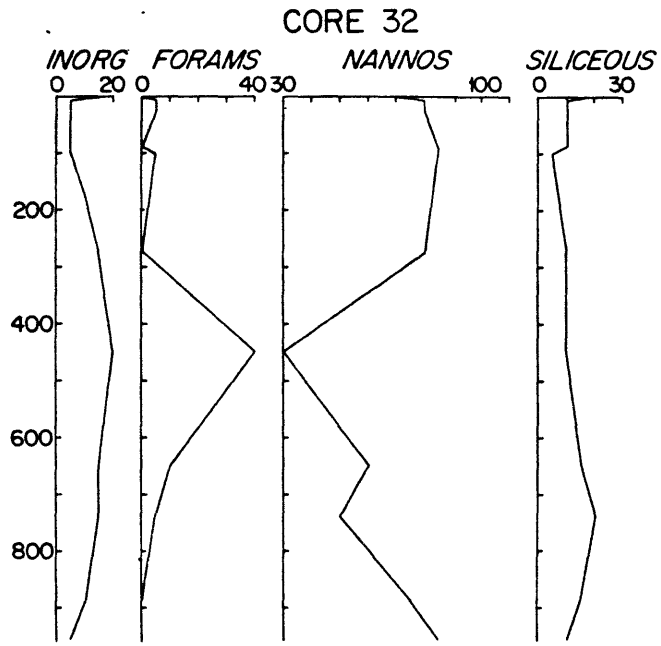
CORE 32
INORG
FORAMS
NANNOS
SILICEOUS
0
20
0
40
30
100
0
30
200
400
600
800

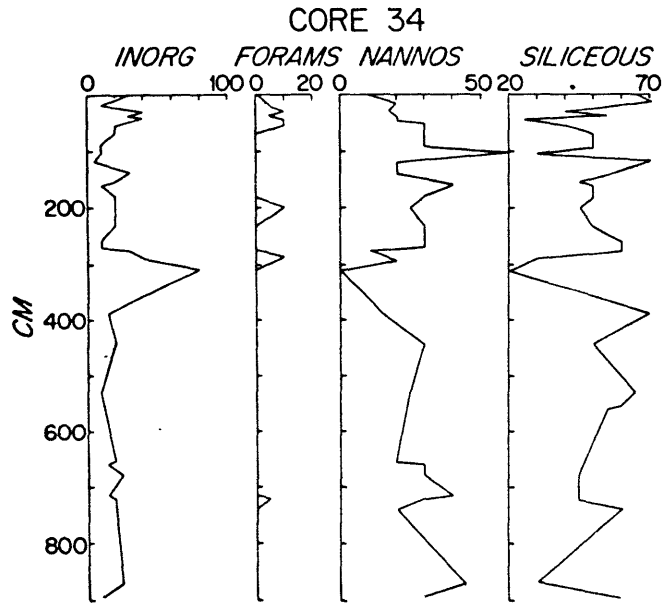
CORE 34
INORG
FORAMS
NANNOS
SILICEOUS
0
100
0
20
0
50
20
70
CM
200
400
600
800

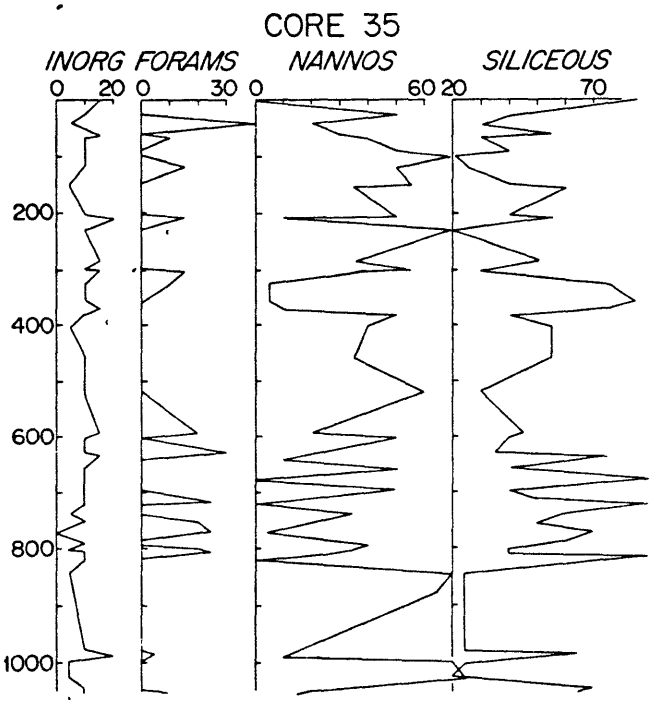
CORE 35
INORG
FORAMS
NANNOS
SILICEOUS
0
20
0
30
0
60
20
70
200
400
600
800
1000

489-523 cm	Darkly mottled gray green lutite rich, siliceous nanno ooze.
523-600 cm	Gray green lutite bearing, siliceous rich, nanno ooze.
600-666 cm	Gray green lutite rich, siliceous rich, nanno ooze.
666-678 cm	Light gray lutite bearing, siliceous rich, nanno ooze.
678-702 cm	Pale green lutite bearing, foram rich, siliceous nanno ooze.
702-717 cm	Green lutite rich, nanno rich, foram siliceous ooze with steeply dipping basal contact.
717-735 cm	Olive green grading to pale green silica rich, lutite rich, foram rich, nanno ooze.
735-738 cm	Green lutite rich, foram rich, nanno siliceous ooze.
738-761 cm	Pale green foram bearing, lutite rich, silica rich, nanno ooze.
761-814 cm	Olive lutite rich, silica rich, nanno ooze.
814-836 cm	Very light gray lutite bearing, foram bearing, silica rich, nanno ooze.

836-1007 cm Pale gray green lutite rich, siliceous nanno ooze.

1007-1106 cm Pale gray green lutite rich, siliceous nanno ooze.

Core 32 3°13.3'N 52°39.8'E 5123 m

0-6 cm Brown grading to gray lutite rich, silica rich, nanno ooze.

6-44 cm Olive lutite bearing, foram bearing, siliceous bearing nanno ooze mottled gray green at base.

92-125 cm Olive silica bearing, lutite bearing, nanno ooze.

125-430 cm Light gray green lutite bearing, silica bearing, nanno ooze.

430-450 cm Light gray lutite rich, silica rich, foram nanno ooze.

450-660 cm Olive grading to gray green foram bearing, lutite bearing, silica rich, nanno ooze.

660-740 cm Gray green foram bearing, lutite rich, silica rich, nanno ooze.

740-906 cm Gray green mottled light gray in upper section (740-751), and all olive in lower section (880-906), lutite bearing, silica rich, nanno ooze.

906-959 cm Gray green lutite bearing, silica rich, nanno ooze.

Core 34 2°52'N 50°13'E 5004 m

0-18 cm Brown grading to pale green, lutite bearing, nanno rich siliceous ooze.

18-40 cm Olive grading to greenish nanno irch, lutite siliceous ooze.

40-202 cm Intensely mottled olive, gray, and pale green grading to olive by 156 cm, lutite rich, occassionally foram rich, nanno siliceous ooze with indurated black lutite at 43 and 146 cm.

202-236 cm Olive lutite rich, nanno siliceous ooze.

236-308 cm Mottled pale green and gray with olive lutite rich, nanno siliceous ooze to 280 cm; with gray and pale green, grading to olive, foram bearing, nanno rich, siliceous lutite and black indurated lutite 298-308 cm.

308-419 cm Olive with gray mottling at base lutite rich, nanno rich, siliceous ooze.

419-454 cm Light gray with dark gray mottles grading to pale green mottles, lutite rich, nanno siliceous ooze.

454-666 cm Pale green grading to olive with pale green and some gray lutite rich nanno siliceous ooze.

666-686 cm Pale green intensively mottled with olive, light, and dark gray micronodule bearing, lutite bearing, nanno siliceous ooze with small pebbles at base.

686-715 cm Pale green mottled olive and gray grading to olive lutite rich, nanno siliceous ooze with pebbles at base.

715-729 cm Pale green intensely mottled light and dark gray and olive foram bearing, lutite rich, nanno siliceous ooze.

729-827 cm Olive with some gray micronodule bearing, lutite rich, nanno siliceous ooze.

827-871 cm Light olive mixed with pale green grading to pale green micronodule bearing, lutite rich, nanno siliceous ooze.

871-895 cm Olive with pale green lutite bearing, nanno siliceous ooze.

Core 35 0°56.8'N 53°19.8'E 5101 m

0-26 cm	Brown grading to green lutite rich, siliceous nanno ooze.
26-42 cm	Off white lutite bearing, nanno rich, siliceous foram ooze.
42-62 cm	Olive lutite rich, nanno siliceous ooze with black specs.
62-69 cm	Light gray lutite bearing, foram bearing, siliceous nanno ooze.
69-90 cm	Very light gray green lutite bearing, siliceous nanno ooze with black specs.
90-119 cm	White lutite bearing, foram rich, siliceous rich, nanno ooze.
119-150 cm	Gray green lutite bearing, siliceous nanno ooze.
150-200 cm	Olive lutite bearing, nanno siliceous ooze.
200-204 cm	White lutite bearing, siliceous nanno ooze.
204-229 cm	White and green foram bearing, lutite rich, siliceous nanno ooze.
229-285 cm	Olive lutite rich, nanno siliceous ooze.
285-300 cm	Gray and olive lutite bearing, siliceous nanno ooze.

300-325 cm White foram rich, lutite rich, nanno siliceous ooze.

325-358 cm Olive nanno bearing, lutite bearing, siliceous ooze.

358-383 cm Gray green and gray mottled green lutite rich, nanno siliceous ooze.

383-403 cm Olive lutite bearing, nanno siliceous ooze.

403-520 cm Olive grading to light gray green lutite bearing, siliceous nanno ooze.

520-595 cm White lutite rich, foram rich, nanno rich, siliceous ooze.

595-603 cm Light gray lutite bearing, siliceous nanno ooze.

603-627 cm White lutite bearing, nanno rich, foram siliceous ooze.

627-657 cm Olive lutite bearing, siliceous nanno ooze.

657-680 cm Light and dark mottled olive, lutite bearing, siliceous ooze.

680-698 cm Gray lutite bearing, siliceous nanno ooze.

698-717 cm Gray lutite bearing, nanno rich, foram rich, siliceous ooze.

717-740 cm Bright green gray lutite bearing, nanno siliceous ooze.

740-755 cm Black mottled olive, lutite bearing, foram rich, nanno rich, siliceous ooze.

755-774 cm White nanno bearing, foram rich, siliceous ooze.

774-788 cm Dark gray green to brown lutite bearing, nanno siliceous ooze.

788-795 cm Pale off-white green lutite bearing, nanno siliceous ooze.

795-803 cm Olive layers in light gray lutite bearing, foram rich, nanno siliceous ooze.

803-807 cm White lutite bearing, nanno rich, foram rich, siliceous ooze.

807-980 cm Olive and green lutite bearing, siliceous rich, nanno ooze.

980-987 cm Light gray and green foram bearing, nanno bearing, lutite rich, siliceous ooze.

987-1028 cm Greenish gray lutite bearing, siliceous rich, nanno ooze.

1050-1053 cm White lutite bearing, foram bearing, nanno rich, siliceous ooze.

Core 36 0°14.5'N 56°03.5'E 4576 m

0-16 cm	Light buff with gray mottles siliceous nanno ooze.
16-122 cm	Dark buff with grayish buff and gray mottles grading to dark buff mottled lighter, lutite bearing, siliceous rich, nanno ooze.
122-160 cm	Light buff to off white lutite bearing, occasionally foram bearing, siliceous rich, nanno ooze.
160-199 cm	Off white foram bearing, lutite rich, siliceous nanno ooze with abrupt lower contact.
199-261 cm	Light buff lutite rich, siliceous rich, nanno ooze.
261-280 cm	Light gray and pale green lutite bearing, silica bearing, foram rich, nanno ooze.
280-288 cm	Pale green micronodule bearing, silica rich, nanno rich, foram ooze with sharp and dipping bottom contact.
288-312 cm	Olive grading to light gray, grading to olive, lutite bearing, siliceous nanno ooze.
312-320 cm	Off white lutite bearing, siliceous nanno ooze with dipping upper contact and irregular lower contact.

Figure 39.

Visually estimated percentages of principal components in smear slides from cores 36, 40, 41, and 59.

CORE 36

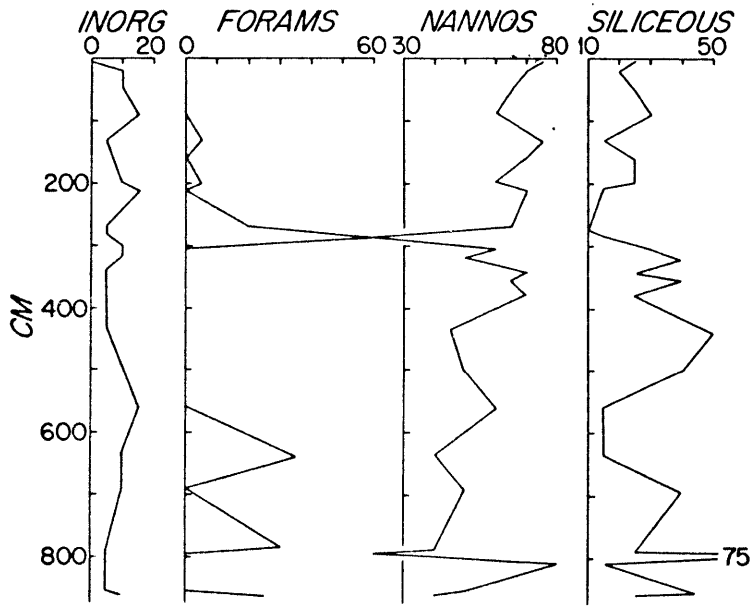

CORE 40

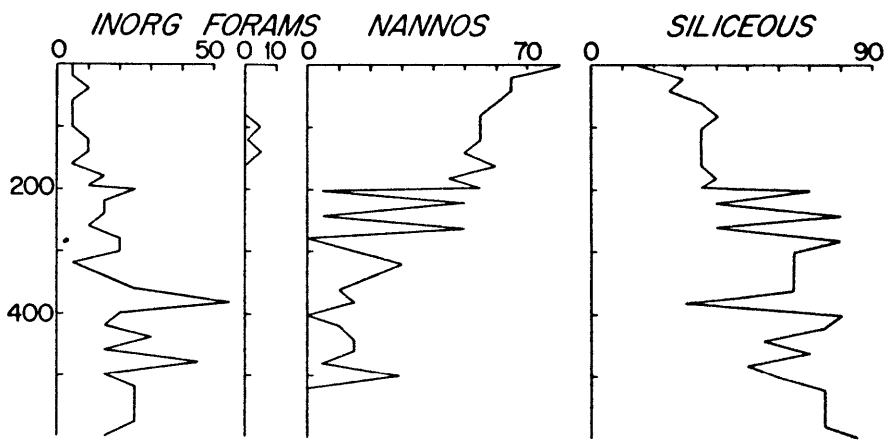

CORE 41

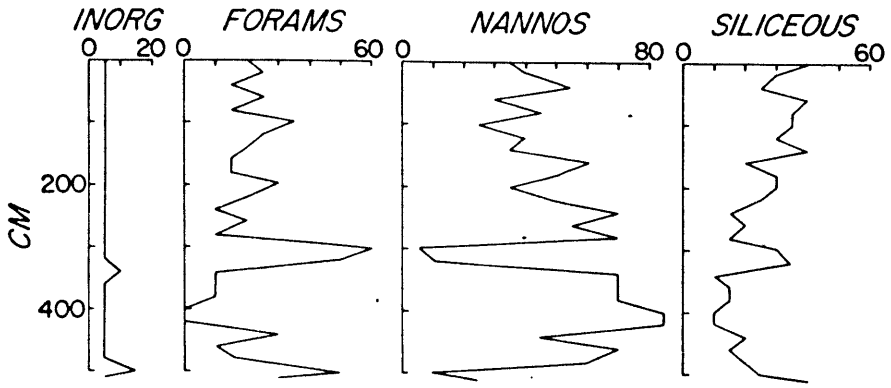

CORE 59

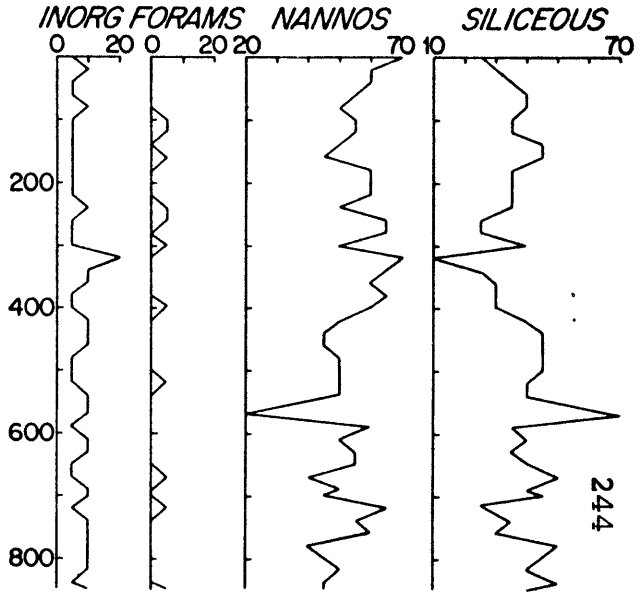

320-340 cm Light gray green, grading to buff, lutite bearing, siliceous nanno ooze.

340-373 cm Buff mottled light gray, grading to light gray, lutite bearing, siliceous nanno ooze.

373-425 cm Light grayish buff grading to dark gray grading to greenish gray lutite bearing, siliceous nanno ooze.

425-449 cm Brownish olive grading to medium olive lutite bearing, nanno siliceous ooze.

449-496 cm Light greenish gray grading to light gray lutite bearing, nanno siliceous ooze.

496-521 cm Pale grayish green grading to pale green lutite bearing, siliceous nanno ooze.

521-571 cm Light gray grading to pale greenish gray grading to gray lutite bearing, siliceous rich, nanno ooze.

571-649 cm Off white lutite bearing, micronodule bearing, silica rich, foram nanno ooze with sharp bottom contact.

649-703 cm Olive grading to pale gray green with olive mottles lutite bearing, siliceous nanno ooze.

703-803 cm Off white lutite bearing, foram siliceous nanno ooze.

803-866 cm Gray olive with pale green mottles, lutite bearing, siliceous nanno ooze with off white lutite bearing, micronodule bearing, siliceous foram and nanno ooze pockets and lenses.

Core 40 1°36'N 59°40'E 5426 m

0-199 cm Dark buff occasionally foram bearing, lutite bearing, siliceous nanno ooze with base of unit containing forams and mud lumps.

199-206 cm Orangey buff nanno bearing, lutite rich, siliceous ooze.

206-212 cm Gray grading to buff biogenic ooze.

212-297 cm Tan lutite rich, nanno siliceous ooze light tan with gray 212-226 cm, grayish tan with light tan mottles 226-272 cm, orangey tan 274-287 cm, gray buff at base.

297-374 cm Intergrading tan and buff lutite rich, nanno siliceous ooze.

374-381 cm Tan and black nanno bearing lutite rich, micronodule rich, siliceous ooze.

381-407 cm Tan lutite rich, siliceous ooze.

407-415 cm Tan and black biogenic ooze.

415-432 cm Light and dark buff nanno bearing, lutite rich, siliceous ooze.

432-439 cm Black and buff biogenic ooze.

439-468 cm Dark buff lutite rich, nanno rich, siliceous ooze.

468-477 cm Grayish buff grading to orangey buff biogenic ooze.

477-480 cm Black and buff nanno bearing, lutite rich, micronodule rich, siliceous ooze.

480-549 cm Grayish buff nanno bearing, lutite rich, siliceous ooze with gray grading to orange 506-549 cm.

549-553 cm Black and orangey buff lutite rich, siliceous ooze.

553-599 cm Buff with black mottles 584 cm and 590 cm lutite rich, siliceous ooze.

Core 41 1°34'N 65°39'E 3433 m

0-172 cm Light and dark buff with gray lutite bearing, foram rich, siliceous nanno ooze.

172-243 cm Light buff to off white with gray lutite bearing, foram rich, siliceous nanno ooze.

243-282 cm Gray and buff lutite bearing, silica rich, foram rich, nanno ooze.

282-293 cm Off white lutite rich, biogenic ooze abruptly terminating at base.

293-295 cm Buff lutite bearing, biogenic ooze.

295-336 cm Off white lutite bearing, nanno bearing, siliceous foram ooze with abrupt bottom contact.

336-351 cm Gray grading to off white with yellow lutite bearing, silica bearing, foram bearing, nanno ooze.

351-511 cm Off white varying to gray lutite bearing, silica rich, foram bearing, to foram nanno ooze.

Station 59 3° 24'S 45°00.5'E 4444 m

0-103 cm Mottled dark gray green lutite bearing, occasionally micronodule or foram bearing, siliceous nanno ooze.

103-132 cm Light gray green to off white with darker mottles, grading to gray green below 114 cm, lutite bearing, foram bearing, siliceous nanno ooze.

132-216 cm	Mottled very dark gray green with faint yellow layers lutite bearing, occasionally foram bearing, siliceous nanno ooze.
216-224 cm	Light gray lutite bearing, siliceous nanno ooze.
224-296 cm	Very dark gray green with black specs and yellow areas, lutite bearing, micronodule bearing, foram bearing, siliceous nanno ooze.
296-311 cm	Light greenish gray darkly mottled and having black specs, lutite bearing, foram bearing, siliceous nanno ooze.
311-335 cm	Dark green gray micronodule bearing, silica bearing, lutite rich, nanno ooze.
335-395 cm	Light green gray with yellowish indurated layers at 360, 375, 385 cm lutite bearing, micronodule bearing, siliceous nanno ooze.
395-412 cm	Light gray lutite bearing, foram bearing, siliceous nanno ooze.
412-430 cm	Dark gray grading at 417 cm to light gray micronodule bearing, lutite bearing, siliceous nanno ooze with black specs.

430-480 cm	Alternating dark green gray, yellow gray and light gray mottled lutite bearing, siliceous nanno ooze.
480-590 cm	Mottled yellow greenish gray grading to dark gray grading to light gray lutite bearing, occasionally foram bearing, siliceous nanno ooze.
590-650 cm	Light gray with dark gray mottles occasionally micronodule bearing, lutite bearing, siliceous nanno ooze.
650-671 cm	Dark gray with some mottles at 664 cm lutite bearing, foram bearing, nanno siliceous ooze.
671-710 cm	Yellowish greenish gray occasionally micronodule bearing, lutite bearing, siliceous nanno ooze.
710-721 cm	Off white with grayish mottling lutite bearing, foram bearing, siliceous nanno ooze.
721-850 cm	Greenish gray occasionally micronodule bearing, occasionally foram bearing, lutite bearing, siliceous nanno ooze.

Station 60 3°31.2'S 46°59.9'E 4832 m

0-18 cm Very dark gray lutite bearing, siliceous rich, nanno ooze with layering from 14-18 cm.

18-70 cm Gray grading by 30 cm to buff with dark gray and dark brown mottles grading to greenish gray below 60 cm, lutite bearing, siliceous nanno ooze.

70-120 cm Very dark gray grading to grayish white lens at 75 cm grading to lighter gray at 76 cm grading to various shades of greenish gray below 79 cm, lutite bearing, nanno siliceous ooze.

120-172 cm Very dark gray mottled lighter with coarser mica bearing material at 136 cm grading to light greenish gray 136-158 cm grading to very drak gray, siliceous bearing, lutite nanno ooze.

172-221 cm Very light greenish gray lutite bearing, siliceous nanno ooze.

221-284 cm Greenish gray with very dark gray sections at 246 cm and 250 cm grading to very dark gray by 268 cm, nanno bearing, silica bearing, lutite at 282 cm with coarser mica bearing material at base of unit.

Figure 40.

'Visually estimated percentages of principal components in smear slides from cores 60, 61, 62, and HF3.

CORE 60

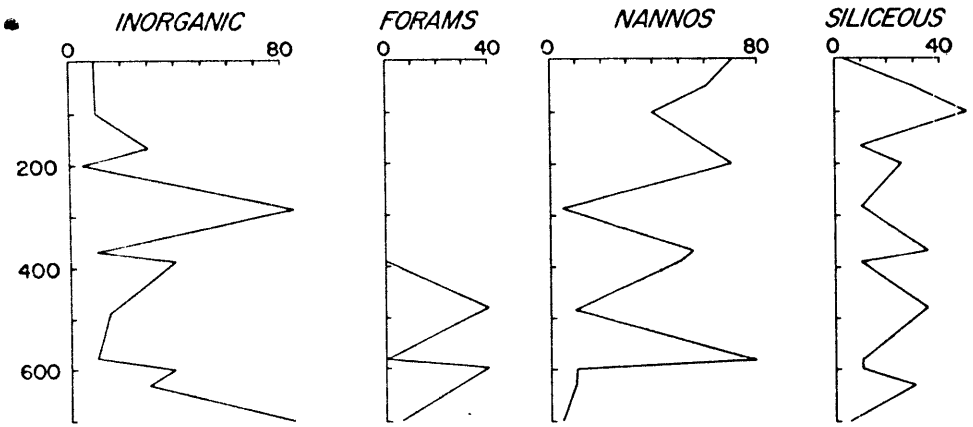

CORE 61

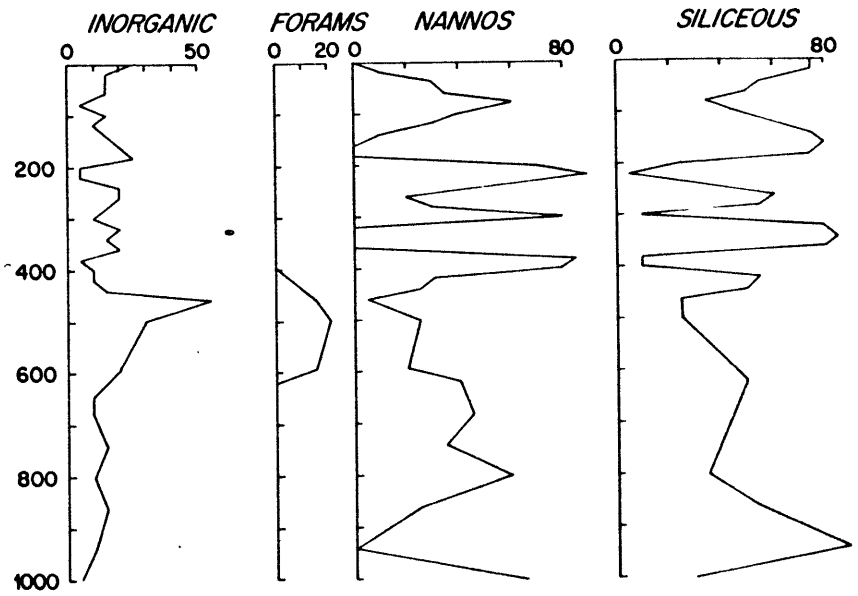

CORE 62

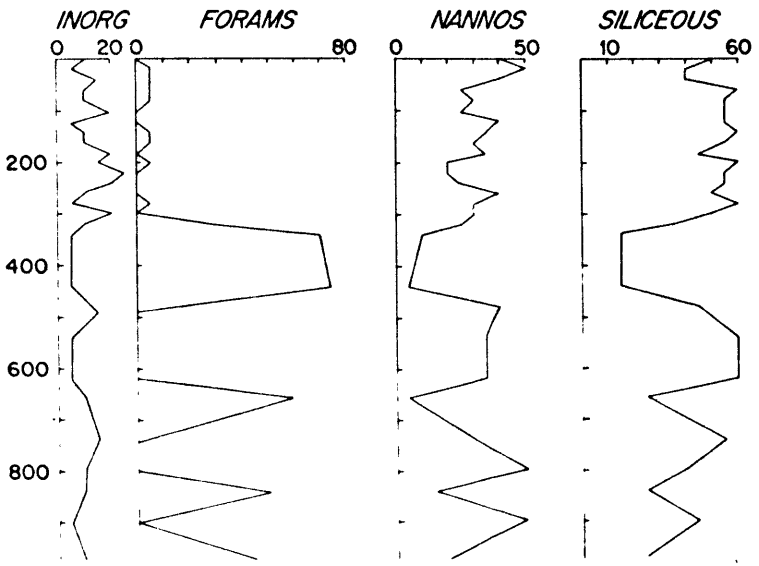

HF3

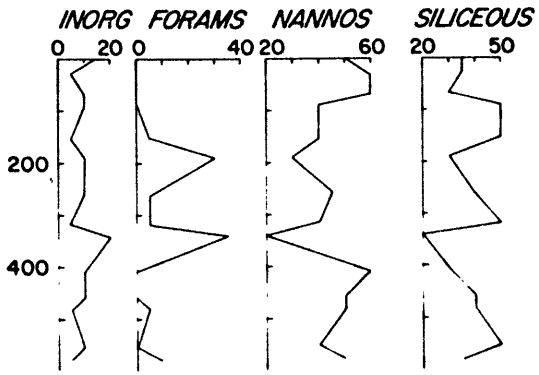

284-297 cm	Light greenish gray grading to very dark gray lutite terminating abruptly.
297-323 cm	Light greenish gray lutite bearing, siliceous nanno ooze grading into very dark gray silica bearing, lutite nanno ooze with abrupt basal contact.
323-350 cm	Same as above.
350-365 cm	Same as above.
365-408 cm	Same as above.
408-443 cm	Same as above.
443-494 cm	Greenish gray with green mottles at 450 cm grading to light gray green at 471 cm nanno bearing, lutite rich, siliceous foram ooze.
494-530 cm	Light greenish gray grading into very dark gray with finely laminated micaceous layers 520-530 cm.
530-558 cm	Light greenish gray grading to very dark gray and terminating abruptly.
558-594 cm	Very light green gray nanno bearing, lutite bearing, nanno ooze.
594-621 cm	Gray green silica bearing, nanno bearing, lutite foram ooze grading at 603 cm to very light green gray.

621-647 cm Light green gray nanno bearing lutite siliceous foram ooze.

647-815 cm Off white nanno bearing, silica bearing foram bearing, coarse sand.

Station 61 3°26.6'S 49°49.2'E 4897 cm

0-24 cm. Brown nanno bearing, lutite rich, siliceous ooze.

24-48 cm Yellowish buff mottled brown lutite rich, nanno siliceous ooze.

48-64 cm Greenish gray buff grading to greenish gray lutite rich, nanno siliceous ooze.

64-98 cm Light gray grading to greenish gray grading to yellowish green gray lutite bearing, siliceous nanno ooze.

98-128 cm Very dark green gray lutite bearing, nanno siliceous ooze.

128-195 cm Light yellowish green gray lutite rich, occasionally nanno bearing, siliceous ooze.

195-224 cm Buff grading to yellow lutite bearing, silica rich, nanno ooze.

224-246 cm Light grading to dark yellowish green lutite rich, siliceous nanno ooze.

246-263 cm Yellowish gray green lutite rich, nanno rich, siliceous ooze.

263-300 cm Gray green mottled lighter yellow lutite bearing, siliceous nanno ooze.

300-328 cm Very dark gray green mottled lighter lutite bearing, siliceous nanno ooze.

328-380 cm Yellowish greenish gray with darker mottles (coarser 328-329 cm) lutite rich, siliceous ooze occasionally nanno ooze.

380-406 cm Very light gray with darker mottles grading to darker gray lutite bearing, silica bearing, nanno ooze.

406-455 cm Very dark gray micaceous ?, foram bearing, lutite rich, nanno siliceous ooze.

455-602 cm Gray green micronodule bearing, foram rich, nanno rich, siliceous sand.

602-624 cm Light gray grading to dark gray lutite bearing, nanno siliceous ooze.

624-700 cm Light green gray lutite mottled dark gray and off white grading at 639 cm to gray green mottled light and dark lutite bearing, siliceous nanno ooze.

700-752 cm Dark gray green grading at 712 cm to light gray green with cross bedding grading at 725 cm to light with darker mottles, lutite bearing, nanno siliceous ooze.

752-858 cm Alternating very dark and lighter gray green, lutite bearing, siliceous nanno ooze.

858-865 cm Very light gray mottled green lutite rich, nanno siliceous ooze.

865-1005 cm Dark gray green lutite, mottled lighter and darker with yellow layer at 966 cm of lutite bearing, siliceous nanno ooze.

Station 62 6°46.4'S 48°41.8'E 4425 m

0-28 cm Medium brown grading to light brown foram bearing, lutite bearing, siliceous nanno ooze.

28-96 cm Dark brown mottled light grading at 39 cm to brownish off white mottled dark, foram bearing, lutite bearing, nanno siliceous ooze.

96-136 cm Buff mottled grayish and brown lutite bearing, to lutite rich, nanno siliceous ooze.

136-145 cm Yellow gray foram bearing, lutite bearing, nanno siliceous ooze.

145-184 cm Buff off white mottled darker occasionally foram bearing, lutite bearing, nanno siliceous ooze.

184-213 cm Gray mottled green, foram bearing, lutite bearing, nanno rich siliceous ooze.

213-270 cm Buff mottled brown and green layered at base, lutite rich, nanno siliceous ooze.

270-319 cm Buff grading from greenish gray laminations to off white to rich brown occasionally foram bearing, lutite bearing, nanno siliceous ooze.

319-471 cm White faintly brownish mottled lutite bearing, nanno rich, siliceous foram ooze.

471-496 cm Gray grading to buff lutite bearing, nanno siliceous ooze.

496-553 cm Yellow off white mottled green and brown, grading tc gray-green buff at base lutite bearing, nanno siliceous ooze.

553-630 cm Dark buff mottled gray and off white grading at 578 cm to off white mottled green and grading to brownish at base lutite bearing, nanno siliceous ooze.

630-646 cm Mottled dark gray-green ooze.

646-661 cm White micronodule bearing, lutite bearing, nanno bearing, siliceous rich, foram ooze with angular upper contact and sharp horizontal basal contact.

661-790 cm Dark buff mottled lighter, grading at 696 cm to off white grading to buff grading at 723 cm to buff with lighter and darker mottles, and then grading at 766 cm to off white with darker mottles lutite rich, nanno siliceous ooze.

790-828 cm Off white lutite bearing siliceous nanno ooze.

828-873 cm Brown mottled light buff ooze with off white lenses at 835-836, 839-842, 846-847, 850-854 cm of lutite bearing, nanno rich, siliceous rich, foram ooze grading at 854 cm to light buff mottled dark brown with lenses at 860-862 and 870-872 cm.

873-967 cm Light and dark buff lutite bearing, siliceous nanno ooze grading at 935 cm to buff lutite lumps, and foram ooze grading at 957 cm to light buff.

967-973 cm White lutite bearing, nanno rich, siliceous rich, foram ooze.

Core FF 3 5°52'N 53°51'E 5099 m

0-55 cm Gray green lutite rich, siliceous nanno ooze.

55-110 cm Gray yellow-green grading to gray-green lutite bearing, siliceous nanno ooze.

110-180 cm Green lutite bearing, foram bearing, nanno siliceous ooze.

180-290 cm Dark green foram bearing, lutite bearing, siliceous nanno ooze with at 189 and 278 cm lighter green lutite bearing, micronodule bearing, foram siliceous nanno ooze.

290-328 cm Gray green lutite bearing, foram bearing, nanno siliceous ooze.

328-455 cm Light green grading at 336 cm to slightly mottled green lutite bearing, occasionally micronodule rich, siliceous nanno ooze with foram ooze at 343 cm.

455-467 cm White green mottled dark green, lutite bearing, siliceous nanno ooze.

467-486 cm Light green lutite bearing, foram bearing, siliceous nanno ooze.

486-559 cm	Dark green mottled black at 545 cm lutite bearing, nanno siliceous ooze.
559-580 cm	Gray-green lutite bearing, foram bearing, siliceous nanno ooze with sharp upper contact.

Core FF 3 8°58.5'N 56°02'E 4001 m

0-106 cm	Off white lutite bearing, occasionally foram bearing to foram rich, siliceous nanno ooze.

Core PC-9 8°59'N 51°44'E 3985 m

0-875 cm	Greenish gray lutite bearing, siliceous rich to siliceous nanno ooze often foram bearing to foram ooze.

Figure 41.

Visually estimated percentages of principal components in smear slides from cores FF3 and PC9.

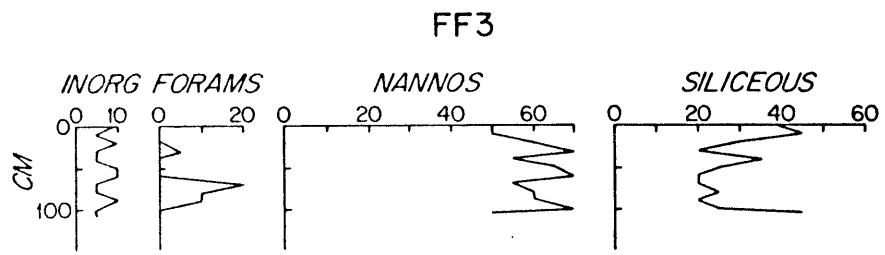
FF3
INORG
FORAMS
NANNOS
SILICEOUS
0
10
20
40
60
CM
100

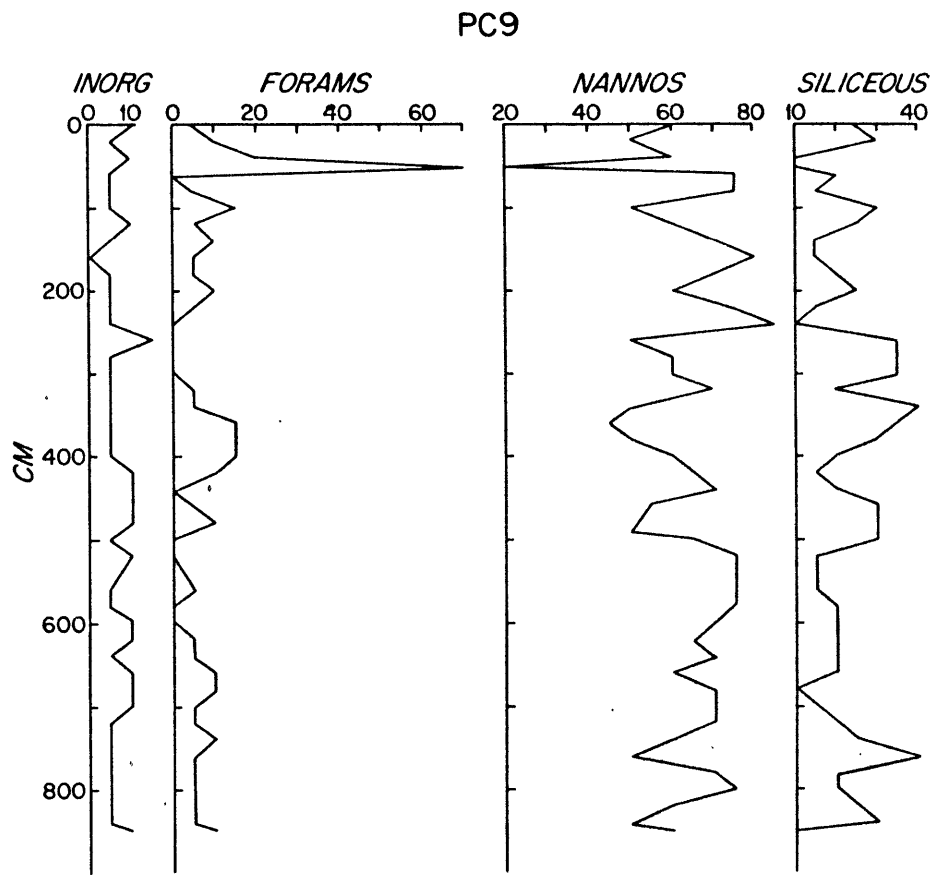
PC9
INORG
FORAMS
NANNOS
SILICEOUS
0
10
20
40
60
80
200
400
600
800
CM

APPENDIX II

Nannofossil Biostratigraphy and Chronostratigraphy of Selected Somali Basin Cores

Introduction

In order to determine sedimentation rates and the age of lithologic changes in the late Cenozoic sediments, several cores were dated using primarily the initial occurrence of Emiliania huxleyi. The principles, preparation methods, and scanning electron microscope results are presented here in order to avoid lengthy discussion in the text.

Late Cenozoic Nannofossil Biostratigraphy and Chronostratigraphy

Several late Cenozoic nannofossil biostratigraphic zonations have been presented including those of Hay et al. (1967), Gartner (1969), Martini and Worsley (1969), Martini (1971), Bukry (1973), Geitzenauer (1972), and Gartner (1973). The first appearance of Emiliania huxleyi and the preceding extinction of Pseudoemiliania lacunosa are the two nannofossil datum levels on which the zonation is based. Correlation of the nannofossil biostratigraphic events with an absolute chronology has been done indirectly on the basis of dated foraminiferal zonations (Gartner, 1969; Bukry, 1973;

Martini, 1971) and directly on the basis of the paleomagnetic stratigraphy of the sediments containing them (Gartner, 1973).

The first occurrence of Emiliania huxleyi has been reported as 140,000 to 200,000 years BP (Gartner, 1969); 170,000 years (Gartner, 1972 on the basis of the Rona and Emiliani, 1969 Pleistocene time scale); 150,000 years (Geitzenauer, 1972); 250,000 to 270,000 (McIntyre, et al., 1970 which if the Hays, et al., 1969 time scale is used is 150,000 years). Thus, the age used for calculations here will be 170,000 years but the variation of plus or minus 30,000 years is implicit due to the present uncertainties.

Determination of the Pseudoemiliania lacunosa extinction datum by several authors has likewise resulted in various estimates. However, Gartner's (1973) direct determination of 300,000 to 350,000 years on the basis of its mid-Brunhes (690,000 to present) occurrence in Equatorial Pacific cores will be used here.

Scanning Electron Microscope Techniques

Due to the extremely small size of Emiliania huxleyi (3-4 microns) and the ease of confusing it with the Gephyrocapsa sp. in the light microscope, all age determinations were made

with the scanning electron microscope. Samples were prepared by suspending a small amount of sediment in a vial, withdrawing from the center of a freshly shaken suspension, and placing the material to dry on a section of glass glued to the standard SEM plug coating with carbon, and then coating with gold. After coating the samples were ready for viewing.

Results

The results of the analyses are summarized in table 7. At each level from each core sampled the preservation was qualitatively noted except in cases where excessive clay or poor sample preparation made such assessment difficult. The presence or absence of Emiliania huxleyi was noted after 15 to 20 minutes of viewing the given sample.

Age Computations and Sedimentation Rates

In table 8 initial occurrence of Emiliania huxleyi has been compiled for 12 cores. In cases where the bottom of the core contained E. huxleyi a minimum sedimentation rate is specified and conversely in cases where it is absent in the samples a maximum rate is noted. Where it appears in a core in samples separated by 1 m or more half of the difference in levels is assigned as the level of initial occurrence with an error of that difference

introduced. The resultant sedimentation rates have been calculated in table 8 on the basis of the age-sediment thickness graph in figure 42.

TABLE 7 (Caption)

ELECTRON MICROSCOPE ANALYSIS FOR
EMILIANIA HUXLEYI FIRST OCCURRENCE

Preservation has been qualitatively determined analogous to the results shown by McIntyre and McIntyre (1971). In their plate 16.2, p. 258, the designation G as used here refers to the upper four photographs which show internal structure of Emiliania huxleyi and Gephyrocapsa oceanica. M as used here is analagous to the next lower photographs where dissolution has proceeded but the specimens are distinct. P indicates the conditions of the lower 4 photographs where only in some instances may E. huxleyi be noted.

Emiliania huxleyi has been indicated as present by Pres. and absent by A. ¢ indicates an excess clay in the sample; N. D. the analysis not determined; and — the analysis not attempted due to inadequate sample material or preparation.

TABLE 7

ELECTRON MICROSCOPE ANALYSIS FOR
EMILIANIA HUXLEYI FIRST OCCURRENCE

Core	Level CM	Preserv.	Emiliania huxleyi
26	1138	M	A
	920	G	A
	653	M-G	A
27	1146	G	Pres.
	0	P	-
29	1154	P	-
30	1106	M-G	A
	935	¢	ND
	678	¢	ND
32	958	M-G	A
	854	M-G	A
	653	M	Pres.
	0	M	Pres.
34	893	G	A
	715	M	A
	530	G	Pres.
35	1053	M	A
	845	G	A
	698	G	Pres.
36	862	G	A
	803	G	A
	638	G	A?
40	603	P¢	ND

TABLE 7 (continued)

Core	Level CM	Preserv.	Emiliania huxleyi
41	511	M-G	A
	480	G	-
	380	G	Pres.?
59	0	M-P	-
	914	G	Pres.
60	815	M	ND
61	0	P	-
	1005	P	ND
62	0	G-M	-
	828	P	ND
HF 3	580	M	A
	482	M	Pres.
	410	G	Pres.
PC 9	853	G	Pres.

TABLE 8

Average Sedimentation Rates
0 - 170,000 Yrs. Based on
Emiliania Huxleyi First Occurrence

Core	Level Absent	Level Present	Initial Occurrence	Rate cm/1000 yr.	Error
26	653		<653	<4.6	
27	-	1146	>1146	>7	
30	1106	-	<1106	<6.5	
32	894	653	773	4.8	±0.7
34	715	530	622	4.5	±0.6
35	845	698	771	4.8	±0.4
36	638	-	<638	<4.5	
41	511	380?	445	3.2?	±0.4
HF3	580	482	531	4.0	±0.3
PC9		853	>853	>5.0	
59	-	914	914	>5.5	

$$\text{Initial Occurrence: Level Present} + \frac{\text{Level Absent} + \text{Level Present}}{2}$$

$$\text{Error} = \frac{\text{Level Absent} - \text{Level Present}}{170} \Big/ 2$$

Figure 42.

Age of nannofossil data plotted versus cm down core with sedimentation rates for various depths shown.

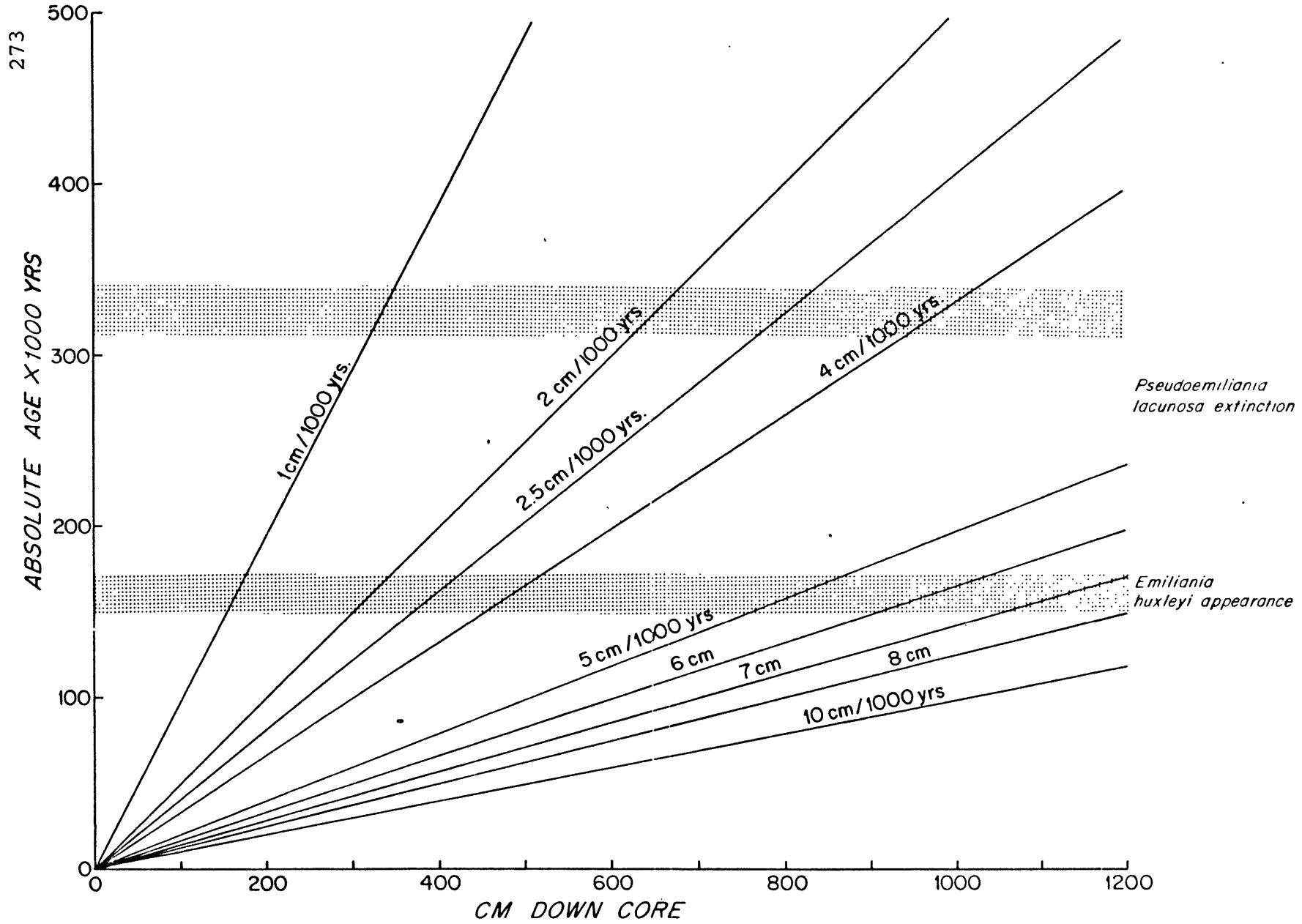
ABSOLUTE AGE X1000 YRS
500
400
300
200
100
0
0
200
400
600
800
1000
1200
CM DOWN CORE
1cm/1000 yrs.
2 cm/1000 yrs.
2.5cm/1000 yrs.
4 cm/1000 yrs.
5 cm/1000 yrs
6 cm
7 cm
8 cm
10 cm/1000 yrs
Pseudoemiliania lacunosa extinction
Emiliania huxleyi appearance

APPENDIX III

Radiocarbon Age Determinations

Introduction and Principles

The Emiliania huxleyi datum (Appendix II) provides a means of identifying the 170,000-year level in cores. To further date cores in the more recent past (40,000 yrs.) radiocarbon dates were attempted on five cores in the basin. The radiocarbon dating method presumes a steady influx of cosmic rays in the upper atmosphere forming the carbon-14, no significant carbon isotopic fractionation in the atmosphere or ocean, and the maintenance of carbon within the sample after the death of the organism (Suess, 1956). Variation in the radiocarbon calendar age relationship is introduced by departures from the above conditions but these discrepancies are usually not significant in terms of the geologic time scale.

Measurement

Analyses were undertaken by a commercial firm Teledyne Isotopes Inc. where the sample is converted to CO_2 and introduced into a Geiger counter to determine the β emissions which are proportional to the number of radiocarbon atoms present. After three counting periods, corrections for background, and corrections

for counting statistics the ages and errors may be assigned (Teledyne).

Results are shown in Table 9.

TABLE 9

RESULTS OF RADIOCARBON

AGE DETERMINATIONS

Core	Sample Internal cm	Total $CaCO_3$ ± 10%	Age in 1000 yrs.	Average Sediment Rate cm/1000 yrs.
26	142-147	77	> 40	< 3.6
30	117-123	N.D.	> 40	< 3.0
36	95-100	63	> 40	< 2.4
59	123-129	51	> 40	< 3.1
PC 9	203-208	76	> 40	< 5.1

N.D. Not Determined.

APPENDIX IV

A Light Microscope Method for Indicating Paleotemperature from Late Cenozoic Calcareous Nannofossils

As nannoplankton live in the photic zone and each nannofossil that accumulates in bottom sediments represents a relatively short time - on the order of weeks - in the surface waters, examination of these organisms should provide excellent paleotemperature information. However, many obstacles have hindered the utilization of this potential. Although some nannoplankton has been cultured many species' preferences for nutrients, temperature, and salinity are not known in detail. In addition mechanisms of bottom accumulation and effects of dissolution may affect the record. Finally, recent material must be examined using an electron microscope which is time consuming and expensive if absolute abundance of each species and subspecies is to be determined. In order to overcome some of these difficulties this appendix will develop a simple ratio that may be determined by light microscope and test its utility with respect to detailed species composition — temperature information from the Pacific (Okada and Honjo, 1973).

Examination of nannofossil sediment assemblages from the Atlantic (McIntyre and Be, 1967) and correlation of these assemblages with surface water temperature in the same areas provides background data for constructing the temperature preferences of several species. In addition examination of assemblages from 0-200 m depth in the Pacific (Okada and Honjo, 1973) yields further information on temperature preference. A composite plot of the results (Figure 43) indicates those species that are indistinguishable in the light microscope, Emiliania huxleyi and Gephyrocapsa sp., span the greatest temperature range while other species generally favor warmer waters. Thus, in cases where other factors aside from temperature do not play a dominant role, the ratio of the sum of Emiliania huxleyi plus Geophyrocapsa spp versus the sum of the number of individual coccoliths of all other species may reflect both present day sea surface temperature and paleotemperatures.

In order to test this hypothesis sea surface temperature and surface water calcareous nannoplankton assemblages from 50°N to 16°S at 155°W in the Pacific (Okada and Honjo, 1973) were used. In table 10 the ratio:

Figure 43.

Nannoplankton temperature ranges in the Atlantic and Pacific compiled from:

McIntyre and Be	1967
McIntyre Be and Roche	1970
Okada and Honjo	1973

In each case the temperature is determined by the temperature of surface water at the time in the case of plankton tows or by a sea surface temperature map in the case of bottom samples.

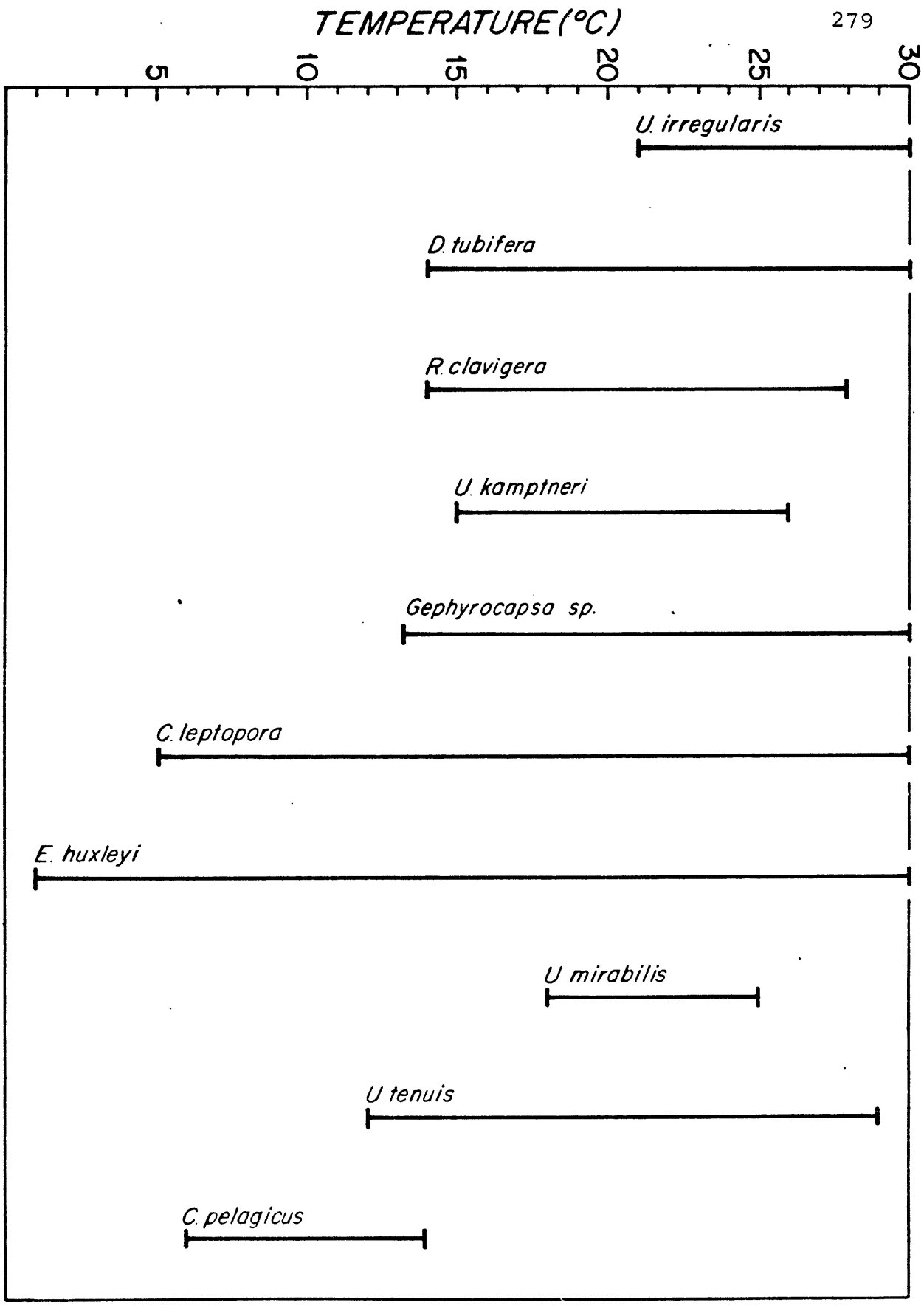
TEMPERATURE(°C)
5
10
15
20
25
30
U. irregularis
D. tubifera
R. clavigera
U. kamptneri
Gephyrocapsa sp.
C. leptopora
E. huxleyi
U mirabilis
U tenuis
C. pelagicus

$$\frac{\text{Gephyrocapsa spp + Emiliania huxleyi coccoliths}}{\text{all other coccoliths}}$$

was computed. Then this ratio was plotted versus latitude along with the temperature (figure 44). As temperature increases from 12°C at 50°N to 25°C at 30°N the ratio falls from over 65 to around 0.05. The ratio fluctuates between 0.01 and 0.12 while the temperature increases to around 28°C at 9°N. Between 9°N and 16°S the temperature remains at 26.5 - 28.9 and the ratio fluctuates between 1 and 10.

Although the ratio is not directly related to temperature, it does define broad regions that can be applied to relative paleotemperature analysis for samples taken down core. In a case where the sea surface temperature and the sediment surface nannofossil ratio is known significant deviations in the ratio may be used to indicate approximate paleotemperature change.

TABLE 10

RATIO OF GEPHYROCAPSA SPP + EMILIANIA HUXLEYI TO OTHER SPECIES DETERMINED FROM OKADA AND HONJO (1973) TOTAL ASSEMBLAGE DATA IN PACIFIC SURFACE WATERS

N Lat.	G + E. H.	Other	Ratio	Temp. °C
50	200	0	--	12.1
49	197	3	65.7	12.2
48	194	6	32.3	12.7
47	189	11	17.2	13.4
46	190	10	19.0	14.1
45	192	8	24.0	15.6
44	158	42	3.8	16.2
41	20	0	--	19.9
40	153	47	3.3	21.0
36	111	89	1.25	24.0
35	112	88	1.27	23.7
34	30	170	.18	23.4
33	29	171	.17	23.5
32	20	180	.11	24.0
31	8	192	.09	24.3
30	0	200	--	24.5
29	0	200	--	25.1
26	1	199	--	25.4
25	13	187	.07	25.3
24	1	199	--	25.7
23	6	194	.03	25.5
22	4	196	.02	25.5
21	11	189	.06	26.0
20	26	174	.15	25.8
19	12	188	.06	26.0
18	4	196	.02	26.1
17	20	180	.11	26.1
16	27	173	.16	26.4
15	29	171	.17	27.0
13.5	34	166	.20	26.9

TABLE 10 (continued)

Lat.	G + E. H.	Other	Ratio	Temp. °C
12	21	179	.12	27.5
11	11	189	.06	27.6
10	11	189	.06	27.7
8.75	11	189	.06	28.0
7.5	21	179	.12	28.7
7	51	149	.34	28.8
6.5	55	145	.38	28.8
6	78	122	.64	28.9
5.5	83	117	.71	28.6
5	112	88	1.27	27.7
4.5	96	104	.92	28.0
4	117	83	1.41	26.9
3.5	128	72	1.78	27.0
3	105	95	1.1	26.9
2.5	97	103	.94	26.9
2	103	97	1.06	26.7
1.5	107	93	1.15	26.8
1	114	86	1.33	27.0
0.5	133	67	1.98	27.4
0	156	44	3.54	28.3
0.5°S	154	46	3.35	27.4
1°S	125	75	1.67	26.6
1.5°S	112	88	1.27	26.7
2°S	111	89	1.25	26.5
2.5°S	115	85	1.35	26.5
3°S	119	81	1.47	27.9
3.5°S	99	101	.98	28.1
4°S	110	90	1.22	27.9
4.5°S	94	106	.88	27.7
5°S	91	109	.84	27.6
5.5°S	98	102	.96	27.9
6°S	110	90	1.22	27.8
6.5°S	88	112	.79	27.8

TABLE 10 (continued)

Lat.	G + E. H.	Other	Ratio	Temp. °C
7°S	107	83	.78	28.0
7.5°S	97	103	.94	28.0
8°S	86	114	.76	28.4
8.5°S	118	82	1.45	28.7
9°S	106	94	1.13	28.4
9.5°S	140	60	2.33	28.6
10°S	92	108	.85	28.4
11°S	74	126	.59	28.4
12°S	10	190	.05	28.7
13°S	7	193	.04	28.2
14°S	7	193	.04	28.0
15°S	11	189	.06	28.3
16°S	12	188	.06	27.8

Figure 44.

Ratio of Geophyrocapsa spp. plus Emiliania huxleyi to other Pacific surface water calcareous nannoplankton species plotted with temperature against latitude. (Data are from Okada and Honjo, 1973).

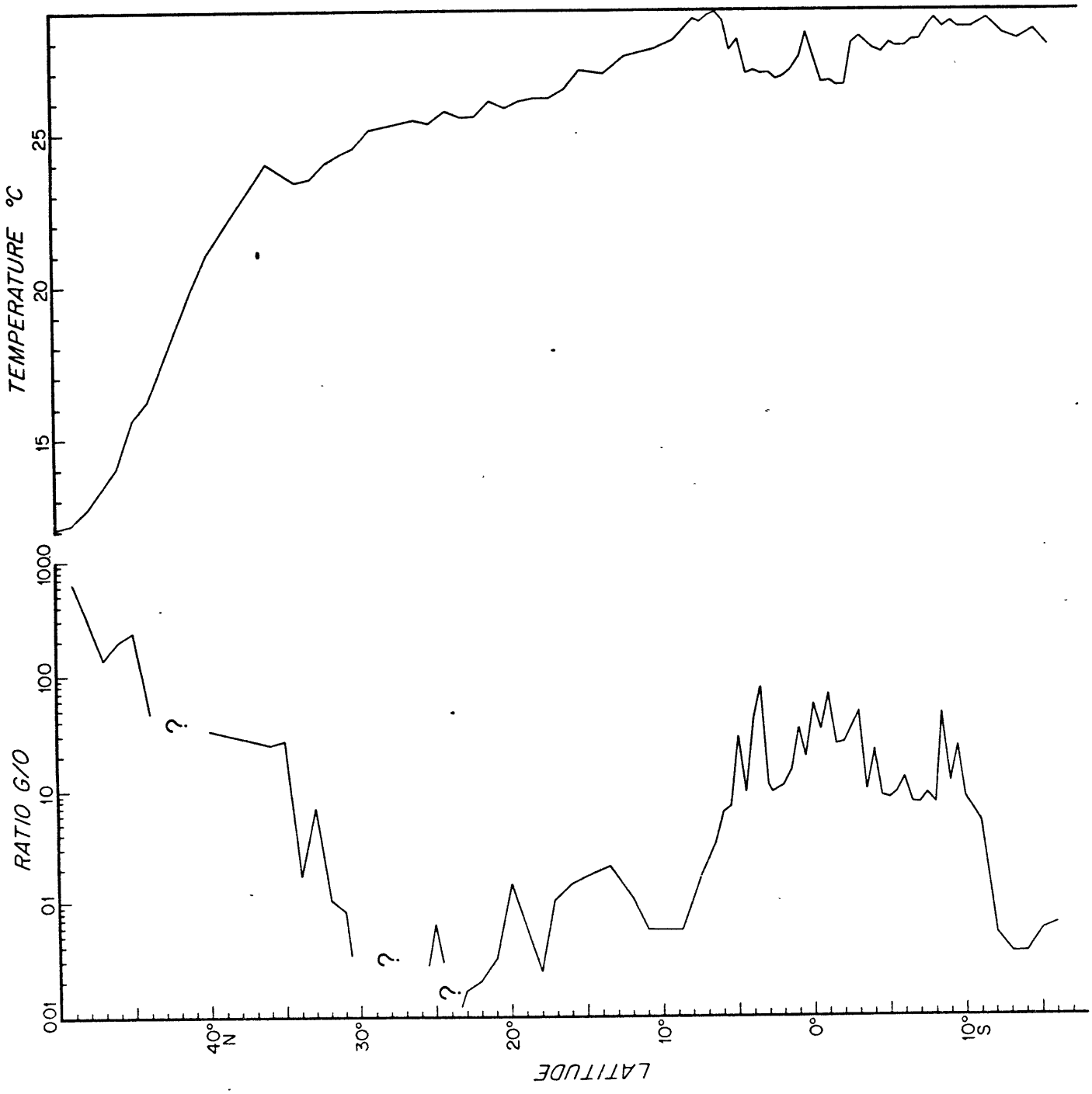
TEMPERATURE °C
15
20
25
RATIO G/O
001
01
1
10
100
1000
?
?
?
40° N
30°
20°
10°
0°
10° S
LATITUDE